AD_____

Award Number: DAMD17-02-1-0195

TITLE: Quantitative Characterization of Pulmonary Pressure-Volume Curve for Improved Care of Acute Lung Injury

PRINCIPAL INVESTIGATOR: Uichiro Narusawa, Ph.D.

CONTRACTING ORGANIZATION: Northeastern University
Boston, Massachusetts 02115

REPORT DATE: March 2003

TYPE OF REPORT: Annual

PREPARED FOR: U.S. Army Medical Research and Materiel Command
Fort Detrick, Maryland 21702-5012

REPORT DOCUMENTATION PAGE

Form Approved
OMB No. 074-0188

1. AGENCY USE ONLY (Leave blank)	2. REPORT DATE	3. REPORT TYPE AND DATES COVERED
	March 2003	Annual (1 Mar 02 - 28 Feb 03)

4. TITLE AND SUBTITLE
Quantitative Characterization of Pulmonary Pressure-Volume Curve for Improved Care of Acute Lung Injury

5. FUNDING NUMBERS
DAMD17-02-1-0195

6. AUTHOR(S):
Uichiro Narusawa, Ph.D.

7. PERFORMING ORGANIZATION NAME(S) AND ADDRESS(ES)
Northeastern University
Boston, Massachusetts 02115

E-Mail: narusawa@coe.neu.edu

8. PERFORMING ORGANIZATION REPORT NUMBER

9. SPONSORING / MONITORING AGENCY NAME(S) AND ADDRESS(ES)
U.S. Army Medical Research and Materiel Command
Fort Detrick, Maryland 21702-5012

10. SPONSORING / MONITORING AGENCY REPORT NUMBER

11. SUPPLEMENTARY NOTES

12a. DISTRIBUTION / AVAILABILITY STATEMENT
Approved for Public Release; Distribution Unlimited

12b. DISTRIBUTION CODE

13. Abstract *(Maximum 200 Words)* *(abstract should contain no proprietary or confidential information)*

Continuous (sigmoidal (tangent-hyperbolic) and error-function) p-V model equations with four parameters are shown to represent clinical p-V curves accurately. The magnitudes of the four parameters, coupled with the normalized p-V equation, distinguish p-V data sets effectively. A mechanistic model of the total respiratory system is developed for the inflation process, relating characteristics of the p-V model equation to the internal respiratory conditions such as alveolar recruitment and elastic distension of tissues. The model is based on the principle of statistical mechanics applied to the total respiratory system as an ensemble of a large number of respiratory elements, each of which consists of a piston-spring subsystem. The ability of the mechanistic model to predict volume limits of the corresponding deflation process justifies its theoretical foundation.

14. SUBJECT TERMS:	15. NUMBER OF PAGES
acute lung injury, mechanical ventilation, P-V curve	108
	16. PRICE CODE

17. SECURITY CLASSIFICATION OF REPORT	18. SECURITY CLASSIFICATION OF THIS PAGE	19. SECURITY CLASSIFICATION OF ABSTRACT	20. LIMITATION OF ABSTRACT
Unclassified	Unclassified	Unclassified	Unlimited

Table of Contents

Introduction

For improved care of patients with acute lung injury, existing clinical data sets are examined to characterize quantitatively the pulmonary pressure-volume (p-V) curves. A mechanistic model of the total respiratory system (TRS) is constructed for the inflation process, making it possible to relate the p-V curve to the corresponding changes in intra-respiratory conditions. The mechanistic model computationally simulates the TRS based on an application of the principle of statistical mechanics to a very large number of elements comprising the TRS. A mechanistic model of the deflation process is currently under investigation.

Body

Research contents are reported in three chapters:

Chapter 1. Quasi-Static Pressure-Volume Curce: Comprehensive Data Analysis, reports research results corresponding to Objective 1 (Examination of accuracies and limitations of the sigmoidal equation) and Objective 2 (Development of a method for quantitative characterization of p-V curves) in Statement of Work of Research Proposal.

Chapter 2. Mechanistic Model: Part I. Model Development for Inflation Process, reports the derivation of the mechanistic model of the total respiratory system, which is part of Objective 3 (Development of a mechanistic respiratory model) in Statement of Work of Research Proposal.

Chapter 3. Mechanistic Model: Part II. Examination of Clinical Data, reports examinations of p-V inflation curves based on the mechanistic model.

Chapter 1. Quasi-Static Pressure-Volume Curve: Comprehensive Data Analysis

Abstract

A p-V model equation with four parameters is used to represent various existing (p-V) curves. The report is focused on the case in which the equation is applied to two existing groups of p-V data (one, twenty nine p-V curves of healthy adults and the other, twenty one p-V curves of patients with acute respiratory distress syndrome) to determine the magnitudes of the parameters for each data set. The equation is found to represent the p-V curves of both data groups extremely well. It is also confirmed that the magnitudes of the four parameters of the error function p-V model equation, combined with the corresponding normalized representation of p-V curves, quantitatively distinguish different respiratory conditions between the two groups as well as between different data sets in each group.

Nomenclature

p	pressure (interpleural pressure difference)
p_{grad}	(volume-) gradient pressure range, Eq.(3)
$p_{cl(u)}$	lower (upper) corner pressure, Eq.(4)
$p_{mci(d)}$	pressure at maximum compliance increase (decrease), Eq.(5)
p_o	pressure at the inflection point (at the maximum local compliance) where $V = (V_U + V_L)/2$
$\overline{p}$	non-dimensional pressure, $p/p_0 - 1$
V	volume
$V_{L(U)}$	lower (upper) volume asymptote (Fig.1)
$\overline{V}$	non-dimensional volume, $(V - ((V_U + V_L)/2)/(\Delta V/2)$, (Eq.(1b))
ΔV	$V_U - V_L$ (Fig.1)

Greek symbols:

α	constant defined in Eq.(1a)
Λ	$\alpha p_0 \Delta V$(non-dimensional parameter) (Eq.(1b))
ω	$\Lambda\bar{p}/2$ (Eq.(1b))

Acronyms:

ARDS	acute respiratory distress syndrome
LIP	lower inflection point, Eq.(6)
TRS	total respiratory system
UIP	upper inflection point, Eq.(6)

Introduction

Quasi-static pulmonary $p-V$ (pressure - volume) curves provide quantitative information on the respiratory system that is important for both research and clinical guidances. A typical inflation p-V curve, obtained for an anesthetized human subject in supine position, consists of a nearly linear region of high compliance (i.e. large dV/dp) sandwiched between two segments with low compliance at low and high pressure regions. The shape of the curve is affected by two mechanisms, the distension of the elastic respiratory wall tissue components and the recruitment of the alveoli ('pop-open' mechanism). The latter is the opening of alveoli overcoming the surface tension at the interface between the gas and the liquid film lining the alveolar surface. A pressure increase (i.e. an increase in the interpleural pressure difference) results in the recruitment of a greater number of alveoli. The high compliance is believed to be associated with both the distension of open parts and the (alveolar) recruitment of collapsed parts of the total respiratory system (TRS).

In order to quantify the characteristics of $p - V$ curves as well as their changes observed in clinical settings, various p-V model equations have been proposed [1 - 8]. One commonly used model equation is developed by dividing the entire p-V curve into three regions, a high-pressure, low-compliance upper region, a high-compliance midregion and a low-pressure, low-compliance lower region. The midregion is represented by a linear equation between p and V; while, the two low-compliance regions are approximated by an exponential function of pressure [9, 10]. The linear-exponential model equation is a piecewise continuous function with the compliance abruptly changing its magnitude at the intersects of the linear and the exponential regions. Venegas, Harris and Simon [8], on the other hand, showed that a single continuous function in a form of sigmoidal (tangent hyperbolic) equation represents various p-V curves extremely well. Parameters in model equations (both piecewise-continuous and continuous equations) are determined from statistical processing of clinical data. More recently the clinical usefulness of the sigmoidal model equation over piecewise-continuous representations is also reported by the same

group of researchers [11].

Accurate and quantitative determinations of the form of p-V model equation and its parameters are prerequisite to the clinical interpretations of p-V curves, including an establishment of ventilator strategy with the p-V curve guidance in intensive care for patients with acute lung injury as well as its more severe form, acute respiratory distress syndrome (ARDS) [12 - 14]. Our objective is to test a hypothesis that the continuous p-V model equation, particularly in a form of an error function equation, is effective in representing p-V curves from different sources, and of different respiratory conditions (a group of patients with ARDS [8] and a group of healthy adults [9]). The former covers both inflation and deflation processes, and the latter includes the inflation p-V curves before and after alveolar recruitment maneuver with a total of fifty p-V curves. The report examines differences and similarities (1) between patients with ARDS and healthy adults, (2) among patients with ARDS as well as among healthy adults, both in terms of parameters of the error function p-V model equation.

Equations for Quasi-Static p-V Curves

A model equation, originally proposed by Venegas, Harris and Simon [8] and subsequently shown to represent p-V curves well for both inflation and deflation processes [11], has the following sigmoidal (tangent hyperbolic) form;

$$\frac{dV}{dp} = -\alpha\,(V - V_U)\,(V - V_L), \quad \frac{V - V_L}{\Delta V} = [1 + exp\,(-\alpha\,\Delta V\,(p - p_0))\,]^{-1}. \qquad (1a)$$

where $\Delta V = V_U - V_L$, V_U = upper volume asymptote, V_L = lower volume asymptote, α = positive constant and p_0 = pressure at the midpoint (inflection point) of the curve. The corresponding non-dimensional form of the sigmoidal equation is [15],

$$\frac{d\overline{V}}{d\overline{p}} = -\frac{\Lambda}{2}\,(\overline{V}^2 - 1), \qquad \overline{V} = \frac{e^{\omega} - e^{-\omega}}{e^{\omega} + e^{-\omega}}\,(= tanh\,(\omega)\,) \qquad (1b)$$

where

$$\overline{V} = \frac{V - (V_U + V_L)/2}{\Delta V/2}, \quad \omega = \frac{\Lambda\,\overline{p}}{2}, \quad \overline{p} = \frac{p}{p_0} - 1, \quad \Lambda = \alpha p_0\,\Delta V.$$

Venegas, Harris and Simon suggested that a p-V equation in terms of the error function is also effective in representing p-V data [8].

The error function, $erf(x)$, is defined as

$$erf(x) = \frac{2}{\sqrt{\pi}} \int_0^x e^{-t^2} dt \qquad with \qquad erf(\infty) = 1, \quad erf(-x) = -erf(x).$$

The error function model equation may be expressed as

$$\frac{dV}{dp} = \frac{\alpha(\Delta V)^2}{4} exp\Big[-\Big(\frac{\sqrt{\pi}}{4}\alpha\Delta V(p - p_0)\Big)^2\Big], \quad \frac{V - V_L}{\Delta V} = \frac{1}{2}\Big[1 + erf\Big(\frac{\sqrt{\pi}}{4}\Lambda\overline{p}\Big)\Big], \quad (2a)$$

$$\frac{d\overline{V}}{d\overline{p}} = \frac{\Lambda}{2} \cdot exp(-\frac{\pi}{4}\omega^2), \qquad \overline{V} = erf(\frac{\sqrt{\pi}}{2}\omega). \quad (2b)$$

Fig.1 is a sketch of a typical p-V model equation (either the sigmoidal or the error-function model equation). The curve varies smoothly between the low pressure asymptote, V_L, and the high pressure asymptote, V_U. The midpoint of the curve where the volume is equal to $(V_U + V_L)/2$ is the inflection point with its pressure denoted by p_0. Both the sigmoidal and the error-function model equations are antisymmetric with respect to the inflection point; that is, $V(p - p_0) - V(p_0) = -(V(p_0 - p) - V(p_0))$ or $\overline{V}(\overline{p}) = -\overline{V}(-\overline{p})$. The compliance, dV/dp, increases along the p-V equation as pressure increases, until the inflection point (= the point of maximum compliance) is reached. Then the compliance decreases with a further increase in pressure. A tangent to the model equation curve at the inflection point has the compliance of $\alpha(\Delta V)^2/4$. The two points of intersection between the tangent and the two volume asymptotes, $V = V_U$ and $V = V_L$ are referred to as the upper and lower corner pressure, $p_{cu(cl)}$, respectively. The pressure difference between the two corner pressures is defined as the (volume-) gradient pressure range, p_{grad}. Also, the pressure at the point of maximum compliance increase (decrease) of the p-V curve, p_{mci} (p_{mcd}), may be specified as the points where the third derivative of $\overline{V}$ with respect to $\overline{p}$ is zero.

For both the sigmoidal and the error-function model equations,

$$\frac{p_{grad}}{p_0}\left(\equiv \frac{\Delta V}{p_0\,(dV/dp)_{max.}}\right) = \frac{4}{\Lambda}, \qquad \overline{p}_{cu(cl)}\,(= \frac{p_{cu(cl)}}{p_0} - 1) = (-)\frac{2}{\Lambda}. \quad (3,4)$$

On the other hand,

$$\overline{p}_{mcd\,(mci)}(=\frac{p_{mcd(mci)}}{p_0}-1)=\begin{cases}(-)1.317/\Lambda & \text{for sigmoidal equation;}\\ (-)1.596/\Lambda & \text{for error-function equation.}\end{cases} \quad (5)$$

Fig.2 is the (non-dimensional) $\overline{p}-\overline{V}$ curve, corresponding to the p-V curve of Fig.1. The origin ($\overline{p}=0$, $\overline{V}=0$) represents the point of antisymmetry (p_0, $(V_U+V_L)/2$) of Fig.1. The non-dimensional pressure, $\overline{p}$, is the pressure difference, $p-p_0$, as a fraction of p_0 (Eq.(1b). The normalization of volume shifts the upper and the lower volume asymptotes, V_U and V_L in Fig.1 into $+1$ and -1 respectively in Fig.2. With both the location of p_0 and the volume asymptotes made common to all p-V curves, the resulting non-dimensional representations characterize p-V curves in general in terms of a single non-dimensional parameter, Λ. (Eqs.(1b,2b)) From Eq.(3) the parameter, Λ, is four times the ratio of the pressure at the maximum compliance, p_0, to the volume-gradient pressure range, p_{grad}. Since the compliance is maximum at the origin, the first quadrant ($\overline{V}$, $\overline{p}>0$) in Fig.2 is a region of decreasing local compliance with pressure; while, the third quadrant ($\overline{V}$, $\overline{p}<0$) is a region of increasing local compliance with pressure. The origin (p = 0, V = 0) of dimensional p-V curves is transformed into ($\overline{p}=-1$, $\overline{V}(V=0)$) on a $\overline{p}$-$\overline{V}$ curve; hence, the physiological lower limit of $\overline{p}$ is -1. Various pressure locations on $\overline{p}-\overline{V}$ diagram are proportional to $1/\Lambda$ as shown in Eqs.(3-5). Eqs.(3-5) also imply over the pressure range of $p>0$ that there is no lower corner pressure (i.e $1+\overline{p}_{cl}<0$) if $\Lambda<2$, and that there is no pressure for maximum compliance increase (i.e. $1+\overline{p}_{mci}<0$) if $\Lambda<1.317\,(1.596)$ for the sigmoidal (error-function) model equation. Both the sigmoidal and the error-function model equations are capable of representing p-V curves over their entire ranges as continuous functions.

Piecewise-continuous model equations are also used to represent p-V curves. Shown below is a three-region model equation [9], relevant to the present study, consisting of a linear midregion ($V_{LIP}\le V\le V_{UIP}$) and two exponential regions at high ($V_{UIP}\le V$) and low pressure ($V\le V_{LIP}$) ranges. (The subscripts, L(U)IP (lower (upper) inflection point),

indicate the points where the linear midregion equation intersect with the exponential equations.)

$$
\begin{aligned}
V_{max} - V(p) &= (V_{max} - V_{UIP}) \cdot exp\Big(\frac{V_{max} - V_{UIP}}{C_{lin}}(p - p_{UIP})\Big) \\
&\qquad\qquad\qquad\qquad\qquad\qquad for \quad V_{UIP} \le V \le V_{insuff}, \\
V(p) - V_{LIP} &= C_{lin}\,(p - p_{LIP}) \qquad\qquad for \quad V_{LIP} \le V \le V_{UIP}, \qquad (6) \\
V_{min} - V(p) &= (V_{min} - V_{LIP}) \cdot exp\Big(\frac{V_{LIP} - V_{min}}{C_{lin}}(p - p_{LIP})\Big) \quad for \quad V \le V_{LIP},
\end{aligned}
$$

where C_{lin} = compliance at the linear midregion, $V_{min(max)}$ = volume asymptote of the lower (upper) exponential region,

Data Analyses

The two data sources with a total of 50 p-V data sets consists of (A) ARDS patients by Harris et al (2000) [11], and (B) healthy adults by Svantesson et al (1998) [9]. For the data source A, p-V data points were made available to us by the authors. The data source B provides model parameters of the piecewise-continuous model equation, Eq.(6), as well as data ranges for each data set. Information on the data sources relevant to the present study is summarized below.

Data Source **A**

21 data sets of ARDS patients by Harris, Hess, Venegas [11], Original p-V data points made available by the authors, Inflation and deflation data in supine position.

Data Source **B**

29 data sets of healthy adults (both male and female) by Svantesson, Sigurdsson, Larsson, Jonson [9], 14 data sets before and 15 data sets after alveolar- recruitment maneuver, Inflation data in supine position

The parameters of Eq.(6) (V_{min}, V_{max}, V_{LIP}, V_{UIP}, V_{insuff}, C_{lin}, p_{LIP}, p_{UIP}) are tabulated for all data sets in [9].

Data sets from the source A are analyzed by minimizing the difference between data points and the model equation (either the sigmoidal or the error-function model equation)

through the application of the method of least squares to obtain the parameters, $\Lambda, \Delta V, p_0$ and V_U (or V_L). To analyze the data source B, ten to twenty five computational data points, depending on the data range, are generated from Eq.(6). Then, the method of least squares is applied to determine the parameters, Λ, p_0, ΔV and V_U (or V_L) of the error function model equation. Parameters of p-V model equations are determined for all data sets in Data Source A (for both inflation and deflation data) and B (for both before- and after-recruitment maneuver). Discussion beyond the validity test of the error function model equation, however, is focused on the inflation data sets of the two data sources. Results of data analyses are summarized in Table.1 (for Data Source A) and in Table.2 (for Data Source B).

Results and Discussion

Fig.3 shows a typical data set of an ARDS patient from the data source A as well as the sigmoidal and the error function model equations, Eqs.(1a)(2a), determined by the method of least squares. The parameters of the model equations, (Λ, p_0, ΔV, V_U), are (1.470, 13.308, 3.491, 2.750) for the sigmoidal equation and (1.627, 13.324, 3.156, 2.584) for the error function equation. Both equations represent the data points well over the entire data range. Substantial differences between the two equations occur in high and low pressure regions away from the data range as they approach different asymptotes of $V = V_U$ and V_L. It should also be noted that there is no lower corner pressure for the data set since Λ is less than 2 (Eq.(4)), and that the pressure at maximum compliance increase, p_{mci}, is very low at 1.385 cmH_2O for the sigmoidal model equation and at 0.254 cmH_2O for the error function equation (Eq.(5)).

An example of the analysis of the data source B is shown in Fig.4. The dotted curve represents the piecewise continuous equation, Eq.(6), with

$(V_{min}, V_{max}, V_{LIP}, V_{UIP}, V_{insuff}, C_{lin}, p_{LIP}, p_{UIP})$

$= (-2230$ [mL], 5870, 1513, 2884, 4125, 157 [mL/cmH_2O], 14.4 [cmH_2O], 23.1),

reported in [9]. The solid curve is the corresponding error function model equation, Eq.(2a),

obtained by applying the method of least squares to computational data points generated over the data range of $0 \leq V \leq V_{insuff}$. Since "true" data points are unknown in the linear region of Eq.(6), we imposed a constraint that the inflection point, p_0, of the error function equation is located in the midregion of Eq.(6). The parameters of the error function equation thus determined are (Λ, p_0, ΔV, V_U) =(2.0800,18.224,5.58750, 4.9114). Due to the error minimization Eq.(2a) is nearly identical to Eq.(6) over the data range indicated by the two triangle marks; which is valid for other 28 data sets from Data Source B. A continuous change of the compliance (i.e. non-linear p-V change) in the region near p_0 has been described previously in terms of the sigmoidal (tangent hyperbolic) model equation [15]. It should also be mentioned here that, of twenty nine inflation data sets, p_0 (the inflection point) is between p_{LIP} and p_{UIP} in eighteen data sets, equal to p_{UIP} in eight data sets, equal to p_{LIP} in one data set, and $p_0 = p_{UIP} = p_{LIP}$ in two data sets.

Fig.5. is a plot of the error function equation, Eq.(2a), with $\sqrt{\pi}\,\Lambda(p/p_0 - 1)/4$ and $(V - V_L)/\Delta V$ as x- and y- axis respectively. All (both inflation and deflation) data points of Data Source A are also shown in the figure, confirming very good agreements with the equation. The coefficient of determination, R^2, is 0.999247, which is comparable in magnitude to that of the sigmoidal equation, $R^2 = 0.9992$ reported in [11], thus indicating that both the sigmoidal (tangent hyperbolic) p-V equation, Eq.(1a), and the error function equation, Eq.(2a), are very effective in representing quasi-static p-V curves. Shown in Fig.6 are comparisons between the sigmoidal equation and the error function equation in terms of two parameters in the equations, Λ (Fig.6(a)) and p_0 (Fig.6(b)) for twenty one data sets from Data Source A. Due to differences in functional form the magnitude of Λ is slightly higher for the error function equation than for the sigmoidal equation. On the other hand, the inflection point, p_0, being the point of antisymmetry, should be identical in theory for both model equations. Fig.6(b) confirms it as the magnitudes of p_0 determined by the method of least squares are very close between the two equations. Differences in the magnitudes of Λ and p_0 between the two continuous-function model equations would

result in function-specific values for such quantities as $p_{cu\,(cl)}$, $p_{mcd\,(mci)}$ of Eqs.(4,5) which characterize p-V curves, indicating the importance of using the same p-V model equation in order to analyze clinical data in a consistent manner.

Although quantitative comparisons of parameters cannot be made among different p-V model equations in a mathematically rigorous manner, a comparison between the linear-exponential model equation, Eq.(6), and the error function equation, Eq.(2a), is presented in Fig.7 in a form of p_{mci} vs p_{LIP} in Fig.7 (a) and p_{mcd} vs p_{UIP} in Fig.7 (b) for Data Source B. It may be seen that the parameters from both equations distinguish two data groups, Before recruitment maneuver and After recruitment maneuver, successfully and also that p_{mcd} of Eq.(2a) and p_{UIP} of Eq.(6) distinguish the two groups more clearly than p_{mci} and p_{LIP}. Values of $p_{LIP\,(UIP)}$ must be located directly from p-V curves; while, $p_{mci\,(mcd)}$ are automatically generated from the model equation once parameters of the model equation are determined.

As shown in Eqs.(2a,b), when p and V are made non-dimensional the resulting non-dimensional p-V equation, Eq.(2b), contains Λ (=the ratio of $(p_{cu} - p_{cl})$ to p_0) as the only parameter representing a shape of $\overline{p} - \overline{V}$ curves with $\Lambda/2$ being the gradient, $d\overline{V}/d\overline{p}$, at the origin (where $\overline{p} = 0$ i.e. $p = p_0$.). The $p\,dV$ work associated with the process from the initial to the end-of-inflation pressure was suggested as a quantity representing the pressure range actually covered by a specified p-V curve [15]. However, in analyzing data sets from different sources we found that the end-of-inflation pressure (volume) is data-(or investigator-) dependent, and may not be appropriate as a comprehensive indicator for data interpretation. Here we selected two volume differences to distinguish p-V data sets accounting for the range of data relative to the entire range covered by the p-V equation; one is $V_U - V(p = 0)$ as a volume scale indicating the total available volume of a specified TRS, and the other is $V(p = 20\,cmH_2O) - V(p = 0)$ as a volume scale representing volume range covered by the specified TRS. The volume at $p = 20\,cmH_2O$ is selected arbitrarily; however, in all the data sets we analyzed, p-V curves were obtained beyond $p = 20\,cmH_2O$.

Fig.8 shows Λ vs p_0 in (a) and $[V_U - V(p=0)]$ vs $[V(p=20\,cmH_2O) - V(p=0)]$ in (b) obtained from the error function model equation for all inflation data sets. In terms of Λ, a wide range ($1 \leq \Lambda \leq 6$) is covered by ARDS patients; while, the range of Λ for healthy adults is $\sim 1.5 - 3.5$. The alveolar recruitment maneuver lowers the magnitude of Λ of the group of healthy adults as a whole. A similar observation may be made on p_0. Both $[V_U - V(p=0)]$ and $[V(p=20\,cmH_2O) - V(p=0)]$ in Fig.8(b) are low in magnitude for patients with ARDS. On the other hand, the recruitment maneuver shifts the location of the whole group to the right in Fig.8(b). Two data sets, No.20 and 5, representing extreme points in Fig.8 (a) and (b) respectively, clearly show they are quite different from those of healthy adults, if Fig.8(a) and (b) are examined together.

According to Data Source B [9], after a p-V curve before the recruitment maneuver is recorded, the lungs are inflated to an airway pressure of $40\,cmH_2O$ and maintained for 15 s, followed by six pressure-controlled breaths (six breaths/min.) delivered at an airway pressure of $30\,cmH_2O$. Then a second large insufflation is delivered before recording a p-V curve after recruitment maneuver. To examine the p-V curves of healthy adults as well as effects of the alveolar recruitment maneuver in more detail, a ratio of the pressure at the inflection point, (p_0 (**before** *maneuver*)/p_0 (**after** *maneuver*)), is plotted against a ratio of Λ (Λ (**before** *maneuver*)/Λ (**after** *maneuver*)) in Fig.9. Each data point is accompanied by two numbers indicating the data set number and his or her age in the bracket (unfilled circle for male and filled circle for female). The data sets of the younger may be seen to be located to the left half of the figure, compared to the older, implying that, for the healthy young adults, Λ after the maneuver either increases slightly or remains roughly the same as Λ before the maneuver. In order to discuss implications of Fig.9 further, Figs.10 and 11 show the error function p-V equations before- and after-maneuver along with the corresponding non-dimensional $\overline{p} - \overline{V}$ equations for three data sets in Fig.10 from the region of $\Lambda\,(before\ maneuver)/\Lambda\,(after\ maneuver) < \sim 1.2$, and for three data sets in Fig.11 from the region of $\Lambda\,(before\ maneuver)/\Lambda\,(after\ maneuver) > \sim 1.2$. The

equations are plotted over the measurement range covered by Data Source B. Numerical values of these data sets are tabulated below.

Data No. (Age)	1 (33)	6 (25)	7 (60)	11 (55)	13 (50)	15 (58)
$\Lambda\,(before)/\Lambda\,(after)$	0.730	0.982	1.143	1.390	1.303	1.625
$p_0\,(before)/p_0\,(after)$	1.726	1.196	1.840	1.312	2.083	1.753

Referring to Fig.10, the high p_0 ratios of Data 1 and 7, compared to Data 6, are results of substantial reduction in p_0 after the maneuver for these data sets as observed in the p-V equations. The triangular marks on the $\overline{p}-\overline{V}$ curves in Figs.10 and 11 indicate locations of $p = 20cmH_2O$; hence, on $\overline{p}-\overline{V}$ diagrams, a large change in p_0 is reflected by a large shift of the triangle from the before-recruitment location to the after-recruitment location. Different degrees of changes in the magnitude of Λ over the alveolar recruitment maneuver for the three data sets cannot directly be observed from the p-V diagrams. However, on the $\overline{p}-\overline{V}$ diagrams, $\Lambda/2$ is the slope of $\overline{p}-\overline{V}$ equation at the origin.(See Eq.(2b).) Therefore, the before-recruitment (solid) curve lies above the after-recruitment (dotted) curve in the third quadrant ($\overline{p} < 0$, $\overline{V} < 0$) for Data 1 for which $\Lambda\,(before) = 0.730 \cdot \Lambda\,(after)$. For Data 6 with $\Lambda\,(before)$ being close to $\Lambda\,(after)$ two curves are nearly identical. In Data 7 the after-recruitment curve lies slightly above the before-recruitment curve as $\Lambda\,(before) = 1.143 \cdot \Lambda\,(after)$. The data sets in Fig.11 all have the two ratios well above unity with the high Λ ratios resulting in the after-recruitment curves to lie above the before-recruitment curves, and the high p_0 ratios of Data 13 and 15 being reflected in the large shifts in triangles between the two curves in the $\overline{p}-\overline{V}$ diagram.

From Eq.(2a) the maximum local compliance ($= dV/dp\ at\ p = p_0$) may be expressed as

$$\frac{dV}{dp}\,(p = p_0) = \frac{\Lambda \cdot \Delta V}{4\,p_0}. \tag{7}$$

Fig.12 is a plot of $[dV/dp\,(p = p_0)$ after recruitment maneuver] vs $[dV/dp\,(p = p_0)$ before

recruitment maneuver] of Data Source B. Changes in the maximum local compliance (= compliance at the inflection point) are small between before- and after-recruitment data with a maximum change of less than 0.035 $[L/cmH_2O]$. It should be mentioned again that the local compliance like other parameters may be obtained mathematically in a continuous p-V model equation, once the parameters of the equation are determined for a specified p-V curve.

Depicted in Fig.13 are p-V curves and the corresponding $\overline{p} - \overline{V}$ curves of four representative data sets of patients with ARDS, drawn over their measurement ranges. The non-dimensional $\overline{p} - \overline{V}$ curves in Fig.13(b), which, we believe, are more useful for data examinations and interpretations, yield the following observations:

(1.) The magnitude of Λ, which is represented by the slope of a $\overline{p} - \overline{V}$ curve, is the largest for Data 20, and the smallest for Data 4.

(2.) Since the origin of a $\overline{p} - \overline{V}$ curve is the location where the local compliance is the maximum (i.e. $p = p_0$), Data 4 and 17 extend well into the region of decreasing compliance, while, the pressure range of Data 13 is limited to the region of increasing compliance.

(3.) At $p = 20\, cmH_2O$ (shown as a triangle), the compliance is still increasing for Data 13 and 20, close to the maximum for Data 17 and decreasing for Data 4.

(4.) The two volume asymptotes, V_U and V_L, are transformed respectively into $\overline{V} = 1.0$ and -1.0; hence, the volume range of Data 13 is closer to the lower asymptote, while, the overall volume change of Data 4 is small compared to ΔV (difference between the asymptotes).

Furthermore the magnitude of Λ in Table 1 indicates that there is no lower corner pressure for Data 4. For each inflation data set, Table 1 lists the maximum local compliance. Its value ranges between 0.03 and 0.11 $[L/cmH_2O]$; much smaller values compared to the data from healthy adults shown in Fig.12. The maximum local compliance, as shown in Eq.(7), is proportional to the product of Λ and ΔV, and inversely proportional to pressure at the inflection point. Since both Λ and p_0 are roughly in the same order of

magnitude as healthy adults (Fig.8), the factor contributing most to smaller values of the maximum local compliance for patients with ARDS is ΔV as evidenced by its values listed in Table 1 and 2.

Summary and Conclusions

The sigmoidal (tangent hyperbolic) equation is known to represent various quasi-static p-V curves very closely [11]. In the present study it has been shown that the error function model equation also represents quasi-static p-V curves well (Figs.4,5). Major parameters of both the sigmoidal (tangent hyperbolic) and the error function model equations are the non-dimensional compliance, Λ, the maximum local compliance, p_0, the upper (or lower) volume asymptote, V_U (V_L), and the maximum volume available for inflation, ΔV. Although both continuous model equations are antisymmetric with respect to p_0, the non-dimensional parameter, Λ, as well as two volume asymptotes slightly differ between the two equations as those function-specific parameters are selected to follow a specified p-V curve as closely as possible (Fig.6). Two inflation data sources, patients with ARDS (Data Source A) and healthy adults (Data Source B), are analyzed in detail using the error function p-V model equation with the following results;

1. The alveolar recruitment maneuver lowers the pressure at the maximum compliance, p_0; while, Λ remains roughly the same or decreases in magnitude (Figs.8(a), 9). It also reduces the upper volume asymptote, V_U, substantially (Fig.8(b)). The combined effects of these parametric changes due to the maneuver extend the range of p-V curves after the maneuver further into the region beyond the location of the maximum compliance (Figs.10, 11).

2. The range of p_0 and Λ covered by the patients with ARDS is wider than the corresponding ranges of healthy adults (Fig.8(a)). Substantially lower magnitudes of the upper volume asymptote, V_U, and the actual volume change (Fig.8(b)) result in lower values for the maximum local compliance (Table 1) compared to that of healthy adults (Fig.12).

3. The non-dimensional $\overline{p} - \overline{V}$ curves combined with the magnitudes of the four parame-

ters of the model equation are shown to help understand quantitatively the effects of the recruitment maneuver as well as differences among patients with ARDS (Figs.11, 13).

4. An important advantage of the continuous model equations is that various parameters characterizing the shape and the range of p-V curves, such as the maximum local compliance, the pressure at the maximum local compliance and the upper and the lower corner pressures, may be evaluated readily from the model equation once the parameters of the equation are determined from p-V curve data. The mathematically exact relations among the parameters also implies that the magnitude of either pressure or volume at a certain location along a p-V curve may only be interpreted correctly when compared to a characteristic pressure or volume of the p-V curve, as demonstrated, for example, in Figs.11 and 13 when we discussed the location of $p = 20\, cmH_2O$ relative to the pressure at the maximum local compliance.

Captions for Tables and Figures

Table 1. Parameters of Error Function Equation for Data Source A

Table 2. Parameters of Error Function Equation for Data Source B

Fig. 1. Continuous p-V model equation.

Fig. 2. Non-dimensional $\overline{p}$-$\overline{V}$ curve corresponding to Fig.1.

Fig. 3. Example of p-V curve from Data Source A. filled circle = Data D,
solid = error function p-V equation, dotted = sigmoidal p-V equation.

Fig. 4. Example of p-V curve from Data Source B. Dotted curve = piecewise continuous equation, Eq.(6), Solid curve = error function equation, Eq.(2a),
Triangle = upper and lower data limits.

Fig. 5. $(V - V_L)/\Delta V \quad vs \quad (\sqrt{\pi}/4)\,\Lambda(p/p_0 - 1)$ of Data Source A.
Unfilled circle = inflation, Filled circle = deflation.

Fig. 6. (a) Λ_s (sigmoidal model equation) vs Λ_e (error function model equation),
(b) $p_{0\,s}$ (sigmoidal equation) vs $p_{0\,e}$(error function equation).
for inflation data sets of Data Source A.

Fig. 7. (a.) $p_{LIP}\,[cmH_2O]$ vs $p_{mci}\,[cmH_2O]$
(filled (unfilled) circle = before (after) recruitment maneuver).
(b.) $p_{UIP}\,[cmH_2O]$ vs $p_{mcd}\,[cmH_2O]$ of Data Source B.
(unfilled (filled) circle = before (after) recruitment maneuver).
(p_{mci} and p_{mcd} evaluated from error-function equation.)

Fig. 8. (a.) Λ vs p_0, (b.)$[V_U - V(p = 0)]$ vs $[V(p = 20\,cmH_2O) - V(p = 0)]$
for inflation data sets from Data Source A and B.
Square = patients with ARDS, Cross = healthy adults before recruitment maneuver,
Triangle = healthy adults after recruitment maneuver.

Fig. 9. p_0 (**before** *maneuver*)/p_0 (**after** *maneuver*)) vs Λ (**before**)/Λ (**after**)
Two numbers are Data Set No., followed by his or her age in the bracket.

unfilled circle = male, filled circle = female.

Fig.10. $p - V$ curve and the corresponding $\overline{p}$-$\overline{V}$ curve of error function model equation.

Data No.1 (top), No.6 and No.7 (bottom) of Data Source B (healthy adults).

Solid = Before recruitment maneuver, Dotted = After recruitment maneuver.

Triangle = location of $p = 20\,[cmH_2O]$.

Fig.11. $p - V$ curve and the corresponding $\overline{p}$-$\overline{V}$ curve of error function model equation.

Data No.11 (top), 13 and 15 (bottom) of Data Source B.

Solid = Before recruitment maneuver, Dotted = After recruitment maneuver.

Triangle = location of $p = 20\,[cmH_2O]$.

Fig.12. $dV/dp\,(p = p_0)$ (maximum local compliance) before recruitment maneuver vs $dV/dp\,(p = p_0)$ after recruitment maneuver of Data Source B.

Fig.13. (a) $p - V$ curve and (b) the corresponding $\overline{p}$-$\overline{V}$ curve of error function model equation for Data No.4, 13, 17 and 20 of Data Source A (patients with ARDS).

Triangle = location of $p = 20\,[cmH_2O]$.

Table 1. Inflation Parameters of Error Function Equation for Data Source A

Data No	Λ	p_0	ΔV	V_L	(dV/dp) at p_0
1.	2.9652,	22.39,	2.3726,	-0.0709	0.0785
2.	2.7173,	21.98,	1.5612,	-0.0762	0.0482
3.	3.3532,	25.08,	1.6193,	-0.0365	0.0541
4.	1.6273,	13.32,	3.1567,	-0.5727	0.0963
5.	2.7160,	30.36,	1.6216,	-0.0768	0.0362
6.	2.6029,	23.88,	1.5066,	-0.0962	0.0410
7.	1.7288,	20.15,	3.0989,	-0.3645	0.0664
8.	1.8901,	14.95,	1.7905,	-0.2185	0.0565
9.	3.5379,	25.24,	2.7570,	-0.0350	0.0965
10.	2.7981,	26.20,	3.7326,	-0.1583	0.0996
11.	2.4296,	17.89,	1.3424,	-0.0997	0.0455
12.	1.2500,	11.59,	1.2470,	-0.2829	0.0336
13.	3.2725,	29.86,	3.9075,	-0.0861	0.1070
14.	2.7915,	15.31,	1.6284,	-0.0705	0.0742
15.	1.9487,	18.37,	1.8797,	-0.2423	0.0498
16.	2.4566,	26.98,	1.3277,	-0.0787	0.0302
17.	2.1027,	19.31,	1.3316,	-0.1279	0.0362
18.	1.1672,	13.98,	2.0685,	-0.5149	0.0431
19.	3.1381,	26.80,	3.1306,	-0.0851	0.0916
20.	5.4709,	30.03,	1.7695,	-0.0097	0.0805
21.	3.2818,	24.43,	2.8956,	-0.2075	0.0972

p_0 in $[cmH_2O]$, ΔV and V_L in [L], dV/dp in $[L/cmH_2O]$.

Table 2. Parameters of Error Function Equation for Data Source B

Data No	Λ	p_0	ΔV	V_L	V_U
1.F					
B.	1.5136	25.00	5.1043	-0.8889	4.2154
A.	2.0711,	14.48	2.7130	-0.2700	2.4430
2.F					
B.	2.5520	31.70	5.4303	-0.2863	5.7166
A.	1.7587	18.17	4.1416	-0.6590	3.4826
3.F					
B.	2.0979	21.76	3.7676	-0.3399	3.4277
A.	2.2960	18.19	3.1331	-0.2300	2.9031
4.M					
B.	2.1491	21.11	4.5443	-0.3726	4.1717
A.	2.1887	18.57	4.4023	-0.3554	4.0469
5.F					
B.	2.2192	24.60	6.4953	-0.4971	5.9982
A.	1.5729	13.46	5.2884	-0.8895	4.3989
6.M					
B.	2.3950	23.21	4.2092	-0.2567	3.9525
A.	2.4387	19.40	3.9049	-0.2722	3.6327
7.M					
B.	2.6997	31.00	7.3180	-0.2167	7.1013
A.	2.3615	16.85	5.5288	-0.5641	4.9647
8.F					
a	2.2901	30.80	8.2489	-0.5185	7.7304
A.	1.9974	17.20	5.0638	-0.5478	4.5160
9.F					
B.	– – –	– – –	– – –	– – –	– – –.
A.	2.0340	15.90	3.7392	-0.4068	3.3324
10.M					
B.	3.4081	28.80	7.211	-0.0491	7.1627
A.	2.3998	17.92	5.7276	-0.5502	5.1774
11.M					
B.	3.1746	25.86	7.0726	-0.1361	6.9365
A.	2.2828	19.70	6.79820	-0.8620	5.9362
12.F					
B.	2.5060	23.20	5.0810	-0.2476	4.8334
A.	2.3844	16.36	4.3799	-0.3799	4.0000
13.F					
B.	2.3600	29.17	6.81755	-0.4353	6.3822
A.	1.8107	14.00	4.03567	-0.6883	3.3472
14.M					
B.	2.2260	24.55	6.7170	-0.4828	6.2342
A.	2.0800	18.22	5.5875	-0.6761	4.9114
15.F					
B.	3.5047	25.70	4.5022	-0.0027	4.4995
A.	2.1561	14.65	3.3016	-0.4836	2.8180

B = Before recruitment maneuver, A = After recruitment maneuver.
p_0 in $[cmH_2O]$, ΔV, V_L and V_U in [L].

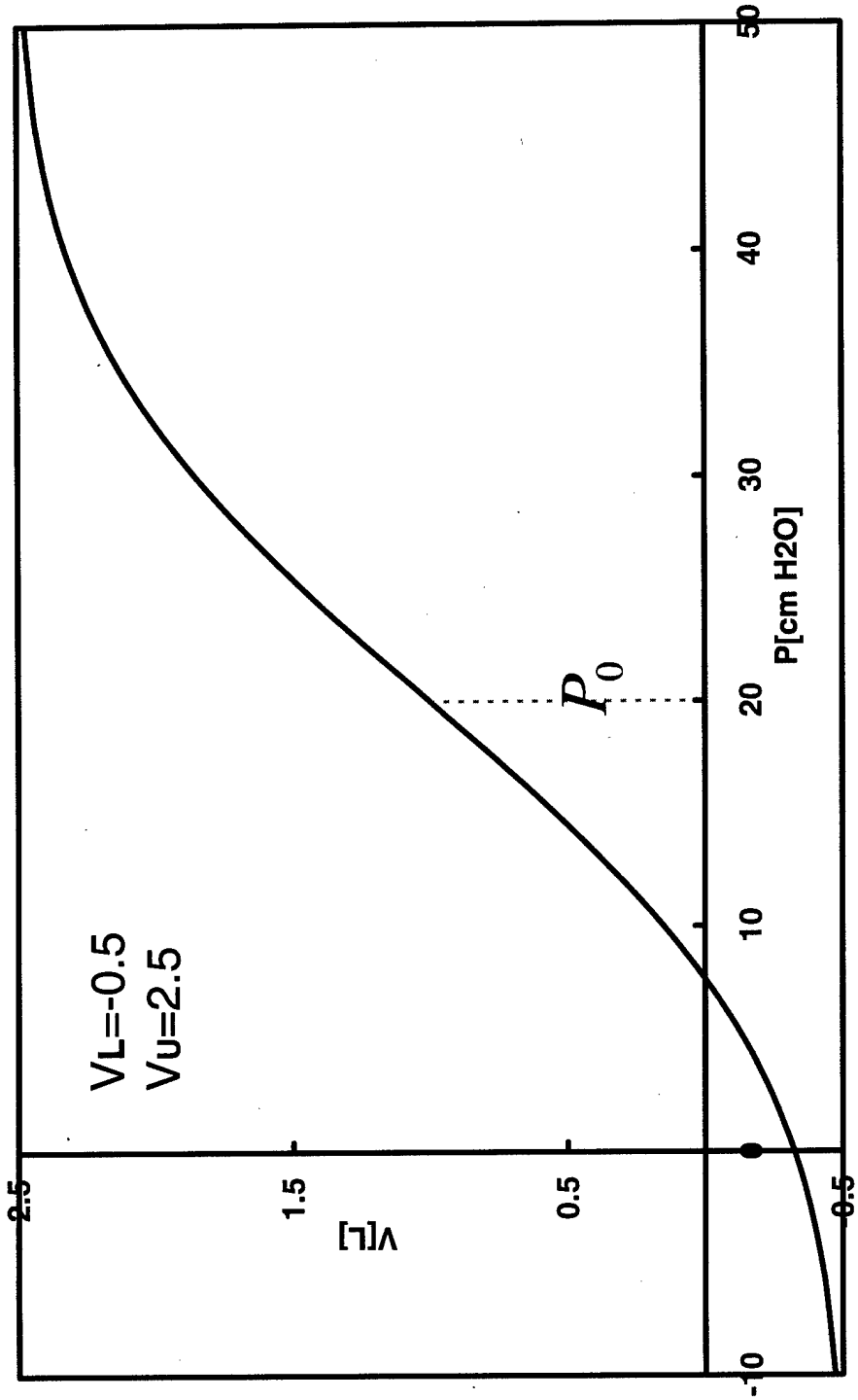

Fig.1. Continuous p-V model equation.

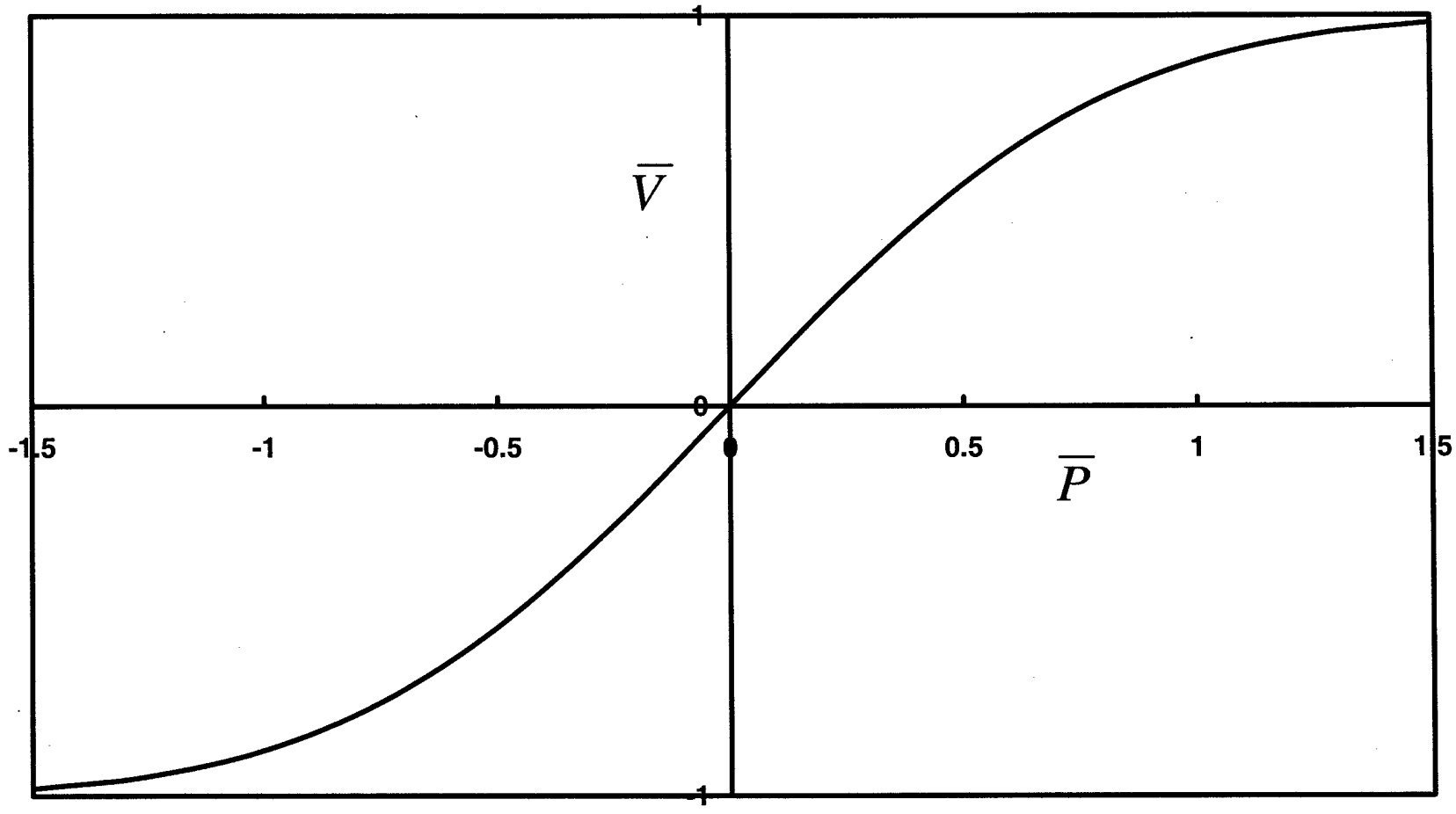

Fig.2. Non-dimensional $\overline{p}-\overline{V}$ curve corresponding to Fig.1.

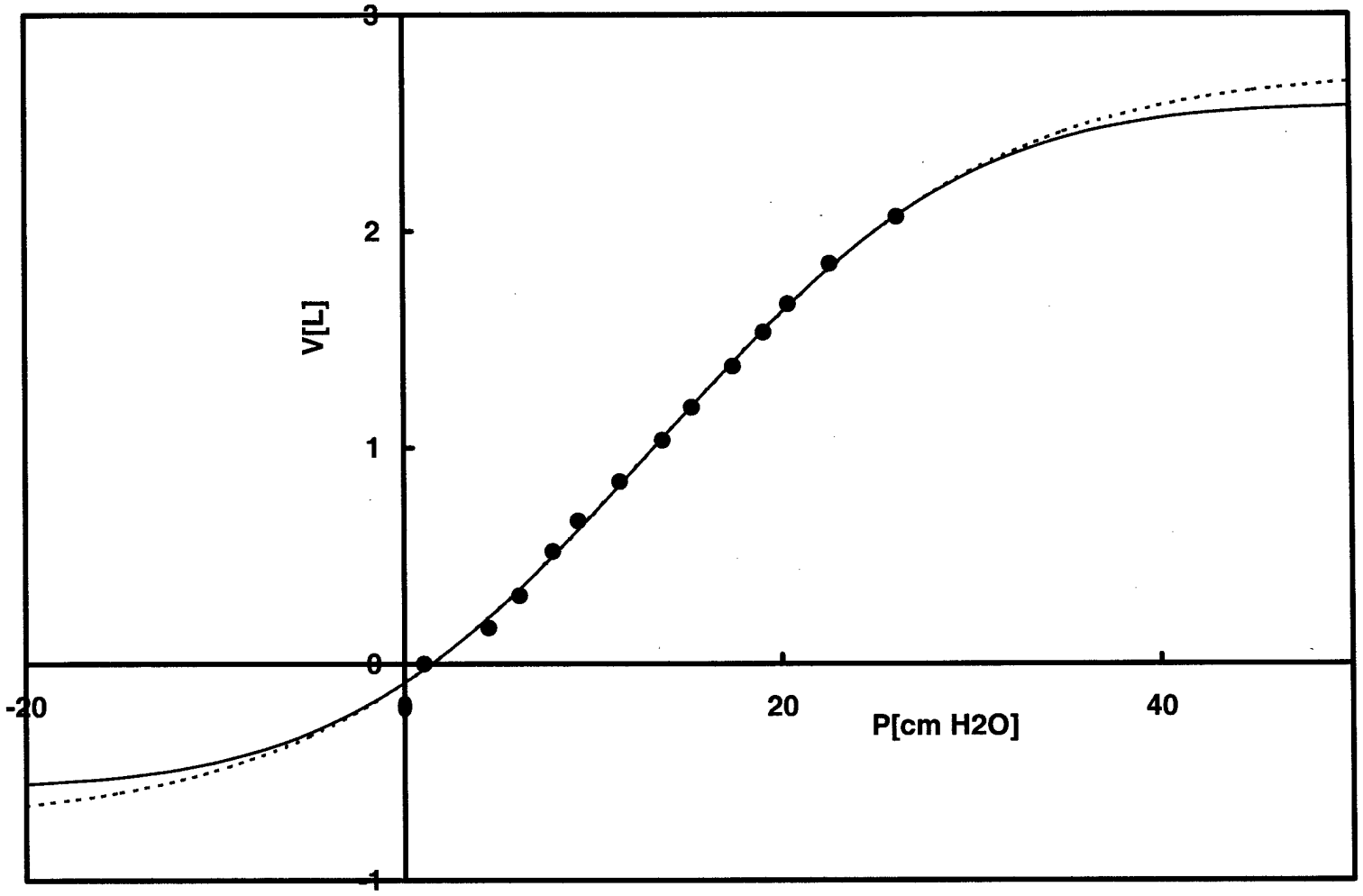

Fig.3. Example of P-V curve from Data source A.
filled circle = Data D, solid = error function p-V equation, dotted = sigmoidal p-V equation

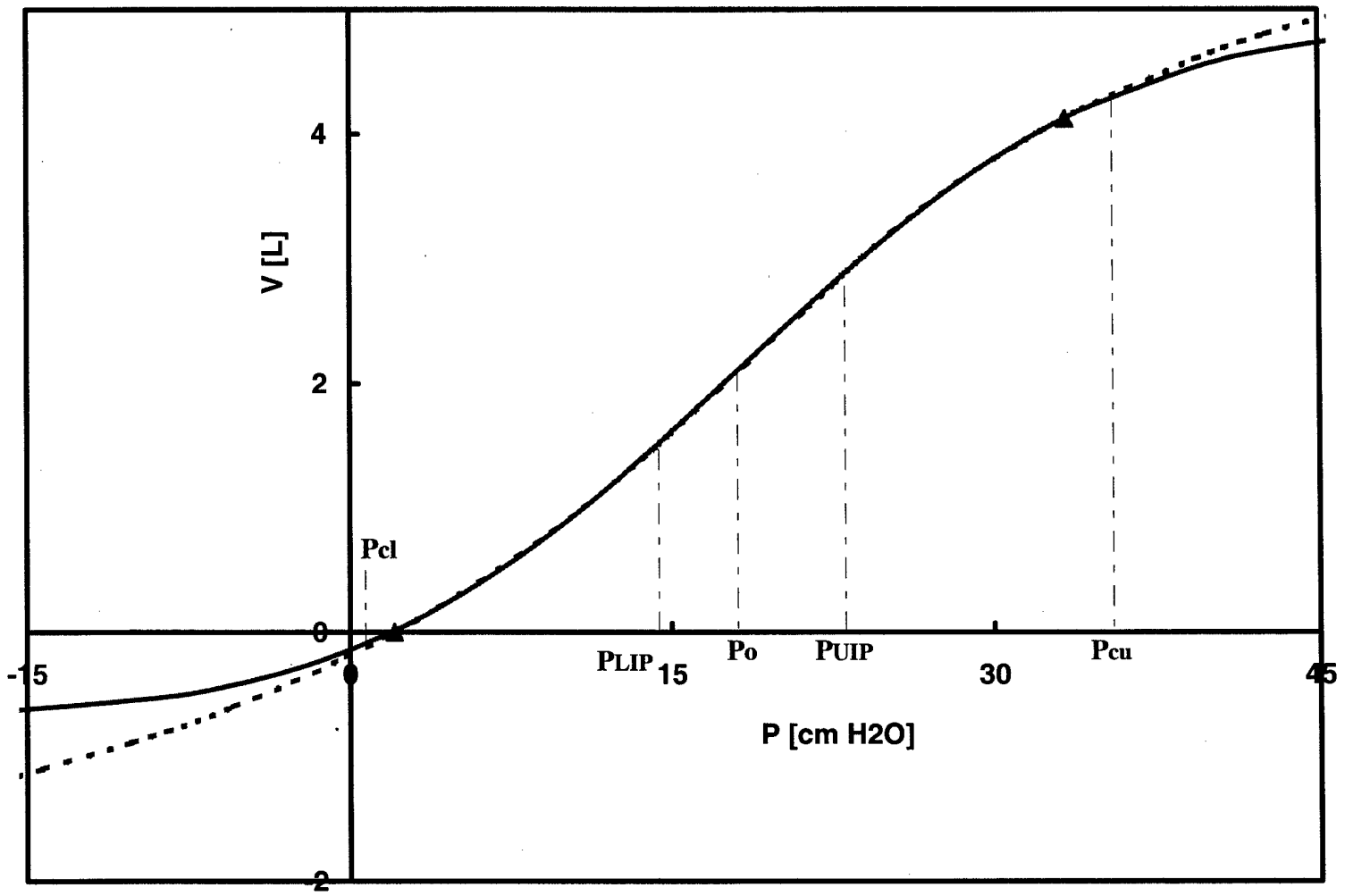

Fig.4. Example of p-V curve from Data Source B.
Dotted curve = piecewise continuous equation, Eq(6), Solid curve = error function equation, Eq(2a), Triangle = upper and lower data limits.

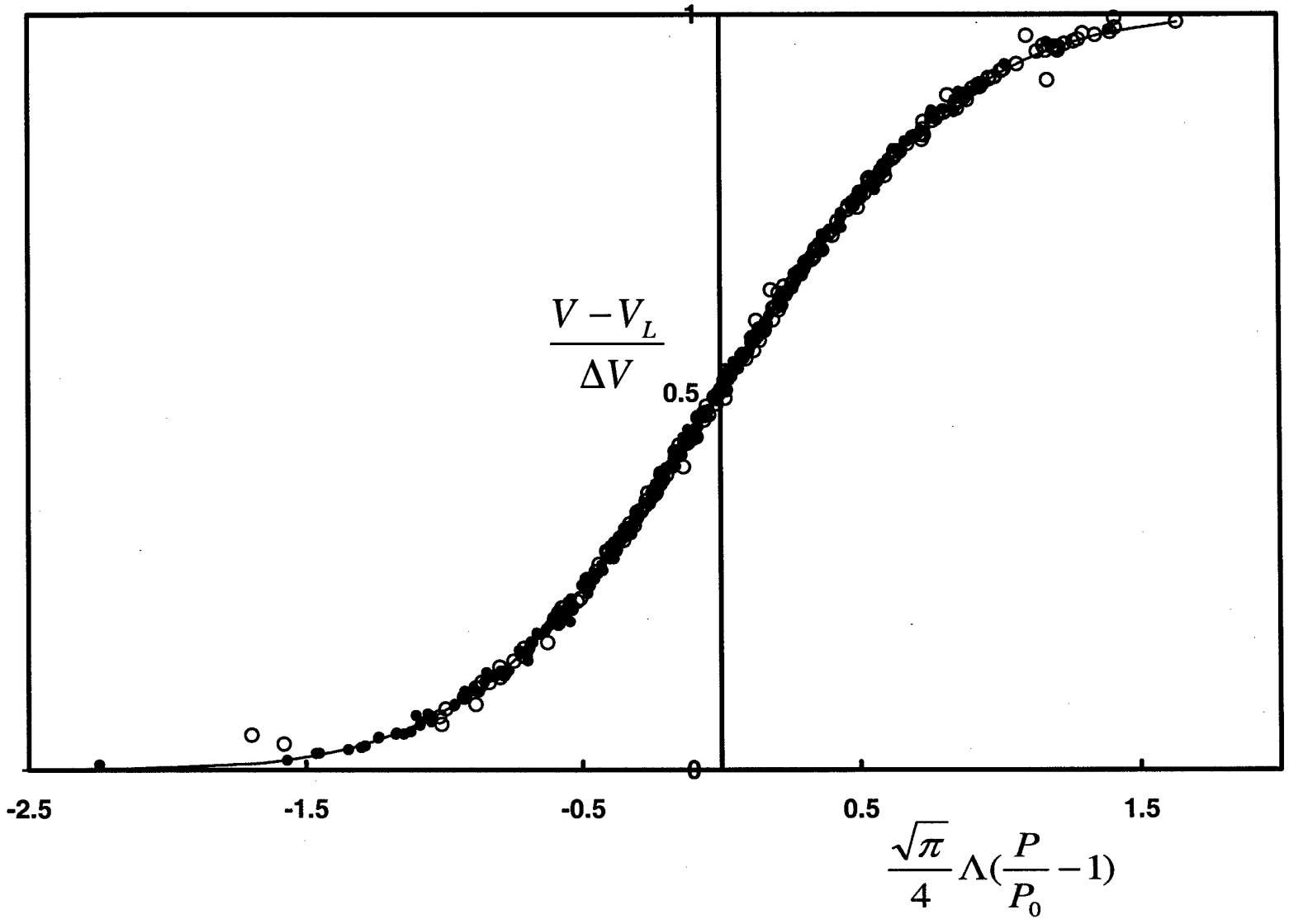

Fig.5. $(V - V_L)/\Delta V$ vs $(\sqrt{\pi}/4)\Lambda(p/p_0 - 1)$ of Data Source A.
Unfilled circle = inflation, Filled circle = deflation.

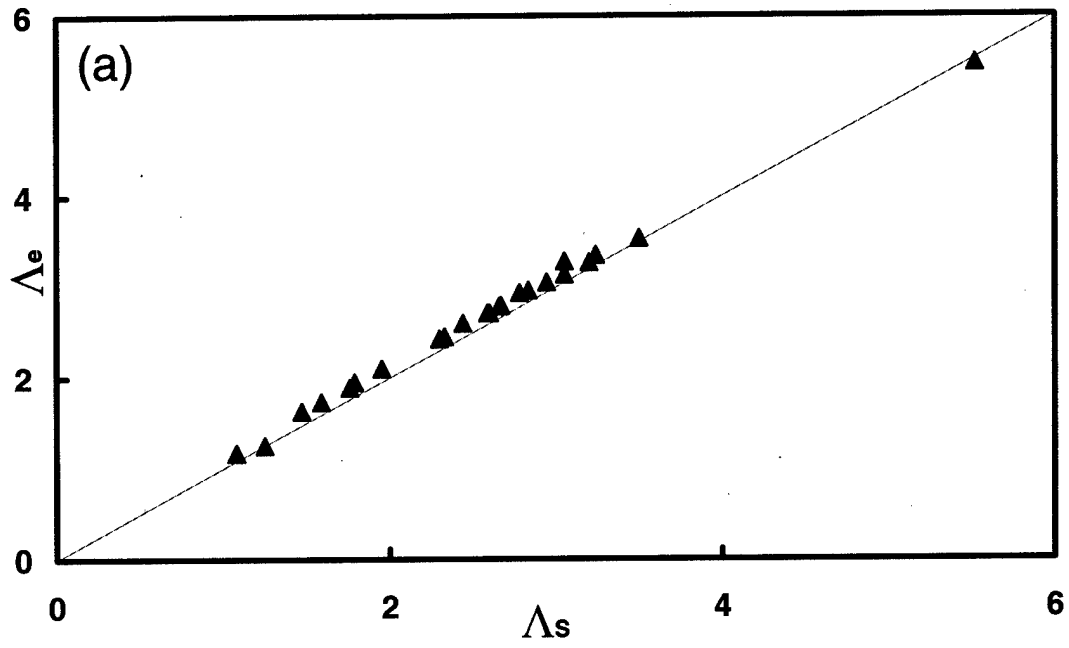

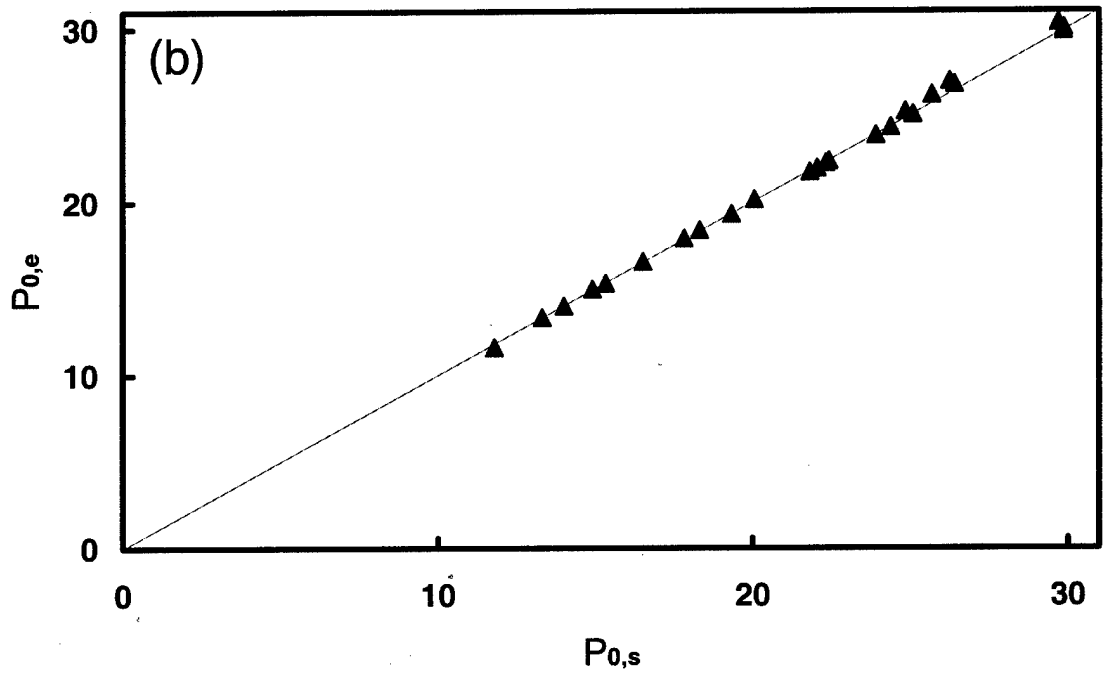

Fig.6. (a) Λ_S (sigmoidal model equation) vs Λ_e (error function) model equation.(b) $p_{0,S}$ (sigmoidal equation) vs $p_{0,e}$ (error function equation) for inflation data sets of Data Source A.

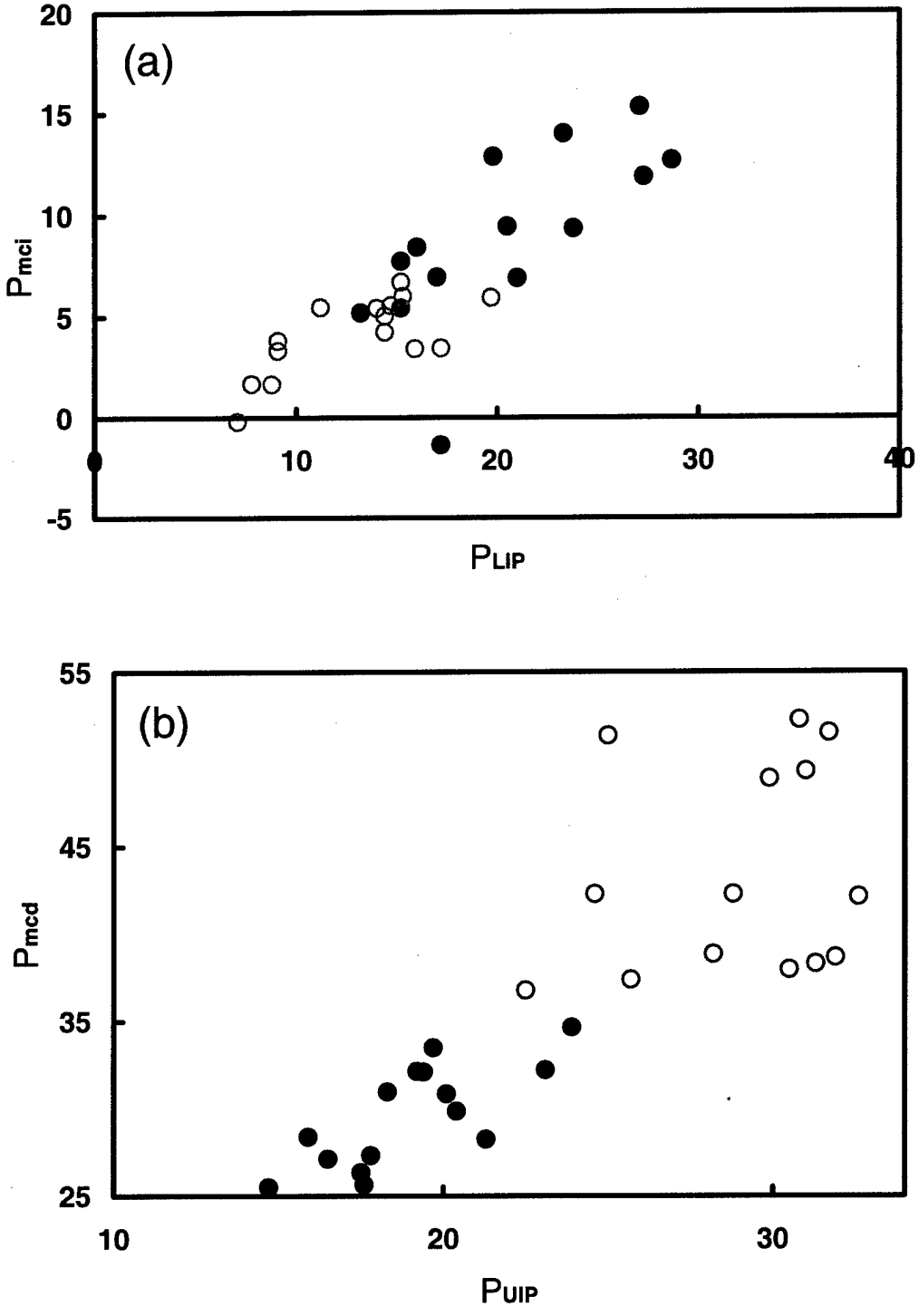

Fig.7. (a) p_{LIP} [cmH2O] vs p_{mci} [cmH2O](filled (unfilled) circle= before (after) recruitment maneuver). (b) p_{UIP} [cmH2O] vs p_{mcd} [cmH2O] of Data Source B.(unfilled (filled) circle = before (after) recruitment maneuver. p_{mci} and p_{mcd} evaluated from errorfunction equation.)

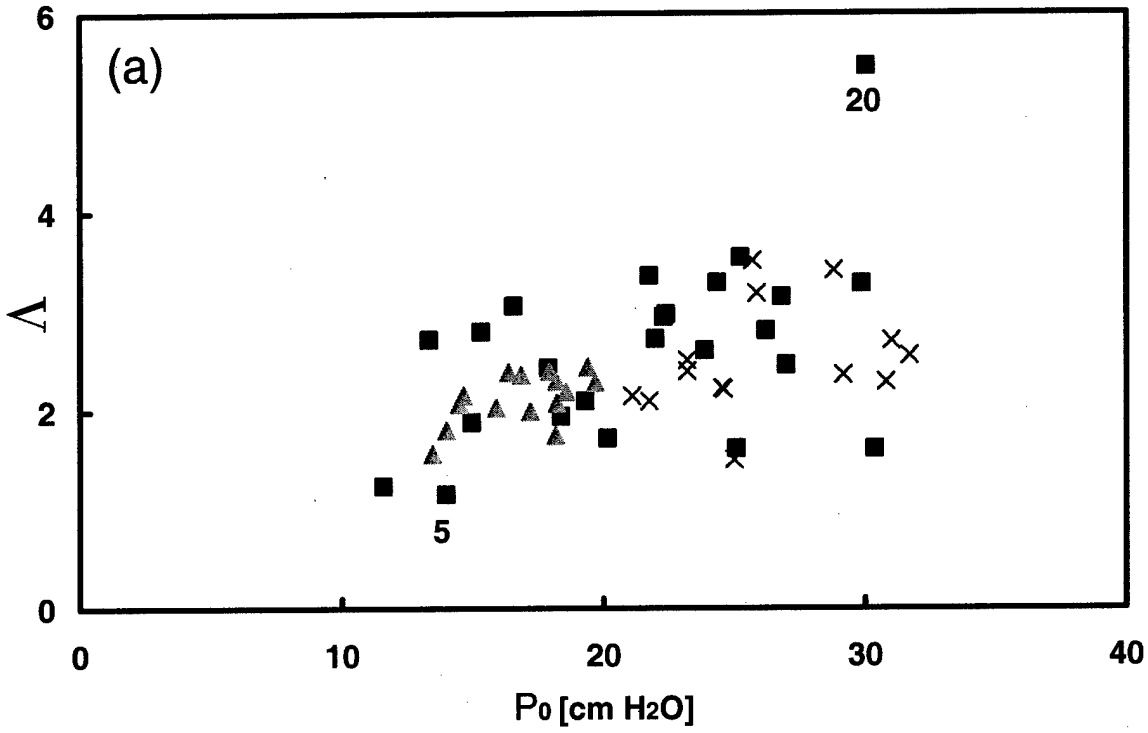

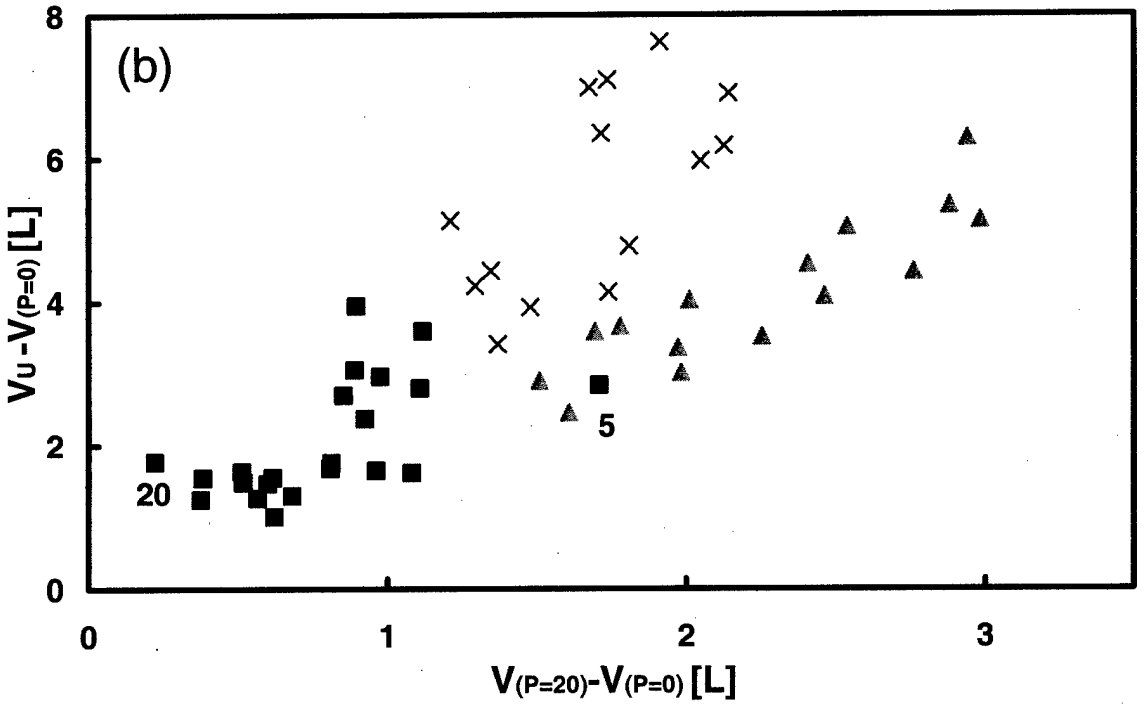

Fig.8. (a.) Λ vs p_0 , (b.) $[V_U - V(p=0)]$ vs $[V(p=20cmH_2O) - V(p=0)]$ for inflation data sets from Data Source A and B.
Square = patients with ARDS, Cross = healthy adults before recruitment maneuver, Triangle = healthy adults after recruitment maneuver.

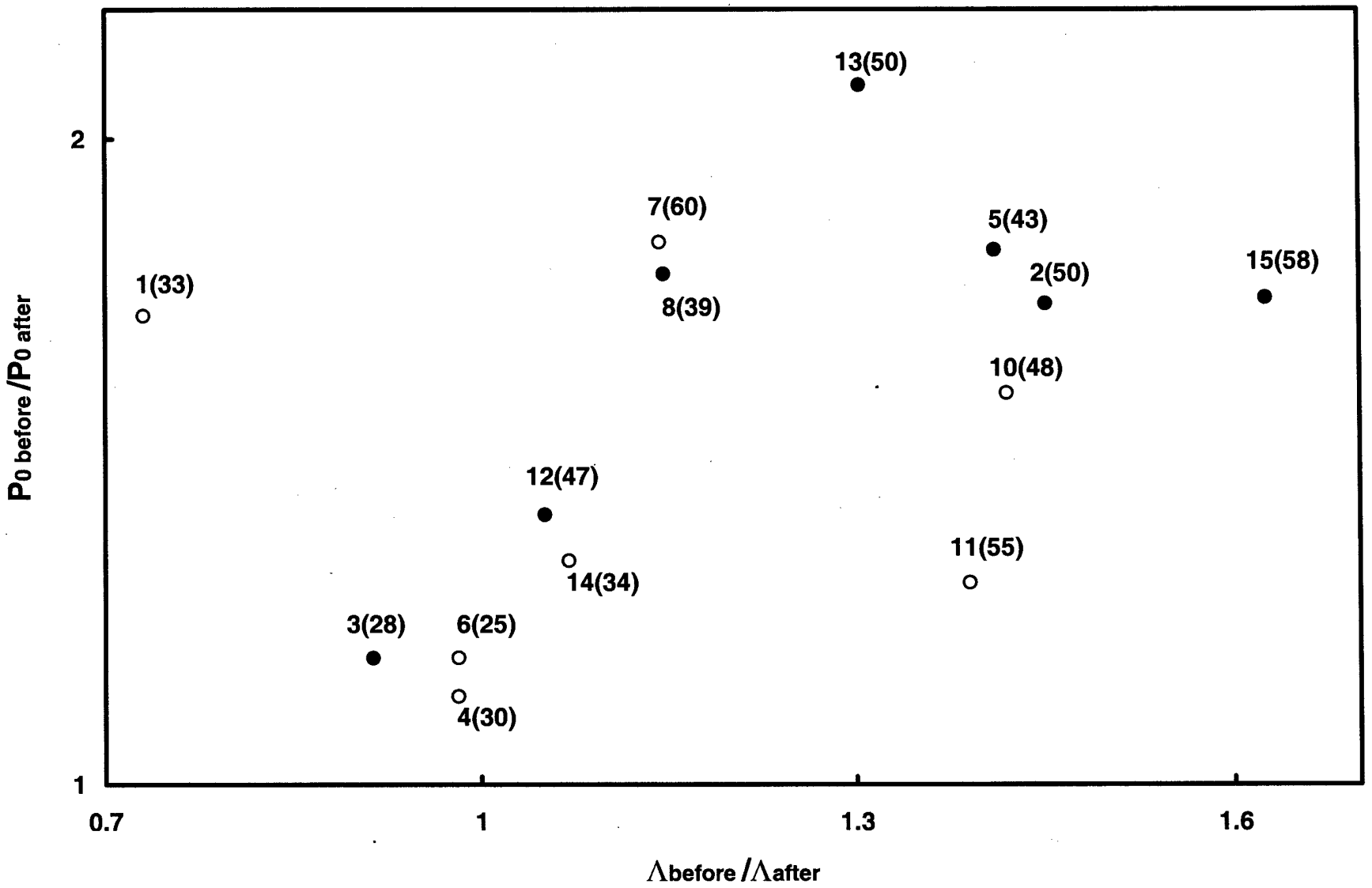

Fig. 9. p_0 (**before** *maneuver*/ p_0 **after** *maneuver* vs Λ (**before**)/ Λ (**after**).
Two numbers are Data Set No., followed by his or her age in the bracket.
unfilled circle = male, filled circle = female.

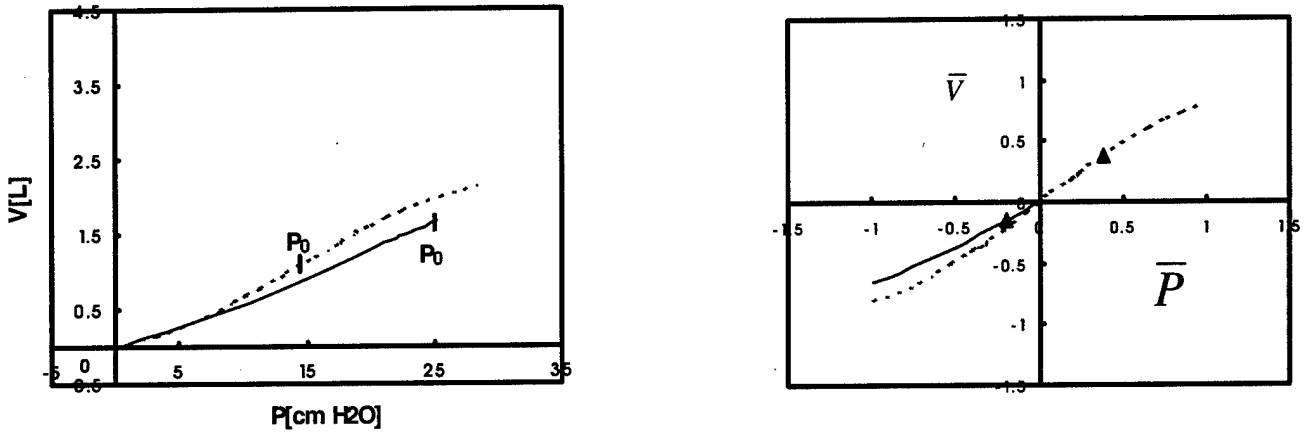

Data No. 1

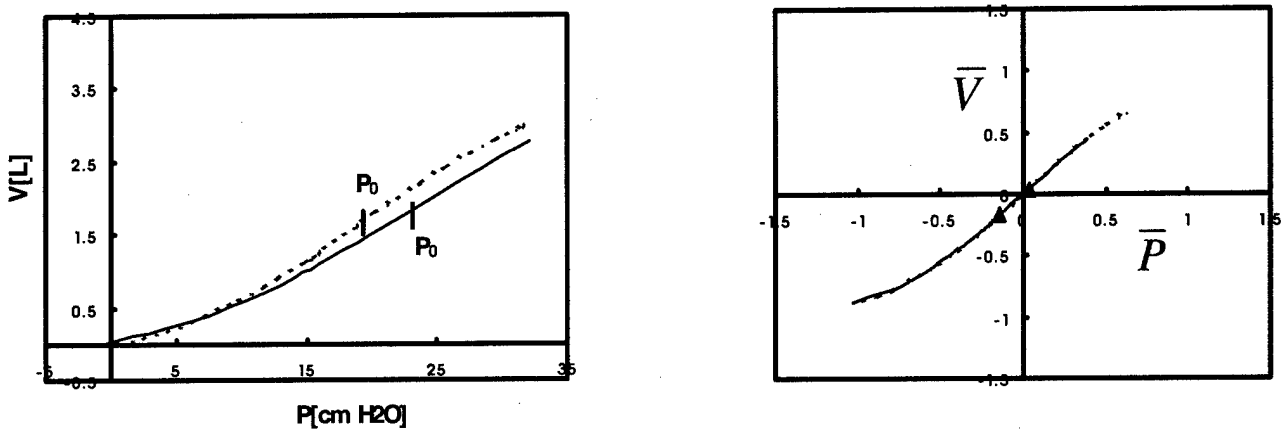

Data No. 6

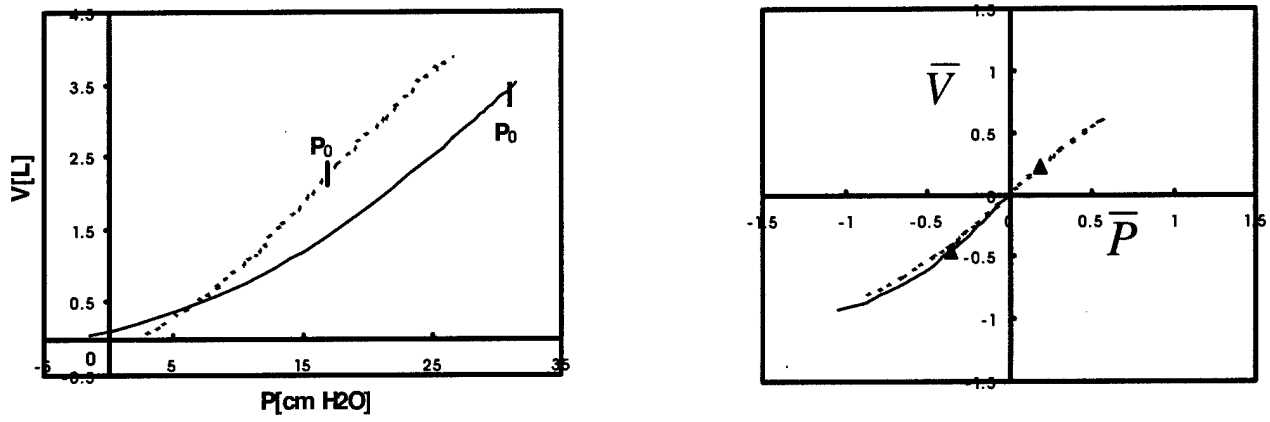

Data No. 7

Fig.10. p-V curve and the corresponding p-V curve of error function model equation. Solid =Before recruitment maneuver, Dotted = After recruitment maneuver, Triangle = location of p=20 [cmH2O].

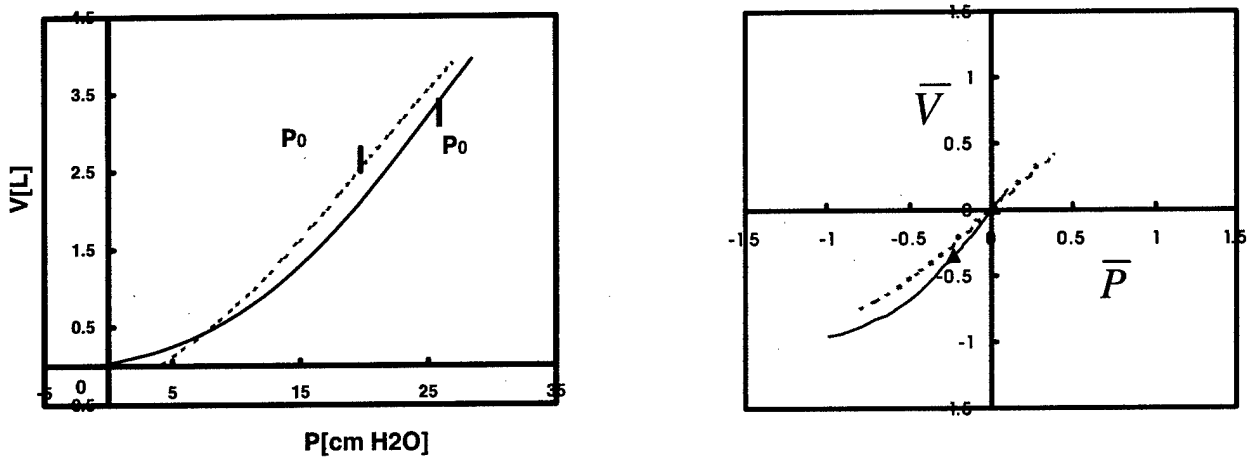

Data No. 11

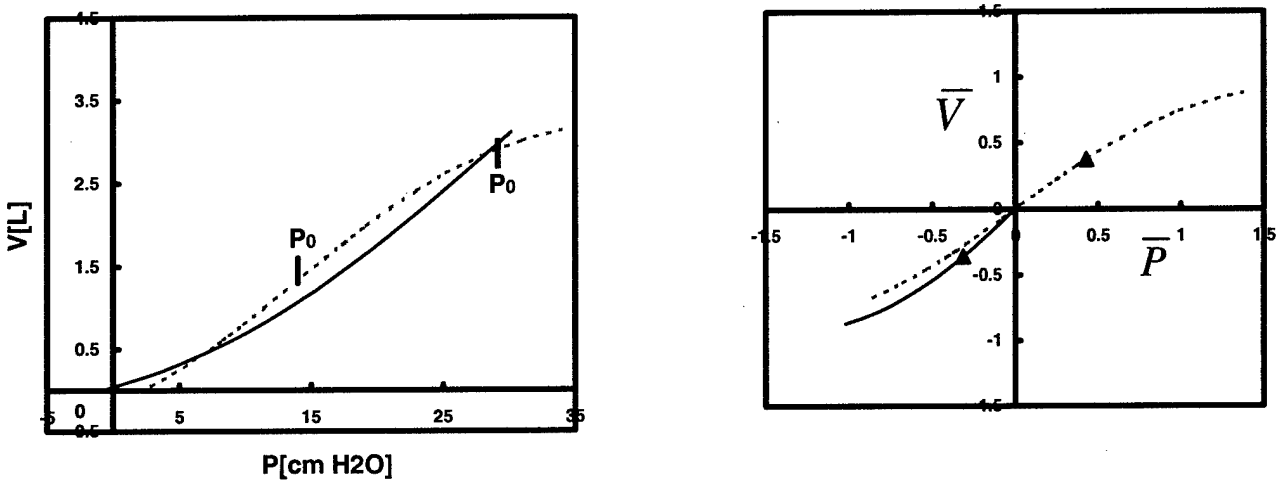

Data No. 13

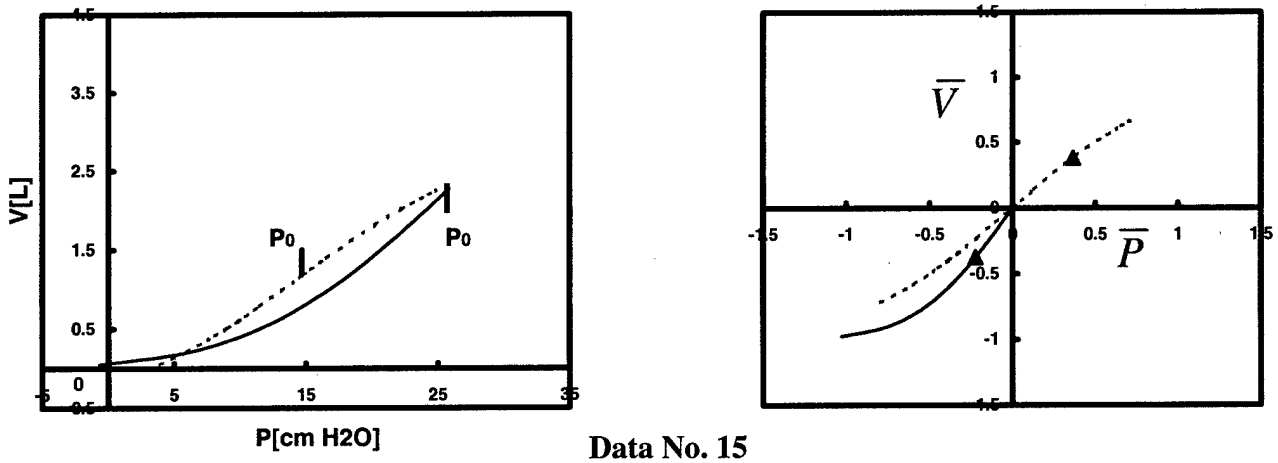

Data No. 15

Fig.11.Solid (Dotted) = Before (After) recruitment maneuver, Triangle = location of p =20[cmH2O].

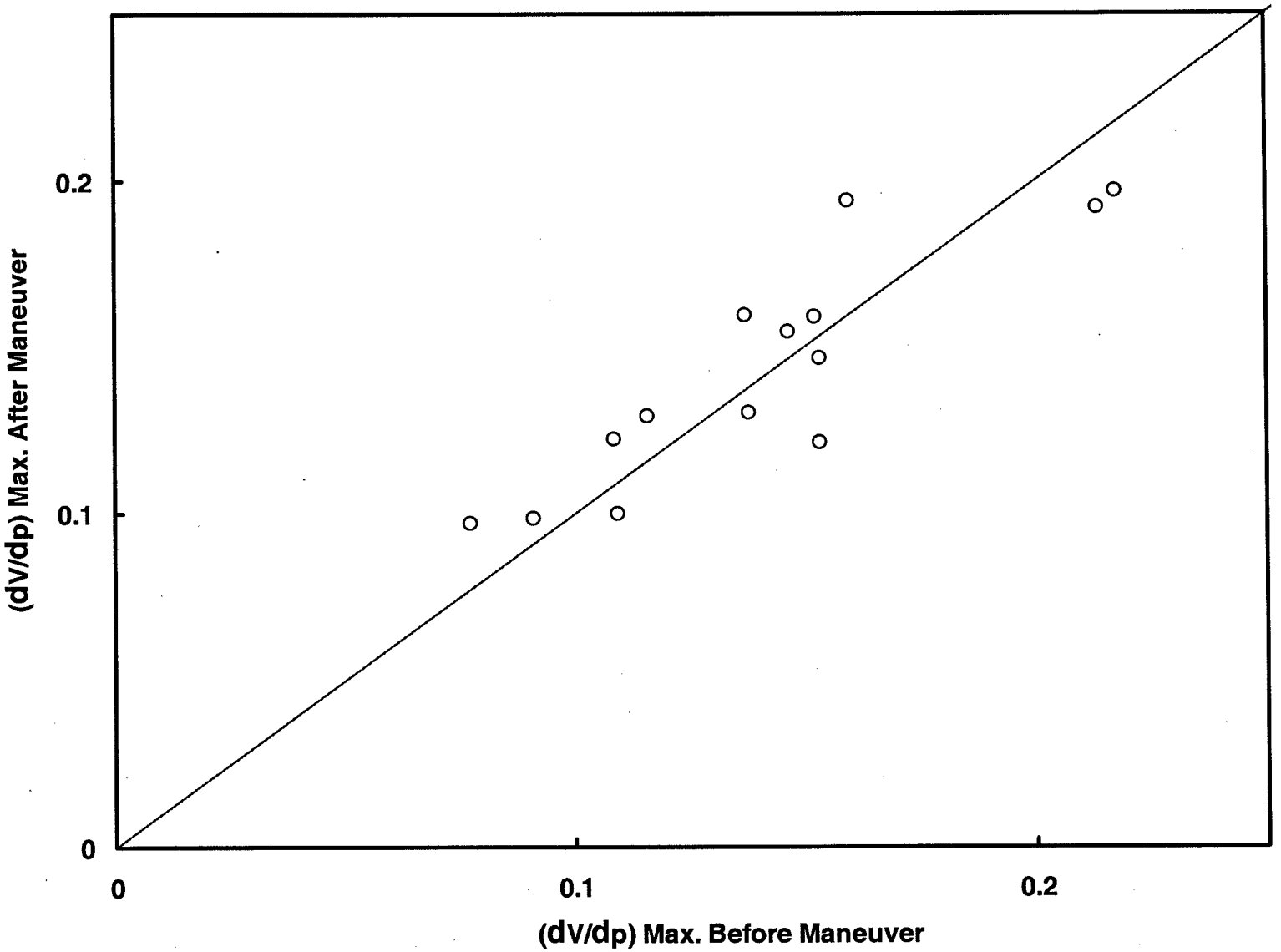

Fig.12. dV/dp ($p = p_0$) (maximum local compliance) before recruitment maneuver vs. dV/dp ($p = p_0$) after recruitment maneuver of Data Source B.

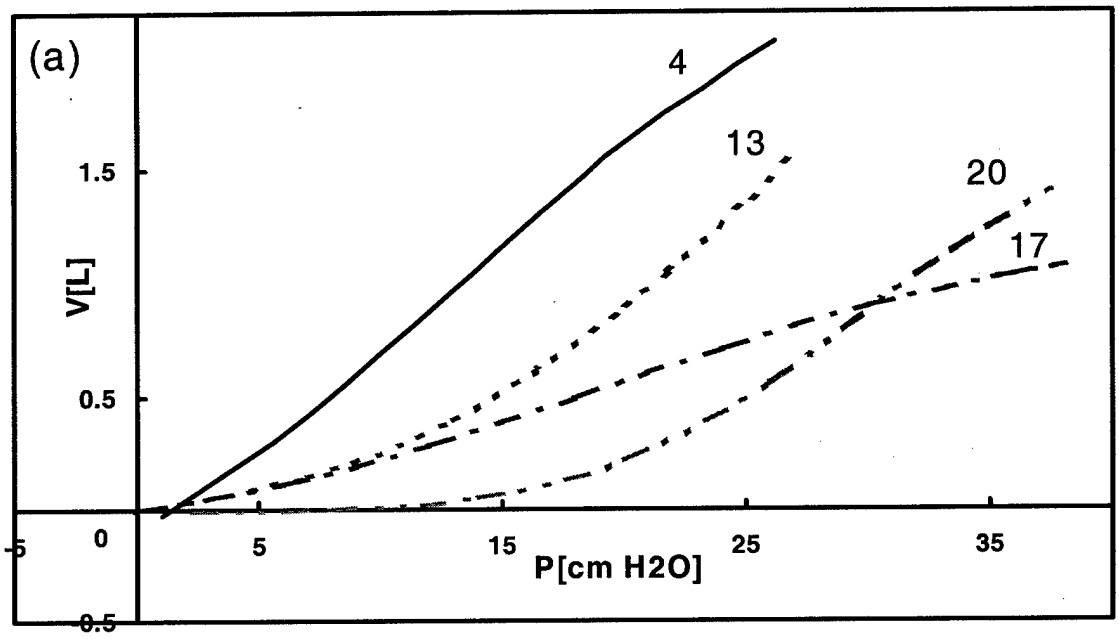

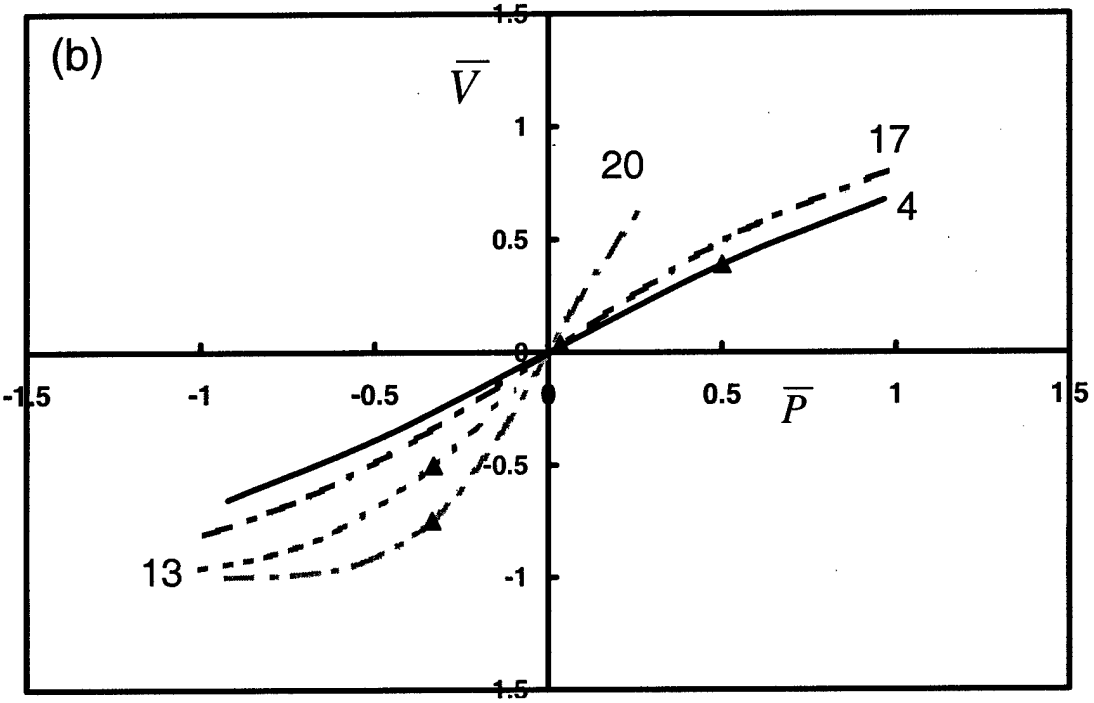

Fig.13. (a) p - V curve and (b) the corresponding $\overline{p}-\overline{V}$ curve of error function model equation for Data No.4, 13, 17 and 20 of Data Source A (patients with ARDS). Triangle = location of p=20[cmH2O]

References

1. Salazar, E., Knowles., J.H., An analysis of pressure-volume characteristics of the lungs. J. Appl. Physiol., 1964, 19, 97-104.
2. Paiva, M., Yernault, J.C., VanErdeweghe, P., Englert, M., A sigmoidal model of the static volume-pressure curve of human lung. Respir. Physiol., 1975, 23, 317-323.
3. Murphy, B.G., Engel, L.A., Models of the pressure-volume relationship of the human lung. Respir. Physiol., 1978, 32, 183-194.
4. Gibson, G. J., Pride, J. B., Davis, J., Schroter, R. C., Exponential description of the static pressure-volume curve of normal and diseased lungs. Am. Rev. Respir. Dis., 1979, 120: 799-811.
5. Greaves, I. A., Colebatch, H. J., Elastic behavior and structure of normal and emphysematous lungs post mortem. Am. Rev. Respir. Dis., 1980, 121, 127-136.
6. Schroter, R. C., Quantitative comparisons of mammalian lung pressure-volume curves. Respir. Physiol., 1980, 42, 101-107.
7. Gugger, M., Wraith, P. K., Sudlow, M. F., A new method of analysing pulmonary quasi-static pressure-volume curves in normal subjects and in patients with chronic airflow obstruction. Clin. Sci. (Lond.), 1990, 78, 365-369.
8. Venegas, J.G., Harris, S.R., Simon, B.A., A comprehensive equation for the pulmonary pressure-volume curve. J. Appl. Physiol., 1998, 84, 1, 389-395.
9. Svantesson, C., Sigurdsson, S., Larsson, A., Jonson, B., Effects of recruitment of collapsed lung units on elastic pressure-volume relationship in anaesthetized healthy adults. Acta Anaesthesiol. Scand., 1998, 42, 721-728.
10. Jonson, B., Svantesson, C., Elastic pressure-volume curves: What information do they convey ? Thorax, 1999, 54, 82-87.
11. Harris, S.R., Hess, D.R., Venegas, J.G., An objective analysis of the pressure-volume curve in the acute respiratory distress syndrome. Am.J.Respir.Crit.Care Med., 2000, 161, 432-439.
12. Amato, M.B., Barbas, C.S., Medeiros, D.M., Schettino, G.D.P., Lorenzi, F.G., Kairalla R.A., Deheinzelin, D., Morais, C., Fernandes, E.D.O., Takagaki, T.Y., Beneficial effects of the "open lung approach" with low distending pressures in acute respiratory distress syndrome. A prospective randomized study on mechanical ventilation. Am.J.Respir.Crit.Care Med., 1995, 152, 1835-1846.
13. Amato, M.B., Barbas, C.S., Medeiros, D.M., Magaldi, G.P., Schettino, G.D.P., Kairalla R.A., Deheinzelin, D., Munozs, C., Oliveira, R., Takagaki, T.Y., Calvalho, C.R., Effect of a protective-ventilation strategy on mortality in the acute respiratory distress syndrome. New Engl. J. Med., 1998, 347-354.
14. ARDS Network, Ventilation with lower tidal volumes as compared with traditional tidal volumes for acute lung injury and the acute respiratory distress syndrome. N. Engl. J. Med., 2000, 342 (18), 1301-1308.
15. Narusawa, U., General characteristics of the sigmoidal model equation representing quasi-static pulmonary pressure-volume curves. J. Appl. Physiol., 2001, 91, 201-210.

Chapter 2. A Mechanistic Model for Quasi-Static Pulmonary Pressure-Volume Curves: Model Development for Inflation Process

Abstract

A mechanistic model of a total respiratory system is proposed to understand differences in quasi-static pressure-volume ($p-V$) curves of the inflation process in terms of the alveolar recruitment and the elastic distension of the wall tissues. In the model, based on the Boltzmann statistics, the total respiratory system consists of a large number of elements, each of which is a subsystem of a cylindrical chamber fitted with a piston attached to a spring. The alveolar recruitment is simulated by allowing a distribution of the critical pressure at which an element opens; while the wall distension is represented by the piston displacement. Various parameters in the error-function $p-V$ model equation are related to the properties of the mechanistic model. The parameters of the model-based p-V equation are determined for each clinical data set for a total of twenty one $p-V$ data sets of patients with acute respiratory distress syndrome by a computational minimization procedure between the equation and the data points, results of which show excellent agreements between the two.

Nomenclature

A	$(k/A_s)\widehat{y}_0 = p_0$
A_s	piston surface area on which pressure is acting (Fig.4)
B	$(k/A_s)\widehat{y}_T = p_0 \cdot \widehat{y}_{T0}$, threshold pressure for onset of saturation
C	$(\hat{\beta}/2)^{1/2} \cdot p_0 = \sqrt{\pi}\Lambda/4$
$f,\ F$	distribution functions (Eqs.(6) & (13c))
$I_i\,(i = 1-5)$	functions defined in Eq.(13b)
k	spring constant [N/m] (Fig.4)
N	total number of TRS elements
N_j	number of elements at energy level j
p	pressure (interpleural pressure difference)
$\overline{p}$	non-dimensional pressure, $p/p_0 - 1$
p_{cj}	critical pressure at which an element, j, 'pops open'.
$\widehat{p}_{cj}$	p_{cj}/p_0 (Eq.(13c))
p_f	pressure at the end of inflation process
p_o	pressure at the inflection point in p-V equation, Eq.(1)
$U(p)$	total energy of TRS at p=p
ΔU	$\equiv U(p = p_f) - U(p = 0)$
V	volume
V_p	volume change from the state of $p = 0$
$V_{L(U)}$	lower (upper) volume asymptote (Fig.1)
$\overline{V}$	non-dimensional volume, $(V - ((V_U + V_L)/2)/(\Delta V/2)$, (Eq.(2))
$\widehat{V}_j$	volume of an element j
ΔV	$V_U - V_L = N\widehat{V}_0(\widehat{y}_{T0} + 1)$
$\widehat{V}_0$	'pop-open' volume $(= A_s\widehat{y}_0)$ (Fig.4)
$\widehat{y}_j$	piston displacement of an element j (Fig.4)

$\widehat{y}_0$	'pop-open' displacement, $(= \widehat{V}_0/A_s)$ (Fig.4)
$\widehat{y}_T$	piston stroke limit (Fig.4)
$\widehat{y}_{T0}$	$\widehat{y}_T/\widehat{y}_0$

Greek symbols:

α	constant of proportionality (Eq.(1a))
β	constant in the distribution function (Eq.(4))
$\widehat{\beta}$	$= (A_s^2/k)\,\beta$ (Eq.(5))
$\widehat{\epsilon}_j$	energy stored in an element j (Eq.(3))
Λ	$\alpha p_0 \Delta V$(non-dimensional parameter) (Eq.(1))
σ	$(8/\pi)^{1/2}/\Lambda$, Standard deviation (Eq.(13c))
ω	$\Lambda\bar{p}/2$ (Eq.(2))

Superscript:

$\widehat{\ }$	related to a single TRS element

Acronyms:

ARDS	acute respiratory distress syndrome
TRS	total respiratory system

Introduction

Quasi-static pulmonary $p-V$ (pressure - volume) curves are used routinely to obtain quantitative information on the respiratory system that is important for both research and clinical guidances, as the conditions of gas exchange, the primary role of the respiratory system, are related to the characteristics of the curve. During the inflation (inspiration) and the deflation (exhalation) processes, the respiratory system changes its volume (measured in L ($= 10^{-3}\,m^3$) or mL), lung (alveolar) pressure as well as the pleural pressure (the pressure of the thin liquid film that couples the lungs and the chest wall pleurae). The pressure, p, refers to the interpleural pressure difference (i.e. the difference between the lung pressure and the pleural pressure) measured in water head $[cm \cdot H_2O]$ ($1\,cmH_2O = 98\,Pa$). Clinical p-V curves are commonly obtained for an anesthetized human subject in supine position by sequentially adding (or withdrawing) incremental gas volumes ($\sim$ 50-100 mL) in a stepwise manner (with a duration of $\sim$ 5 seconds per step)[1,2]. Fig.1 is a typical inflation p-V curve, consisting of a nearly linear region of high compliance (i.e. large dV/dp) sandwiched between two segments with low compliance at low and high pressure regions. The shape of the $p-V$ curve is affected by two mechanisms, the distension of the elastic respiratory wall tissue components and the recruitment ('pop-open' mechanism) of the alveoli. The latter is the opening of alveoli overcoming the surface tension at the interface between the gas and the liquid film lining the alveolar surface. A pressure increase (i.e. an increase in the interpleural pressure difference) results in the recruitment of a greater number of alveoli. The high compliance is believed to be associated with both the distension of open parts of the lungs and the (alveolar) recruitment of collapsed parts of the lungs [3]. Some protective ventilation strategies, based on patients' quasi-static p-V curves, have been proposed for lung disease patients in intensive care units. Amato and coworkers [4,5] demonstrated, based on their clinical study involving patients with acute respiratory distress syndrome (ARDS), that a ventilator strategy guided by the p-V curve resulted in reduced lung trauma, a high weaning rate and improved survival compared with

a conventional ventilator strategy without the p-V curve guidance. Also, a recent ARDS Network report [6] on a clinical study involving 861 patients shows lower mortality in the group treated with lower tidal volume than in the group treated with traditional higher tidal volumes. Although a use of p-V curves is not mentioned, the report underscores the importance of optimized ventilator strategy.

In order to quantify the characteristics of $p-V$ curves as well as their changes observed in clinical settings, various p-V model equations have been proposed [7-12]. Parameters in model equations are determined from statistical processing of clinical data. It is important that these parameters should have some physiological interpretations. Also, to understand the shape of p-V curves in terms of mechanical behavior of lungs, multi-compartment lung models were developed and used to obtain information on the effects of lung elasticity and a degree of alveolar recruitment on p-V curves [3,13]. Although these analyses serve to relate the internal elastic conditions of the total respiratory system (TRS) to general p-V curve behavior, there has been no attempt to interpret individual differences in p-V curves directly in terms of internal elastic properties, alveolar recruitment and their changes. From an analytical viewpoint the quasi-static p-V curves are more amenable to theoretical studies because at each state we may be able to apply equilibrium principles. An overall objective of this report is to test the hypothesis that a mechanistic model, based on the continuous alveolar recruitment and the elastic distension of the wall tissues, is effective in understanding a relation between the observed pulmonary behavior (as p-V curves) and the corresponding internal respiratory response (in terms of the mechanistic model).

Continuous Equation for Quasi-Static p-V Curves

In the past piecewise-continuous equations were used to generate such quantities as compliance, the lower and upper inflection points that may reflect the internal conditions of TRS [7-12]. There are two continuous model equations that simulate various p-V curves accurately over the entire range of p-V data. One is a sigmoidal (tangent hyperbolic) equation, and the other an error-function equation, both originally proposed by Venegas

and his coworkers [1]. Since the analytical development to follow utilizes the error function representation of p-V curves, its characteristics are discussed below in some detail.

The error function p-V equation, plotted in Fig.1, may be expressed as

$$\frac{dV}{dp} = \frac{\alpha}{4} \cdot \Delta V^2 \cdot exp\Big[-\Big(\frac{\sqrt{\pi}}{4}\Lambda\Big)^2\Big(\frac{p}{p_0} - 1\Big)^2\Big], \tag{1a}$$

$$V = V_U - \frac{\Delta V}{2} + \Big(\frac{\Delta V}{2}\Big) \cdot erf\left(\frac{\sqrt{\pi}}{4}\Lambda\Big(\frac{p}{p_0} - 1\Big)\right), \tag{1b}$$

where $\Delta V = V_U - V_L$, V_U = the upper asymptote, V_L = the lower asymptote, α = positive constant, p_0 = a pressure at the midpoint (inflection point) of the curve and Λ (non-dimensional) = $\alpha p_0 \Delta V$ [1,2,14] with

$$erf(x) = \frac{2}{\sqrt{\pi}} \int_0^x e^{-t^2} dt \qquad erf(\infty) = 1, \quad erf(-x) = -erf(x).$$

The corresponding non-dimensional forms are,

$$\frac{d\overline{V}}{d\overline{p}} = \frac{\Lambda}{2} \cdot exp\Big(-\frac{\pi}{4}\omega^2\Big), \qquad \overline{V} = erf\Big(\frac{\sqrt{\pi}}{2}\omega\Big). \tag{2}$$

where $\overline{V} = [V - (V_U + V_L)/2]/(\Delta V/2)$, $\overline{p} = (p/p_0) - 1$, $\omega = \Lambda\overline{p}/2$.

Eq.(2) satisfies the following conditions:

$\overline{V}(\overline{p} = 0) = 0$, $\overline{V}(\overline{p}) = -\overline{V}(-\overline{p})$ (antisymmetry with respect to $p = p_0$),

$d\overline{V}/d\overline{p}(\overline{p} = 0) = \Lambda/2$, $\overline{V}(\overline{p} \to \pm\infty) = \pm 1$, $d\overline{V}(\overline{p} \to \pm\infty)/d\overline{p} = 0$.

A clinical data source of p-V curves we use in the present analyses are twenty one data sets of ARDS patients (both inflation and deflation data) in supine position by Harris et al [2], made available by the authors. Data sets are analyzed by minimizing the difference between data points and the error function model equation through the application of the method of least squares to obtain the parameters, $\Lambda, \Delta V, p_0$ and V_U (or V_L). Plotted in Fig.2 (Fig.3) are 264 inflation data points (225 deflation data points) in terms of Eq.(1b), $(V - V_L)/\Delta V$ vs $\sqrt{\pi}\Lambda(p/p_0 - 1)/4$. Agreement is excellent between the data and the p-V equation with R^2 (the coefficient of determination) = 0.99938 for the inflation- and = 0.99907 for the deflation- data points.

Development of a Mechanistic Model

An overall objective of the development of a mechanistic TRS model is to derive an equation for the volume participating in the p-V variations. We consider a TRS comprised of a very large number of elements with N = total number of elements. Based on the characteristics of a single element that are common to all elements, a distribution of elements is derived over a distribution parameter. The mechanistic model of an element is shown in Fig.4. An arbitrary element, j, consists of a cylindrical chamber containing a piston (with its surface area, A_s, $[m^2]$), which is attached to a spring with its spring constant, $k\,[N/m]$. The element is closed when the piston is located at the left end of the cylinder in Fig.4. When pressure acting on the left end of the piston reaches a certain critical value, the piston suddenly moves to a new position ('pop-open' mechanism) with the elemental volume, $\widehat{V}_0$, in the figure indicating an elemental volume increase due to the sudden piston displacement of $\widehat{y}_0$. Once the element is open with its volume of $\widehat{V}_0$, any further increase in pressure results in a volume increase as the piston moves to the right until it reaches the end of the cylinder. (The symbol, $\widehat{\ }$, indicates an elemental quantity.) In the model the pop-open volume, $\widehat{V}_0\,(= A_s\,\widehat{y}_0)$, and a further volume increase due to piston displacement represent the opening of alveoli and the elastic distension of the wall tissues respectively. We define p_{cj} as the critical pressure at which the element, j, 'pops open'.

Referring to Fig.4, the elemental volume, $\widehat{V}_j$, at $p\,(\geq p_{cj})$ is equal to $\widehat{V}_0 + A_s\widehat{y}_j$; which, upon application of a quasi-static force balance across the piston, $A_s\,(p - p_{cj}) = k\widehat{y}_j$, may be expressed as, $\widehat{V}_j = \widehat{V}_0 + (A_s^2/k)\,(p - p_{cj})$. Also the piston position of an element reaches its stroke limit of $\widehat{y}_T$ when pressure, p, reaches $(p_{cj} + (k/A_s)\widehat{y}_T)$. The mechanistic model of an element, therefore, goes through three stages in the inflation process — closed, open & unsaturated (i.e. $\widehat{y}_j < \widehat{y}_T$) and open & saturated (i.e. $\widehat{y}_j = \widehat{y}_T$). The model assumes that the critical 'pop-open' pressure, p_{cj}, as well as the location of the piston for open elements, $\widehat{y}_j$, vary from element to element at an arbitrary quasi-static state (p, V), and that other quantities such as k, A_s, $\widehat{V}_0$ and $\widehat{y}_T$ are constant and common for all elements. The energy

level of an open and unsaturated element, j, consists of the activation energy required to pop open the element, $\widehat{\epsilon}_{j\,A}$, and the energy stored in the spring, $\widehat{\epsilon}_{j\,S}$. For $\widehat{\epsilon}_{j\,A}$, we assign the compression/expansion work under constant pressure; i.e. $\widehat{\epsilon}_{j\,A} = p_{cj}\widehat{V}_0$; while, $\widehat{\epsilon}_{j\,S}$ is equal to $k\,\widehat{y}_j^2/2$, which may be expressed in terms of p_{cj} as $\widehat{\epsilon}_{j\,S} = (A_s^2/2k)(p - p_{cj})^2$ from an application of the force balance.

In summary, at a quasi-static (-equilibrium) state at $p = p$, a TRS element, j, belongs to one of the following states:

if $p < p_{cj}$, the element, j, is closed with $\widehat{V}_j = 0, \quad \widehat{\epsilon}_j = 0.$

if $p_{cj} = p$, the element, j, pops open with $\widehat{V}_j = \widehat{V}_0, \quad \widehat{\epsilon}_j = p_{cj}\widehat{V}_0.$

if $p - (k/A_s)\widehat{y}_T < p_{cj} < p$, the piston of the open and unsaturated element, j, moves to a location, $\widehat{y}_j$, with $\widehat{V}_j = \widehat{V}_0 + A_s\,\widehat{y}_j, \;\; \widehat{\epsilon}_j = p_{cj}\widehat{V}_0 + (A_s^2/2k)(p - p_{cj})^2.$

if $p_{cj} \le p - (k/A_s)\widehat{y}_T$, the piston of the open and saturated element, j, remains at the stroke limit, $\widehat{y}_T$, with $\widehat{V}_j = \widehat{V}_0 + A_s\,\widehat{y}_T, \quad \widehat{\epsilon}_j = p_{cj}\widehat{V}_0 + (k/2)\widehat{y}_T^2.$

The state of an element follows the sequence above during the inflation process as p increases. To obtain an explicit form of the distribution function of TRS elements over the distribution parameter, p_{cj}, we focus on open and unsaturated elements, for which the elemental energy shown above may be rewritten as,

$$\widehat{\epsilon}_j\,(\textit{open, unsaturated}) = \frac{A_s^2}{2k}\Big[p_{cj} - \big(p - \frac{k\widehat{V}_0}{A_s^2}\big)\Big]^2 + \frac{\widehat{V}_0}{2}\Big(2p - \frac{k\widehat{V}_0}{A_s^2}\Big). \tag{3}$$

According to the Boltzmann statistical model ([15,16] for example), which assumes that there is no limit in the number of elements per energy state, the most probable distribution N_j/N (a fraction of elements at an energy level, $\widehat{\epsilon}_j$), may be expressed as

$$N_j\,/\,N \;=\; e^{-\beta\widehat{\epsilon}_j}\Big/\sum_j e^{-\beta\widehat{\epsilon}_j} \qquad (\beta \;=\; \textit{unspecified constant}) \tag{4}$$

A substitution of Eq.(3) into Eq.(4) with the summation replaced by an integral over the whole range of p_{cj} for a large number of elements, yields

$$\frac{dN_j}{N\,dp_{cj}} = exp\bigg(-\frac{\widehat{\beta}}{2}\Big(p - p_{cj} - \frac{k}{A_s^2}\widehat{V}_0\Big)^2\bigg)\Big/\int_{-\infty}^{\infty} exp\bigg(-\frac{\widehat{\beta}}{2}\Big(p - p_{cj} - \frac{k}{A_s^2}\widehat{V}_0\Big)^2\bigg)dp_{cj} \tag{5}$$

where $\widehat{\beta} = (A_s^2/k)\,\beta$. It should be noted that the integration in the denominator ranges from $-\infty$ and $+\infty$. As summarized above, any arbitrary element remains active (open and unsaturated) only in a certain range of p_{cj}; therefore, the application of Eq.(5) over the entire range of $-\infty < p_{cj} < \infty$ assumes that the distribution function that is valid for active elements is also applicable in evaluating the number of closed as well as saturated elements. Then, upon performing the integration of the denominator in Eq.(5), we obtain for dN_j/N(= a number fraction of elements, for which the magnitude of p_{cj} ranges between p_{cj} and $p_{cj} + dp_{cj}$),

$$\frac{dN_j}{N} = f \cdot dp_{cj}, \qquad f = \left(\frac{\widehat{\beta}}{2\pi}\right)^{\frac{1}{2}} \cdot exp\Big(-\frac{\widehat{\beta}}{2} \cdot (p - p_{cj} - \frac{k}{A_s^2}\widehat{V}_0)^2\Big) \tag{6}$$

Noting that elements, j, with p_{cj} in the range of $0 \le p_{cj} \le p$, are open at $p = p$, and that $(k/A_s)\,\widehat{y}_T$ $(\equiv B)$ is the pressure at which an element j with $p_{cj} = 0$ reaches the piston stroke limit of $\widehat{y}_T$, the volume change with pressure needs to be evaluated for the following two pressure ranges; pressure range 1: $0 \le p \le B$ and pressure range 2: $B \le p$.

Pressure Range 1: $0 \le p < B$

Since the pressure is below B (the threshold pressure for the onset of saturation), all open elements are active (unsaturated) with $\widehat{y}_j < \widehat{y}_T$. Then the total volume, $V_p(\equiv V(p = p) - V(p = 0)$; i.e. a volume change from the state of $p = 0$), participating in the inflation process is,

$$V_p(p) = N\left[\int_{p_{cj}=0}^{p} (\widehat{V}_0 + A_s\widehat{y}_j)\, f(p = p)\, dp_{cj} + A_s\widehat{y}_j \int_{p_{cj}=p}^{\infty} f(p = p)\, dp_{cj}\right].$$

The first term on the right hand side represents a volume increase due to the elements that pop-open, followed by a piston displacement ($\widehat{y}_j = A_s^2(p - p_{cj})/k$ from the force balance) during the inflation process from $p = 0$ to $p = p$; while, the second term, noting

$$\int_{p_{cj}=p}^{\infty} f(p = p)\, dp_{cj} = \int_{p_{cj}=0}^{\infty} f(p = 0)\, dp_{cj},$$

accounts for the elements that are already open at p =0 and the piston displacement $\widehat{y}_j$ $(= A_s^2 p/k)$ is the only mechanism available for the volume increase.

After expressing $\widehat{y}_j$ in terms of p and p_{cj} as shown above, the equation may be written as,

$$V_p = N\left(\frac{\widehat{\beta}}{2\pi}\right)^{\frac{1}{2}}\left[\int_{-A}^{p-A}(2\widehat{V}_0+\frac{A_s^2}{k}t)\cdot exp(-\frac{\widehat{\beta}}{2}t^2)\,dt+\int_{A}^{\infty}\frac{A_s^2}{k}p\cdot exp(-\frac{\widehat{\beta}}{2}z^2)dz\right] \quad (7)$$

where $A=(k/A_s)\,\widehat{y}_0, \quad t=-z=(p-p_{cj}-k\,\widehat{V}_0/A_s^2)$.

Pressure Range 2: $B \le p$

In this pressure range, the elements with $0 \le p_{cj} \le p-B$ as well as the elements that are already open at p =0 are saturated (i.e. $\widehat{y}_j=\widehat{y}_T$ for the elements); while, the elements with $p-B \le p_{cj} \le p$ remain unsaturated (i.e. $\widehat{y}_j<\widehat{y}_T$); therefore,

$$\begin{aligned} V_p =& N\int_0^{p-B}(\widehat{V}_0+A_s\widehat{y}_T)\cdot f(p=p)\,dp_{cj}+N\int_{p-B}^{p}(\widehat{V}_0+A_s\widehat{y}_j)\cdot f(p=p)\,dp_{cj} \\ &+N\int_p^{\infty}A_s\widehat{y}_T\cdot f(p=p)\,dp_{cj}. \end{aligned} \quad (8)$$

Eqs.(7)(8), after integration, become,

$$V_p\,(0\le p\le B)=N\widehat{V}_0\Big[I_1+\frac{1}{2}\frac{p}{A}(1-I_1)-\frac{I_2(p)}{2\sqrt{\pi}C}+I_3(p)\Big], \quad (9a)$$

$$V_p\,(\quad B\le p\quad)=N\widehat{V}_0\Big[I_1+\frac{\widehat{y}_{T0}}{2}(1-I_1)+\frac{\widehat{y}_{T0}-1}{2}I_4-\frac{I_5}{2\sqrt{\pi}C}+\frac{\widehat{y}_{T0}+1}{2}I_3(p)\Big] \quad (9b)$$

where

$$I_1=erf(C),\quad I_2(p)=exp\big(-C^2(\frac{p}{A}-1)^2\big)-exp(-C^2),\quad I_3(p)=erf\big(C\,(\frac{p}{A}-1)\big),$$
$$I_4=erf\big(C(1-\widehat{y_{T0}})\big),\quad I_5=exp\big(-C^2(\widehat{y}_{T0}-1)^2\big)-exp(-C^2),$$
$$C=\big(\widehat{\beta}/2\big)^{1/2}\cdot A,\quad \widehat{y}_{T0}=\widehat{y}_T/\widehat{y}_0=B/A\,.$$

Therefore, the mechanistic model yields the following p-V equation;

$$\begin{aligned} V\,(0\le p\le B\,) &= V_U \\ &+N\widehat{V}_0\Big(\frac{(1-I_1)}{2}(\frac{p}{A}-\widehat{y}_{T0})-\frac{\widehat{y}_{T0}+1}{2}-\frac{\widehat{y}_{T0}-1}{2}\cdot I_4+\frac{I_5-I_2(p)}{2\sqrt{\pi}C}+I_3(p)\Big), \end{aligned} \quad (10a)$$

$$V\,(B\le p\quad)\quad = V_U-\frac{N\widehat{V}_0(\widehat{y}_{T0}+1)}{2}+\frac{N\widehat{V}_0(\widehat{y}_{T0}+1)}{2}\cdot I_3(p). \quad (10b)$$

In order to relate the present TRS model, intended to describe the internal respiratory conditions, to the p-V curve that quantitatively describes overall variations in TRS conditions, an additional condition that needs to be satisfied is conservation of energy. For a quasi-static process from an initial state of $(p = 0, V = V(p = 0))$ to a final state of $(p = p_f, V = V(p = p_f))$ (p_f = the pressure at the end of a measured p-V curve), the conservation of energy neglecting any dissipative mechanisms may be written as,

$$\Delta U(\equiv U(p = p_f) - U(p = 0)) = \int_{V(p=0)}^{V(p=p_f)} p\, dV\,, \tag{11}$$

where $U(p)$ represents the total energy of TRS at $p = p$ to be evaluated from our mechanistic model; while the right hand side of the equation is work associated with the inflation process that must be evaluated from the p-V model equation. A further development of the energy equation will be discussed in the next section.

Mechanistic Model vs Error Function p-V Equation

Relations between the parameters in the error function $p - V$ equation and the parameters in our mechanistic model are derived based on the observation that the $p - V$ relation, Eq.(10b), for the high pressure region as well as the corresponding equation for the local compliance,

$$V\,(B \le p) = V_U - \frac{N\widehat{V}_0(\widehat{y}_{T0}+1)}{2} + \frac{N\widehat{V}_0(\widehat{y}_{T0}+1)}{2} \cdot erf\big(C\,(\frac{p}{A}-1)\big),$$

$$\frac{dV}{dp}\,(B \le p) = \frac{N\widehat{V}_0(\widehat{y}_{T0}+1)}{2} \cdot \frac{2C}{\sqrt{\pi}p_0} \cdot exp\left(-C^2(\frac{p}{A}-1)^2\right),$$

become identical to the error function model equation, Eq.(1),

$$V = V_U - \frac{\Delta V}{2} + \Big(\frac{\Delta V}{2}\Big) \cdot erf\left(\frac{\sqrt{\pi}}{4}\Lambda\Big(\frac{p}{p_0}-1\Big)\right),$$

$$\frac{dV}{dp} = \frac{\alpha}{4} \cdot \Delta V^2 \cdot exp\Big[-\Big(\frac{\sqrt{\pi}}{4}\Lambda\Big)^2\Big(\frac{p}{p_0}-1\Big)^2\Big],$$

if we set

$$N\widehat{V}_0(\widehat{y}_{T0}+1) = \Delta V, \quad A\Big(\equiv (k/A_s)\,\widehat{y}_0\Big) = p_0, \quad C\left(\equiv \Big(\frac{\widehat{\beta}}{2}\Big)^{1/2} \cdot A\right) = \frac{\sqrt{\pi}}{4}\Lambda. \tag{12}$$

Before further developments are made on the mechanistic model, our results are summarized below, based on the parametric relations, Eq.(12), between the error function p-V equation and the model.

Pressure - Volume $(p - V_p)$ Equation:

$$V_p\,(0 \le p \le p_0 \cdot \widehat{y}_{T0}) = \frac{\Delta V}{\widehat{y}_{T0}+1}\left(I_1 + \frac{(\overline{p}+1)(1-I_1)}{2} - \frac{2\,I_2(\overline{p})}{\pi\Lambda} + I_3(\overline{p})\right),$$

$$V_p\,(p_0 \cdot \widehat{y}_{T0} \le p) = \frac{\Delta V}{\widehat{y}_{T0}+1}\left(I_1 + \frac{\widehat{y}_{T0}}{2}(1-I_1) + \frac{\widehat{y}_{T0}-1}{2}\,I_4 - \frac{2\,I_5}{\pi\Lambda} + \frac{\widehat{y}_{T0}+1}{2}\cdot I_3(\overline{p})\right). \qquad (13a)$$

Pressure - Volume $(p - V)$ Equation:

$$V\,(\,0 \le p \le p_0 \cdot \widehat{y}_{T0}\,) = \frac{V_U + V_L}{2} + \frac{\Delta V}{\widehat{y}_{T0}+1}\left(I_3(\overline{p}) + \frac{(1-I_1)}{2}(\overline{p}+1-\widehat{y}_{T0}) - \frac{\widehat{y}_{T0}-1}{2}\,I_4 + \frac{2(I_5 - I_2(\overline{p}))}{\pi\Lambda}\right),$$

$$V\,(\,p_0 \cdot \widehat{y}_{T0} \le p\,) = \frac{V_U + V_L}{2} + \frac{\Delta V}{2}\,I_3(\overline{p}) \qquad (13b)$$

$$\textit{where}\quad I_1 = erf(C), \qquad I_2(\overline{p}) = exp(-C^2\,\overline{p}^2) - exp(-C^2),$$

$$I_3(\overline{p}) = erf(C\,\overline{p}), \qquad I_4 = erf(C(1-\widehat{y_{T0}})),$$

$$I_5 = exp(-C^2\,(\widehat{y}_{T0}-1)^2) - exp(-C^2), \qquad C = \sqrt{\pi}\Lambda/4.$$

Distribution Function:

$$\frac{dN_j}{N \cdot d\widehat{p}_{cj}} = F(\overline{p}), \qquad F(\overline{p}) = \frac{1}{\sqrt{2\pi}\,\sigma}\cdot exp\Big(-\frac{1}{2}\Big[\frac{\widehat{p}_{cj} - \overline{p}}{\sigma}\Big]^2\Big) \qquad (13c)$$

$$\textit{where}\qquad \widehat{p}_{cj} = p_{cj}/p_0, \qquad \sigma = (8/\pi)^{\frac{1}{2}}/\Lambda\,.$$

The model-based p-V equation, Eq.(13b), consists of two regions. The solution for the high pressure region is identified with the error-function p-V equation. The p-V equation for the lower pressure region as well as the boundary pressure between the high- and low-pressure region contain the parameters of the p-V equation, Λ, p_0, ΔV, V_U $(or V_L)$),

and an additional parameter, $\widehat{y}_{T0}$. Conservation of energy, Eq.(11), is utilized to find the magnitude of $\widehat{y}_{T0}$. Similar to the p-V model equation, Eq.(13b), the evaluation of Eq.(11) depends on the magnitude of the final pressure, p_f, relative to the boundary pressure, $p_0\,\widehat{y}_{T0}$, between the high and the low pressure regions of the model-based p-V equation. As will be shown later in the analyses of clinical data, the magnitude of $\widehat{y}_{T0}$ is less than unity; hence, the conservation of energy is further developed for the case of $p_0 \cdot \widehat{y}_{T0} \leq p_f$ (i.e. $\widehat{y}_{T0} - 1 \leq \overline{p}_f (= p_f/p_0 - 1)$). Accordingly the left hand side of Eq.(11) may be evaluated from the elemental distribution function, $F(\overline{p})$ of Eq.(13c), along with the elemental energy summarized in the paragraphs preceding Eq.(3), yielding,

$$
\begin{aligned}
\Delta U \;&= \frac{N\,p_0^2\,A_s^2}{k}\left[\int_0^{\overline{p}_f+1-\widehat{y}_{T0}} (\widehat{p}_{cj} + \frac{1}{2}\widehat{y}_{T0}^2)\cdot F(\overline{p}=\overline{p}_f)\,d\widehat{p}_{cj}\right. \\
&\quad \left. + \int_{\overline{p}_f+1-\widehat{y}_{T0}}^{\overline{p}_f+1} (\widehat{p}_{cj} + \frac{1}{2}(\overline{p}_f + 1 - \widehat{p}_{cj})^2)\cdot F(\overline{p}=\overline{p}_f)\,d\widehat{p}_{cj}\right] \\
&= \frac{N\,p_0^2\,A_s^2}{k}\left[\int_0^{\overline{p}_f+1-\widehat{y}_{T0}} (\widehat{p}_{cj} - \overline{p}_f)\,F(\overline{p}=\overline{p}_f)\,d\widehat{p}_{cj}\right. \\
&\quad + \frac{\widehat{y}_{T0}^2}{2}\int_0^{\overline{p}_f+1-\widehat{y}_{T0}} F(\overline{p}=\overline{p}_f)\,d\widehat{p}_{cj} + \overline{p}_f\int_0^{\overline{p}_f+1} F(\overline{p}=\overline{p}_f)\,d\widehat{p}_{cj} \\
&\quad \left. + \frac{1}{2}\int_{\overline{p}_f+1-\widehat{y}_{T0}}^{\overline{p}_f+1} F(\overline{p}=\overline{p}_f)\,d\widehat{p}_{cj} + \frac{1}{2}\int_{\overline{p}_f+1-\widehat{y}_{T0}}^{\overline{p}_f+1} (\widehat{p}_{cj} - \overline{p}_f)^2\,F(\overline{p}=\overline{p}_f)\,d\widehat{p}_{cj}\right] \\
&= \frac{N\,p_0^2\,A_s^2}{k}\left[-\frac{2}{\pi\Lambda}[I_5 - I_2(\overline{p}_f)] + \frac{1}{4}\widehat{y}_{T0}^2[I_3(\overline{p}_f) + I_4] + \frac{1}{2}\overline{p}_f[I_1 + I_3(\overline{p}_f)]\right. \\
&\qquad + \frac{1}{4}(I_1 - I_4) + \frac{2}{\pi\Lambda}\Big(\frac{1}{\Lambda}(I_1 - I_4) + \frac{\widehat{y}_{T0}^2}{4}(1 - I_1) \\
&\qquad \left. - \frac{1}{2}\big[(exp(-C^2) - (1-\widehat{y}_{T0})\cdot exp(-C^2(1-\widehat{y}_{T0})^2)\big]\Big)\right]. \qquad (14a)
\end{aligned}
$$

The right hand side of Eq.(11) becomes,

$$
\begin{aligned}
\int_{V(p=0)}^{V(p=p_f)} p\,dV &= p_f V(p=p_f) - \Big[\int_0^{p_0\widehat{y}_{T0}} V(0 \leq p \leq p_0\widehat{y}_{T0})dp + \int_{p_0\widehat{y}_{T0}}^{p_f} V(p_0\widehat{y}_{T0} \leq p_f)dp\Big] \\
&= \frac{p_0\Delta V}{\widehat{y}_{T0}+1}\left[\frac{(\widehat{y}_{T0}+1)}{2}(\overline{p}_f+1)\cdot I_3(\overline{p}_f) + \frac{\widehat{y}_{T0}(\widehat{y}_{T0}-1)}{2}\cdot I_4 - \frac{2}{\pi\Lambda}\widehat{y}_{T0}\cdot I_5\right.
\end{aligned}
$$

$$- \int_{-1}^{\widehat{y}_{T0}-1} I_3(\overline{p})\, d\overline{p} + \frac{4}{\pi\Lambda^2}(I_1 - I_4) - \frac{2}{\pi\Lambda}\widehat{y}_{T0} \cdot exp(-C^2)$$

$$- \frac{\widehat{y}_{T0}+1}{2} \int_{\widehat{y}_{T0}-1}^{\overline{p}_f} I_3(\overline{p})\, d\overline{p} + \frac{\widehat{y}_{T0}^2}{4}(1 - I_1) \Bigg]. \qquad (14b)$$

It should be noted that the factors, $N\, p_0^2\, A_s^2/k$, in Eq.(14a) and $p_0 \Delta V/(\widehat{y}_{T0}+1)$, in Eq.(14b) are identical, thus dropping out of the conservation of energy, Eq.(11), as common factor.

The p-V equation constructed from the mechanistic model, Eq.(13b), contains five unknowns (Λ, p_0, ΔV, V_U (*or* V_L), $\widehat{y}_{T0}$), the magnitudes of which are determined by minimizing the differences between Eq.(13b) and a specified data set based on the method of least squares, under the constraint imposed by the conservation of energy, Eq.(11) and Eq.(14). Because the p-V equation consists of two equations, one for the high pressure region and the other for the low pressure region, and also because algebraic equations resulting from the application of the method of least squares are non-linear, a computational program is developed to find the five unknowns. The program requires a set of initial guess values for the five unknowns. The parameters, Λ, p_0, ΔV, V_U, of the error function p-V equation, Eq.(1b), are used for initial values with the initial value for the fifth unknown, $\widehat{y}_{T0}$, being set to zero. The program employs the Newton-Raphson iterative technique around the value of $\widehat{y}_{T0}$ to minimize the errors between Eq.(13b) and the data points while conservation of energy is satisfied exactly, until the five unknowns converge to a set of solutions.

Discussion of Results

We begin with physical interpretations of parameters of p-V equations in terms of the mechanistic model. The first equation in Eq.(12) is,

$$\Delta V = N\widehat{V}_0(\widehat{y}_{T0}+1)$$

$$= N(\widehat{V}_0 + A_s\, \widehat{y}_T).$$

Noting that $\widehat{y}_{T0}$ is a ratio of the piston displacement by elastic tissue distension to that by alveolar recruitment, ΔV of the error function p-V equation is the maximum possible

volume available for inflation, and is related to the mechanistic model as a product of the total number of elements, N, and the elemental volume available for inflation through both the 'pop-open' mechanism, $\widehat{V}_0$ (corresponding to the volume increase due to the alveolar opening), and the piston displacement, $A_s\widehat{y}_T$ (corresponding to the elastic wall distension of TRS). V_U is related only to the solution of the high pressure region as $V_U = V(p \to \infty)$. On the other hand, under the two-region p-V equation of the mechanistic model, the definition of ΔV needs to be elaborated. Since $V_L \neq V(p \to -\infty)$ in the lower pressure solution of the mechanistic model, ΔV should be interpreted as the maximum possible volume change when the high pressure solution is extended into the low pressure region.

The second equation, $p_0 = (k/A_s)\,\widehat{y}_0$, indicates that the pressure at the midpoint of the p-V curve is an equivalent pressure required to displace the piston against the spring force over the pop-open displacement of $\widehat{y}_0$. It may be rewritten as $p_0\widehat{V}_0 = k\,\widehat{y}_0^2$; therefore, $p_0\widehat{V}_0/2$ is the spring energy required to displace the piston by the amount, $\widehat{y}_0$. This observation implies that the pressure, p_0, is related to both the alveolar recruitment (through $\widehat{y}_0$) and the elastic tissue distension (through k). A higher magnitude of p_0 implies a larger value of the spring constant 9wall elasticity) and/or a greater amount of energy required to pop-open the elements.

The non-dimensional parameter, Λ, is related to the parameter, C, of the mechanistic model through the third equation in Eq.(12), $C = (\sqrt{\pi}/4)\,\Lambda$. As may be seen from Eq.(9), the parameter, C, appears as a factor in the function, $I_3(p)$. Since the function, $I_3(p)$, is a monotonically increasing function of p, an increase in volume, V, becomes more sensitive to a change in pressure when the magnitude of Λ is larger. The observations above may be further extended in terms of the distribution of elements over the critical pop-open pressure, Eq.(13c). The number distribution of elements is a normal distribution with its mean at $\overline{p}\,(= p/p_0 - 1)$ and a standard deviation, σ, which is proportional to $1/\Lambda$. Since the peak of the distribution is located at $\widehat{p}_{cj} = \overline{p}$, the rate of increase in the number of open elements increases (decreases) for $p < p_0\,(p > p_0)$; an observation consistent with

the fact that p_0 is a pressure at the inflection point of the error function p-V equation. A larger value of Λ indicates a smaller standard deviation, indicating a higher peak in number density and a sharper distribution.

The p-V equation, Eq.(13b), of the mechanistic model consists of the low pressure solution in which all open elements are unsaturated, and the high pressure solution where some elements are saturated (fully-distended). The equation has three pressure -dependent terms. A term proportional to $\overline{p}$ in the equation for the low pressure region (the third term) is due to the elastic distension of the elements that are open at p=0. Two other pressure-dependent functions are $I_2(\overline{p})$, originating from volume changes due to the piston displacement, and $I_3(\overline{p})$, which results from both the pop-open volume and the piston displacement. The former is symmetric with respect to $\overline{p}\,(= p/p_0 - 1) = 0$, i.e. $I_2(\overline{p}) = I_2(-\overline{p})$; while, the latter is antisymmetric, i.e. $I_3((\overline{p}) = -I_3(-\overline{p})$. Furthermore, the p-V equation in the high pressure region, $V\,(p_0 \cdot \widehat{y}_{T0} \leq p\,)$, is independent of the magnitude of $\widehat{y}_{T0}$; while, the solution V_p is sensitive to the magnitude of $\widehat{y}_{T0}$ in both the low and the high pressure regions.

Fig.5 shows six representative data sets of patients with ARDS as well as the corresponding p-V equation, Eq.(13b), derived from the mechanistic model for the inflation (**I**) process. Fig.6 is a plot of [the volume predicted by model-based p-V equation at a specified pressure] vs [the corresponding data volume] for all inflation data points from the twenty one data sets. Both figures show very good agreements between the model and the clinical data with R^2 for Fig. 6 being equal to 0.9993. (Various parameters for all data sets are summarized in Table 1.) The solid (dotted) curves in Fig.5 are the solution of the low (high) pressure region (i.e. the first (second) equation in Eq.(13b)) with the composite solution indicating that the p-V curve is not antisymmetric with respect to p_0. However, since the error minimization is applied between the antisymmetric error function p-V equation, Eq.(1b), and the mechanistic model equation, Eq.(13b), the two curves are very close to each other in the low pressure region of $0 \leq p \leq p_0\widehat{y}_{T0}$. Ranges of various

parameters listed in Table 1 are,

$$\Lambda = 1.5 - 5.5, \quad p_0 = 13 - 31\ [cmH_2O],$$

$$\Delta V = 1 - 4\ [L], \quad \widehat{y}_{T0} = 0.289 - 0.695.$$

Since the boundary pressure between the low- and the high- pressure solution, $p_0 \cdot \widehat{y}_{T0}$, is low compared to the end-of inflation pressure for most data sets, the antisymmetric high pressure solution is applicable over a major part of the data sets analyzed. It is also noted here that if the condition of $\widehat{y}_{T0} = 0$ (negligible elastic tissue distension) is imposed, the solution of the mechanistic model, consisting solely of the solution for the high pressure region becomes identical to the (antisymmetric) error function p-V equation although the conservation of energy is not satisfied by the condition. Fig.7 is presented to show the magnitude of the left hand side of conservation of energy divided by $p_0\Delta V$ as the abscissa, and $(-1)\cdot$(the right hand side of conservation of energy divided by $p_0\Delta V$) as the ordinate for all data sets when $\widehat{y}_{T0}$ is set to zero and the parameters (Λ, p_0, ΔV, V_L) of the error function p-V equation are used for the evaluation. The figure shows that the left and right hand side of conservation of energy have opposite signs for all data sets, indicating that conservation of energy is not satisfied at $\widehat{y}_{T0} = 0$.

The range of $\widehat{y}_{T0}$ obtained by the mechanistic model indicates that the fraction of total volume available for the pop-open mechanism (alveolar recruitment), $N\widehat{V}_0/\Delta V$, which is equal to $1/(1 + \widehat{y}_{T0})$, ranges between 0.59 and 0.78.

Summary

A mechanistic model of TRS elements, each consisting of a piston-spring system, is developed to analyze quasi-static pressure-volume curves for the inflation process. The model accommodates both the alveolar recruitment (in terms of the critical pop-open pressure) and the elastic distension of wall tissues (in terms of the piston displacement). Model-based relations (Eq.(12)) are established between the parameters in the $p-V$ curve represented by the error function equation, Eq.(1), and in the mechanistic model. Under the constraint imposed by conservation of energy, the parameters of the model-based p-V

equation is determined for each clinical data set by a computational minimization procedure between the equation and the data points, results of which show excellent agreements between the two (Figs.5 and 6). The p-V equation thus derived, Eq.(13b), consists of two equations; one for the low pressure region where all open elements are active (= unsaturated) as the piston of an element is yet to reach its stroke limit, and the other for the high pressure region where some open elements are saturated. The elemental distribution over the critical pop-open pressure, Eq.(13c), is a normal distribution with its shape (the mean and the standard deviation) affected substantially by the magnitudes of two parameters in the mechanistic model, Λ and p_0.

The present analysis is for the inflation process. The deflation process is different from the preceding inflation because of the absence of the pop-open mechanism, and also becasue of a possibility of airway closure. However, a certain aspect of the deflation process may be predicted from the inflation analysis; which will be discussed in Prat II as a validity test of the mechanistic model. Wide ranges covered by the parameters, Λ, p_0, ΔV and $\widehat{y}_{T0}$, of the p-V equation and the mechanistic model need to be interpreted in terms of the shape and the range of the p-V curves as well as in terms of the elemental distribution and its changes along the corresponding p-V curve; which will also be discussed in Part II.

Figure/Table Captions

Table 1. Summary of Inflation Data Analyses.

Fig.1. A typical quasi-static pulmonary pressure-volume curve.

Fig.2. Error-function p-V equation and inflation data points.

Fig.3. Error-function p-V equation and deflation data points.

Fig.4. A schematic diagram of mechanistic model of TRS element.

Fig.5. Model-based p-V equation, Eq.(13b), vs data points for inflation process.

solid: solution for low pressure region,

dotted: solution for high pressure region.

Fig.6. V (volume predicted by model-based p-V equation) vs V (volume of data) for a specified pressure.

Fig.7. $\Delta U/p_0 \cdot \Delta V$ vs $(-1) \cdot \int p\, dV/p_0 \cdot \Delta V$ when $\widehat{y}_{T0} = 0$

Table 1. Summary of Inflation Data Analysis.

Data No	Λ	p_0 $[cmH_2O]$	ΔV [L]	V_L [L]	$\widehat{y}_{T0}$
A.1.	2.9652	22.398	2.3726	-0.0709	
2.	2.9578	22.411	2.3772	-0.0723	0.347
B.1.	2.7173	21.981	1.5612	-0.0762	
2.	2.7304	21.999	1.5559	-0.0728	0.359
C.1.	3.3532	25.082	1.6193	-0.0365	
2.	3.3664	25.073	1.6139	-0.0342	0.329
D.1.	1.6273	13.324	3.1567	-0.5727	
2.	1.9257	13.999	2.8392	-0.3542	0.379
E.1.	2.7160	30.361	1.6216	-0.0768	
2.	2.6497	30.817	1.6847	-0.0923	0.480
F.1.	2.6029	23.880	1.5066	-0.0962	
2.	2.6423	23.863	1.4874	-0.0873	0.365
G.1.	1.7288	20.156	3.0989	-0.3645	
2.	1.9277	20.731	2.8704	-0.2138	0.447
H.1.	1.8901	14.959	1.7905	-0.2185	
2.	2.0421	15.405	1.7129	-0.1563	0.431
I. 1.	3.5379	25.248	2.7570	-0.0350	
2.	3.5449	25.232	2.7508	-0.0333	0.368
J. 1.	2.7981	26.208	3.7326	-0.1583	
2.	2.7364	26.830	3.9129	-0.1887	0.474
K.1.	2.4296	17.895	1.3424	-0.0997	
2.	2.4708	17.951	1.3304	-0.0916	0.440
L.1.	1.2500	11.592	1.2470	-0.2829	
2.	1.5318	13.213	1.1256	-0.1678	0.695
M.1.	3.2725	29.865	3.9075	-0.0861	
2.	2.9972	30.327	4.2463	-0.2179	0.626
N.1.	2.7915	15.310	1.6284	-0.0705	
2.	2.8046	15.297	1.6219	-0.0681	0.358
O.1.	1.9487	18.374	1.8797	-0.2423	
2.	2.1412	18.837	1.7753	-0.1696	0.389
P.1.	2.4566	26.982	1.3277	-0.0787	
2.	2.4553	27.032	1.3278	-0.0773	0.467
Q.1.	2.1027	19.314	1.3316	-0.1279	
2.	2.2041	19.583	1.2941	-0.1004	0.389
R.1.	1.1672	13.986	2.0685	-0.5149	
2.	1.6209	16.352	1.7396	-0.2530	0.406
S. 1.	3.1381	26.802	3.1306	-0.0851	
2.	3.0894	26.925	3.1878	-0.1030	0.407
T.1.	5.4709	30.038	1.7695	-0.0097	
2.	5.4708	30.037	1.7694	-0.0097	0.289
U.1.	3.2818	24.439	2.8956	-0.2075	
2.	3.2819	24.349	2.8956	-0.2075	0.327

1. Obtained by applying the method of least squares along with error function p-V equation.
2. Results from the mechanistic model.

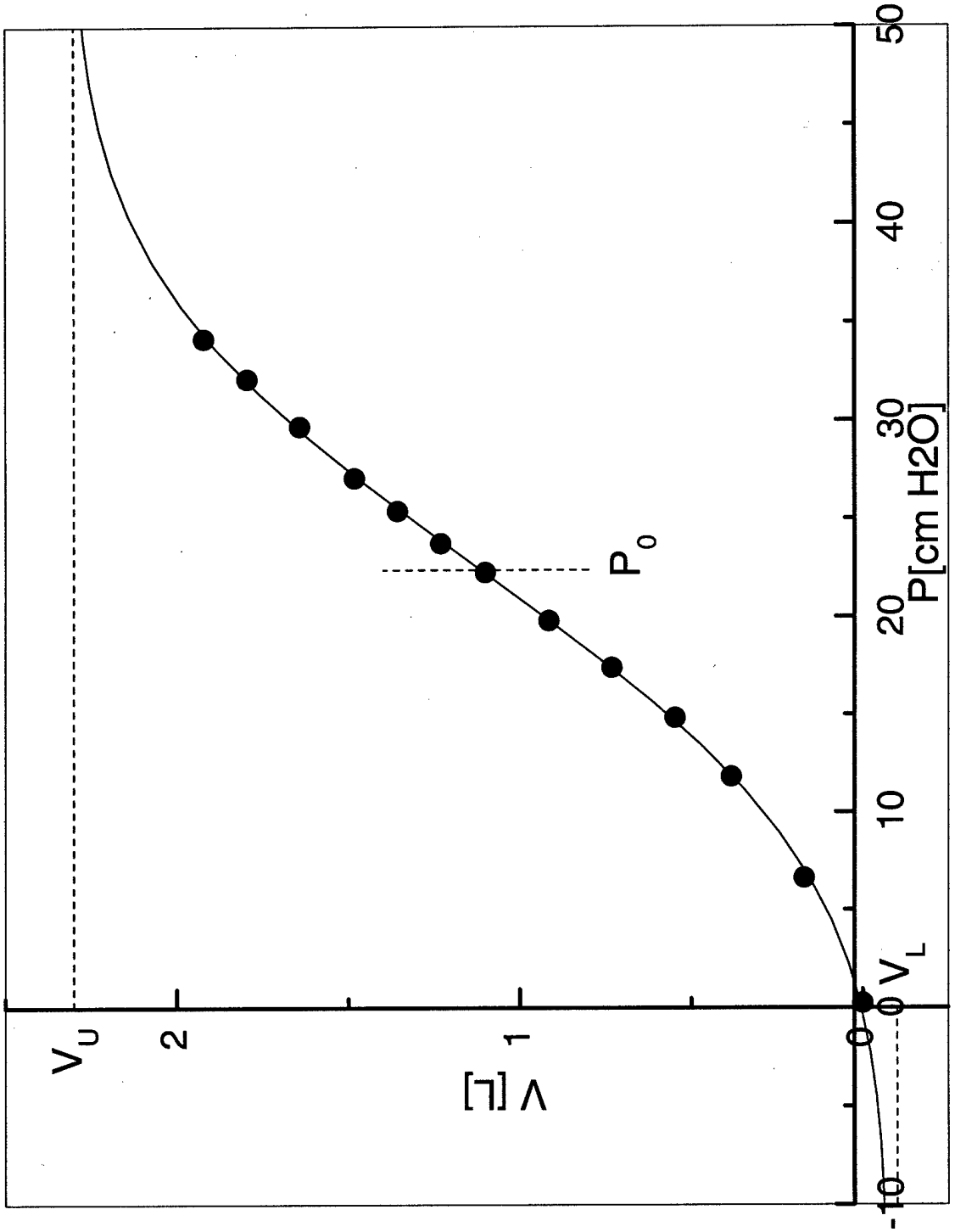

Fig.1. A typical quasi-static pulmonary pressure-volume curve

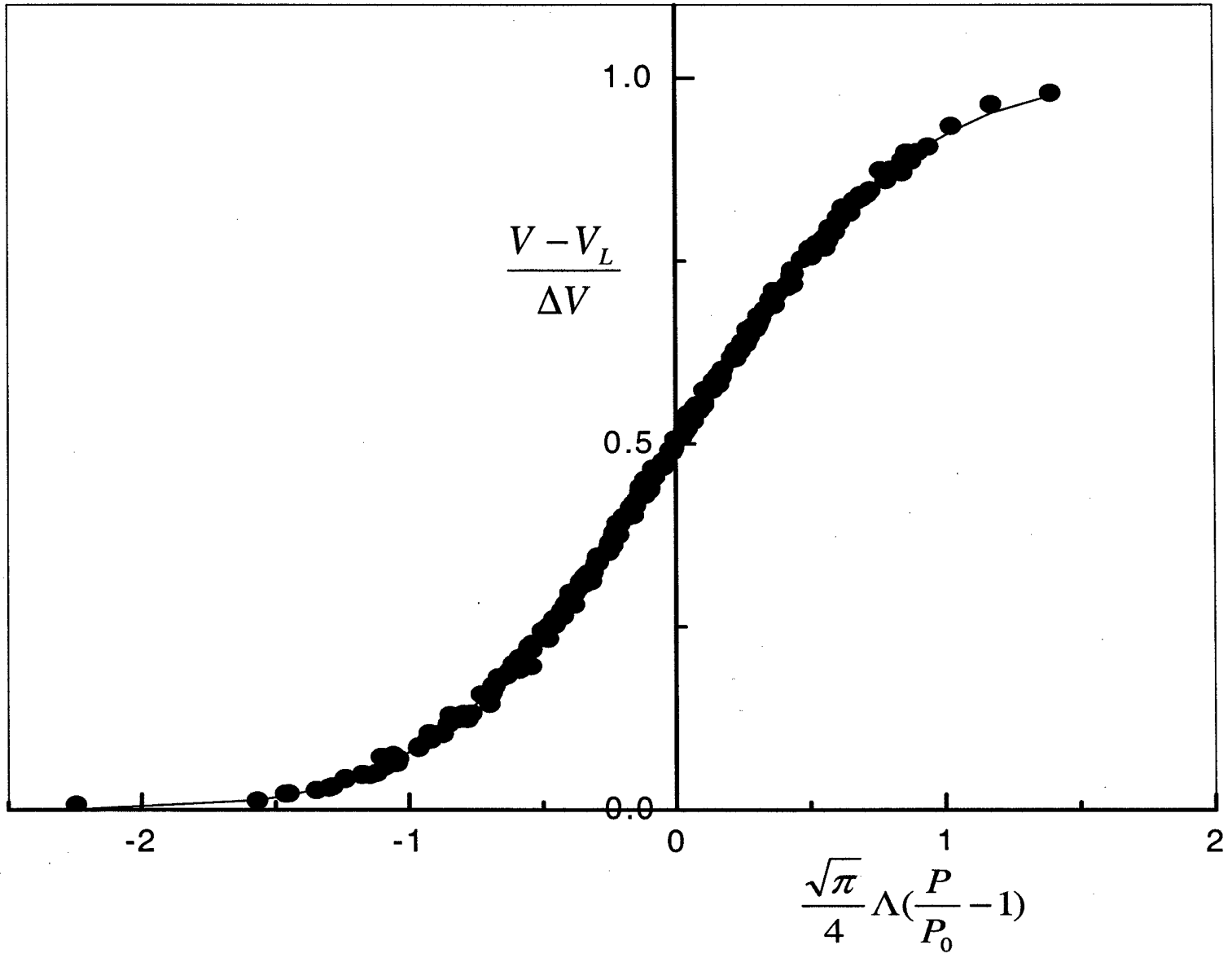

Fig.2. Error-function p-V equation and inflation data points.

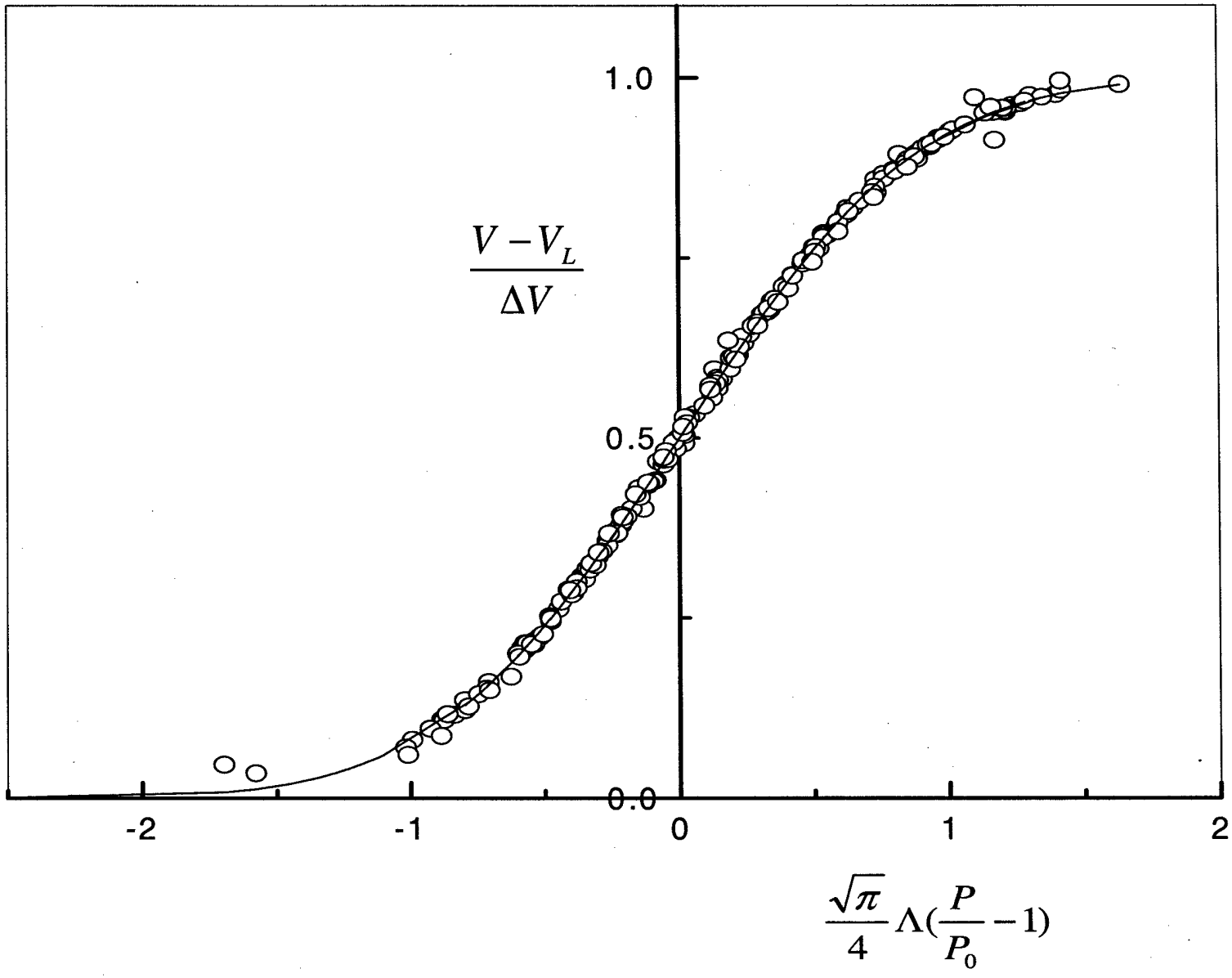

Fig.3. Error-function p-V equation and inflation data points.

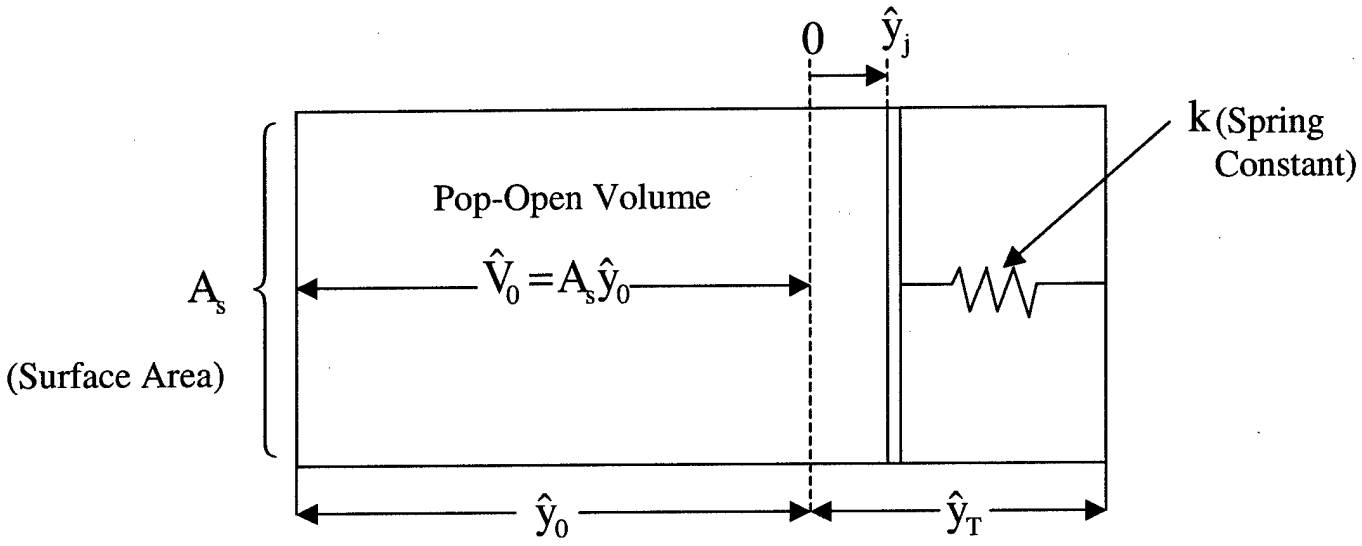

Fig.4. A Schematic diagram of mechanistic model of TRS element

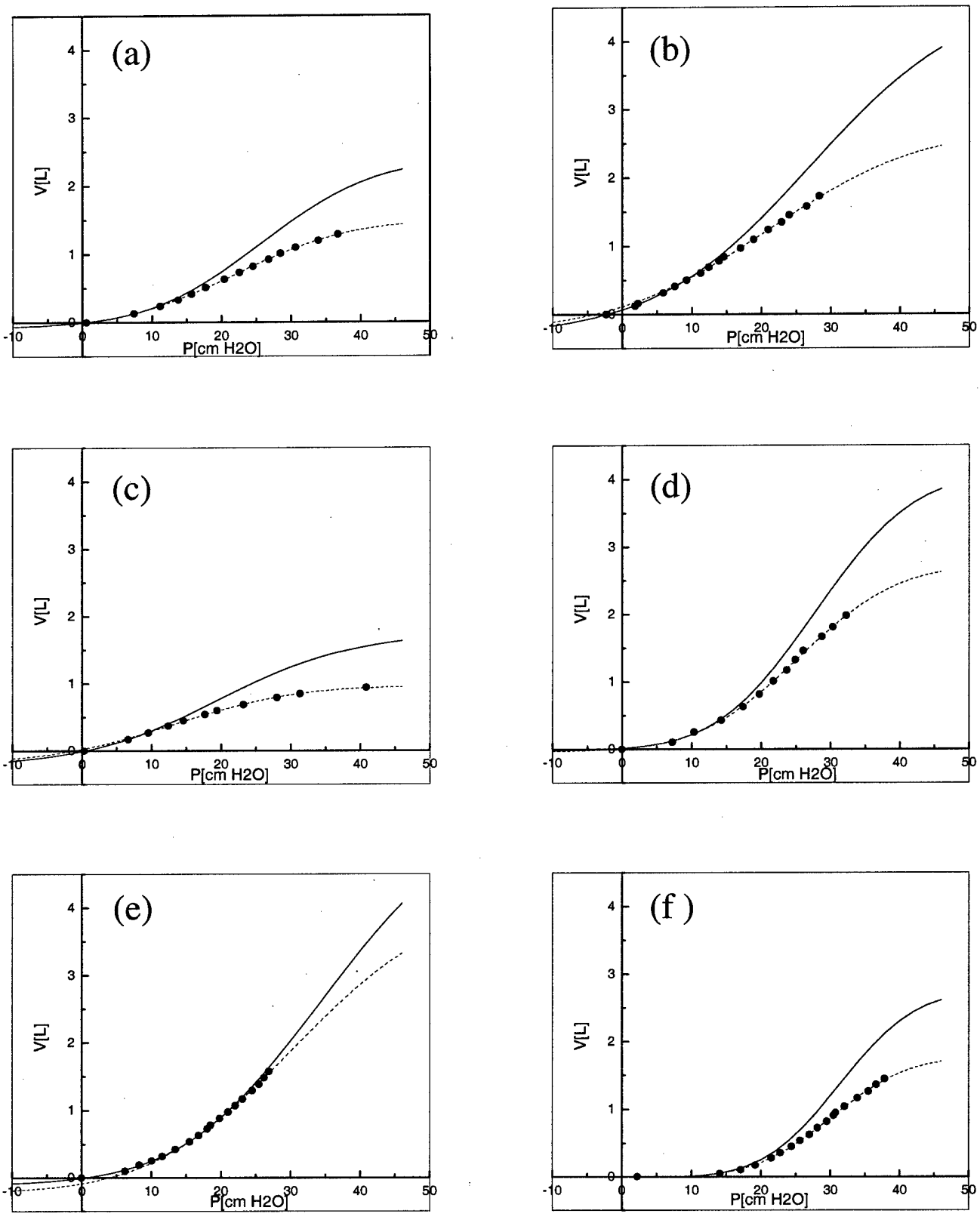

Fig.5. Model based p-V equation, Eq. (13b), vs data points for inflation process.
Solid: solution for low-pressure region,
Dotted: solution for high-pressure region.

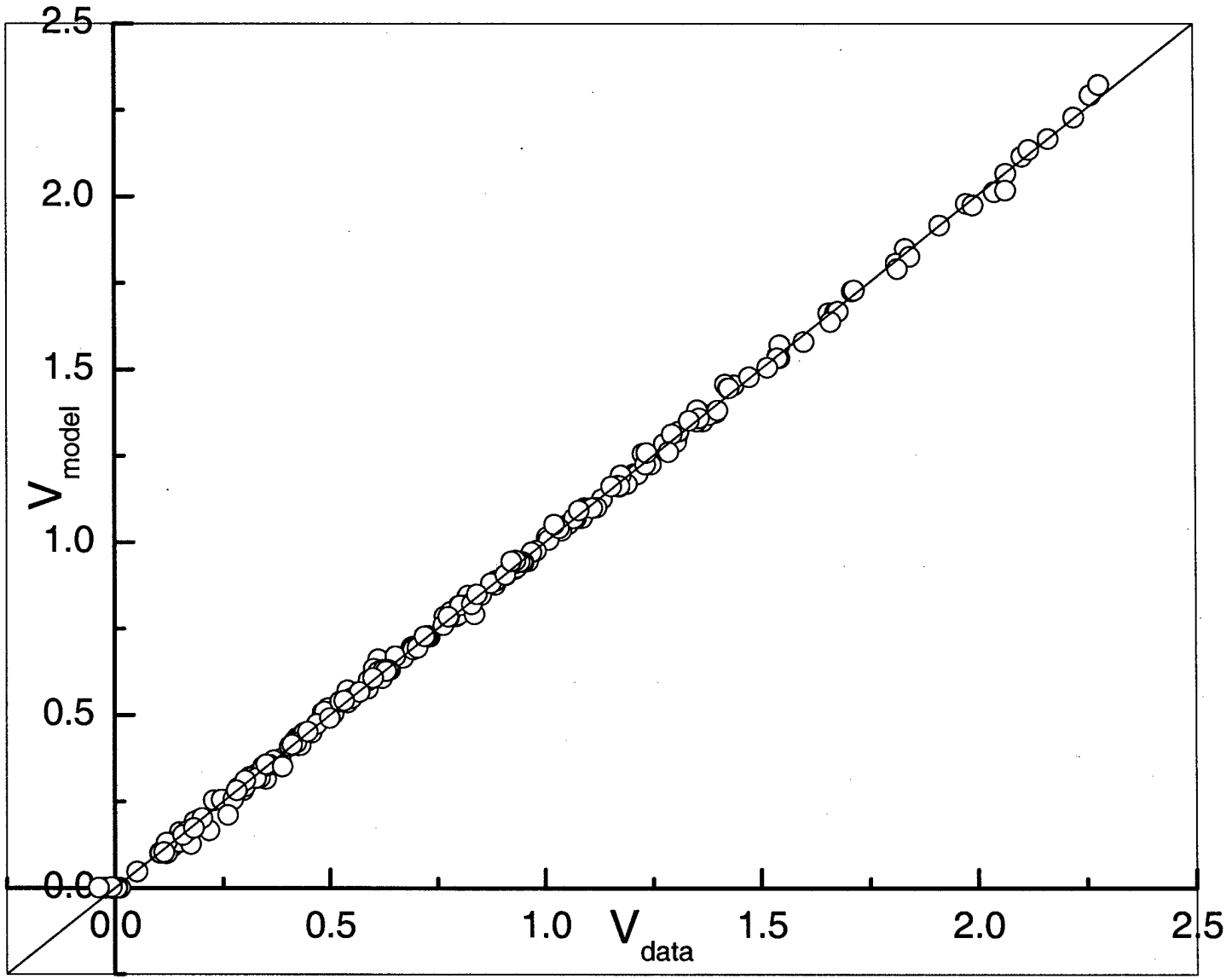

Fig.6. V (volume predicted by model-based p-V equation) vs. V(Volume of data) for a specified pressure.

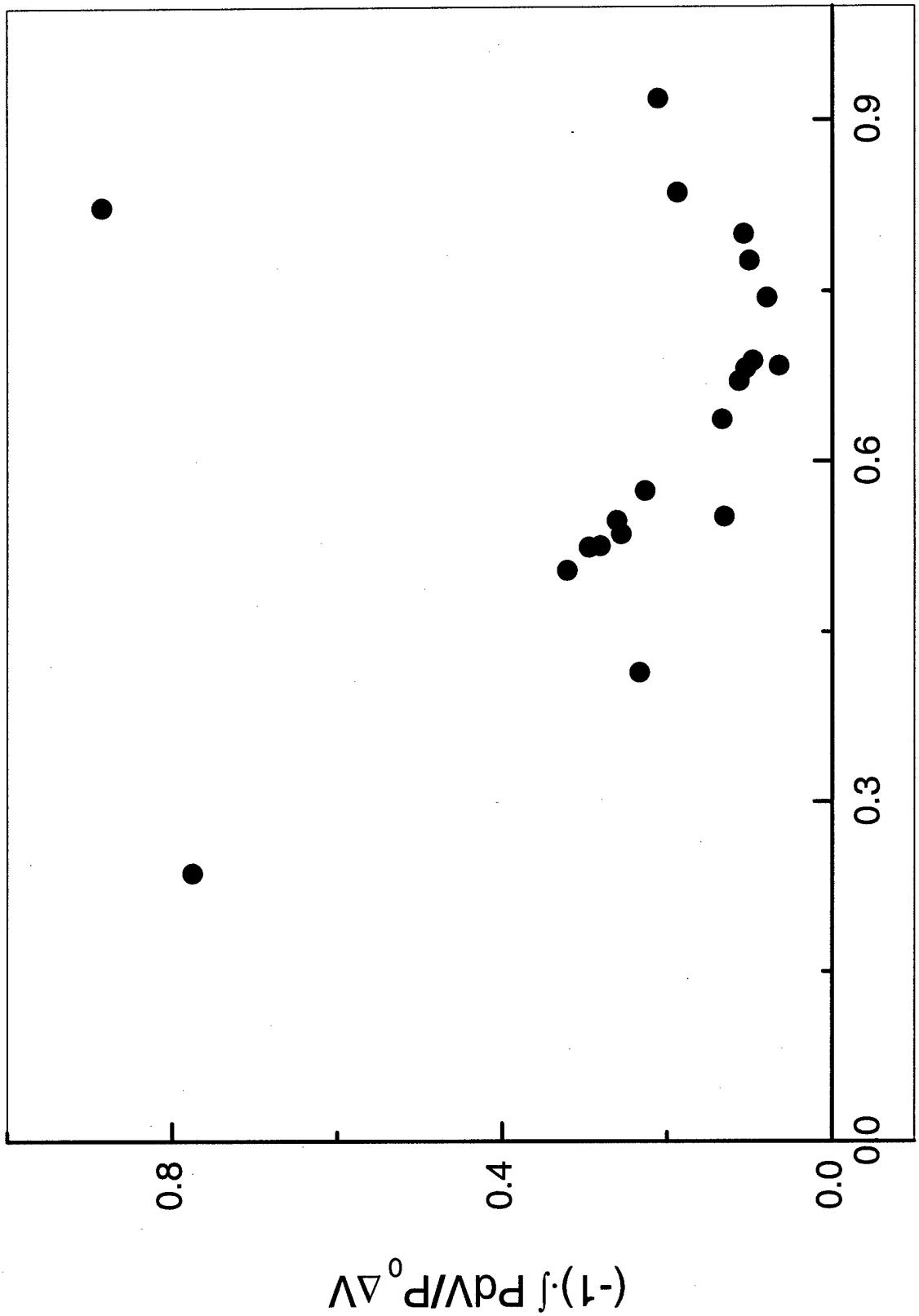

Fig.7. $\Delta U/P_0 \Delta V$ vs. $(-1)\cdot\int PdV/P_0 \Delta V$ when $\hat{y}_{T0} = 0$

References

1. Venegas, J.G., Harris, S.R., Simon, B.A., A comprehensive equation for the pulmonary pressure-volume curve. J. Appl. Physiol., 84, 1, 389-395, 1998.
2. Harris, S.R., Hess, D.R., Venegas, J.G., An objective analysis of the pressure-volume curve in the acute respiratory distress syndrome. Am.J.Respir.Crit.Care Med., 161, 432-439, 2000.
3. Jonson, B., Svantesson, C., Elastic pressure-volume curves: what information do they convey ? Thorax, 54, 82-87, 1999.
4. Amato, M.B., Barbas, C.S., Medeiros, D.M., Schettino, G.D.P., Lorenzi, F.G., Kairalla R.A., Deheinzelin, D., Morais, C., Fernandes, E.D.O., and Takagaki, T.Y., Beneficial effects of the "open lung approach" with low distending pressures in acute respiratory distress syndrome. A prospective randomized study on mechanical ventilation. Am.J.Respir.Crit.Care Med., 152, 1835-1846, 1995.
5. Amato, M.B., Barbas, C.S., Medeiros, D.M., Magaldi, G.P., Schettino, G.D.P., Kairalla R.A., Deheinzelin, D., Munozs, C., Oliveira, R., Takagaki, T.Y., and Calvalho, C.R., Effect of a protective-ventilation strategy on mortality in the acute respiratory distress syndrome. New Engl. J. Med., 347-354, 1998.
6. ARDS Network, Ventilation with lower tidal volumes as compared with traditional tidal volumes for acute lung injury and the acute respiratory distress syndrome. N. Engl. J. Med. 342 (18), 1301-1308, 2000.
7. Salazar, E., and J. H. Knowles. An analysis of pressure-volume characteristics of the lungs. J. Appl. Physiol., 19, 97-104, 1964.
8. Paiva, M., Yernault, J.C., VanErdeweghe, P. and Englert, M., A sigmoidal model of the static volume-pressure curve of human lung. Respir. Physiol., 23, 317-323, 1975.
9. Murphy, B.G., Engel, L.A., Models of the pressure-volume relationship of the human lung. Respir. Physiol. 32, 183-194, 1978.
10. Gibson, G. J., Pride, J. B., Davis, J. and Schroter, R. C.. Exponential description of the static pressure-volume curve of normal and diseased lungs. Am. Rev. Respir. Dis., 120: 799-811, 1979.
11. Bogaard, J. M., Overbeek,S. E., Verbraak, A. F., Vons, ,C., Folgering, H. T., Van, D. M. T. C., Roos, M. and Sterk, P. J.. Pressure-volume analysis of the lung with an exponential and linear-exponential model in asthma and COPD. Eur. Respir. J., 8, 1525-1531, 1995.
12. Svantesson, C., Sigurdsson, S., Larsson, A., Jonson, B., Effects of recruitment of collapsed lung units on elastic pressure-volume relationship in anaesthetized healthy adults. Acta Anaesthesiol. Scand., 42, 721-728, 1998.
13. Hickling, K.G., The pressure-volume curve is greatly modified by recruitment. A mathematical model of ARDS lungs. Am.J. Respir. Crit. Care Med., 158, 194-202, 1998.
14. Narusawa, U., General characteristics of the sigmoidal model equation representing quasi-static pulmonary pressure-volume curves. J. Appl. Physiol., 91, 201-210, 2001.
15. Sonntag, R.E. and Van Wylen, G.J., Fundamentals of Statistical Thermodynamics. John Wiley & Sons, 1966.
16. Fowler, R. and Guggenheim, Statistical Thermodynamics. Cambridge University Press. 1956.

Chapter 3. A Mechanistic Model for Quasi-Static Pulmonary Pressure-Volume Curves: Examination of Clinical Data

Abstract

A p-V equation is developed in Part I based on a mechanistic model of a total respiratory system. In Part II, twenty one $p - V$ data sets of patients with acute respiratory distress syndrome are examined using the mechanistic model, relating the quasi-static pulmonary p-V curve to the corresponding respiratory conditions in terms of a volume increase due to alveolar recruitment and due to elastic tissue distension, the elemental distribution ranging from the closed elements to the saturated (open and fully-distended) elements and its changes with pressure. The compliance (local gradient) of p-V curves is shown to represent the change in the total volume of saturated elements; while the pressure at the maximum compliance is identified as the location where a maximum rate of increase occurs both in the volume increase due to alveolar recruitment and in the volume increase due to an increase in the saturated elements. Validity of the model is provided by its predictions of the upper volume asymptote and the maximum possible volume change of the corresponding deflation process which agree well with the clinical data.

Nomenclature

A_s	piston surface area on which pressure is acting
B	$(k/A_s)\widehat{y}_T = p_0 \cdot \widehat{y}_{T0}$
C	$= \sqrt{\pi}\Lambda/4$
$f,\ F$	distribution functions (Eq.(3))
$I_i\,(i = 1-5)$	functions defined in Eq.(2)
k	spring constant [N/m]
N	total number of TRS elements
N_{open}	total number of open elements
N_{sat}	total number of saturated elements
N_{unsat}	total number of unsaturated elements
N_j	number of elements at energy level j
p	pressure (interpleural pressure difference)
$\overline{p}$	non-dimensional pressure, $p/p_0 - 1$
p_{cj}	critical pressure at which an element, j, 'pops open'.
$\widehat{p}_{cj}$	p_{cj}/p_0
p_f	pressure at the end of inflation
p_o	pressure at the inflection point in model equation
p_{ID}	pressure at the intersect of inflation and deflation processes
V	volume
$V_{pop-open}$	total 'pop-open volume'
V_{sat}	total volume of saturated elements
$V_{open-sat}\,(p = 0)$	total volume of elements open at p = 0 when they are all saturated.
V_p	volume change from the state of $p = 0$
$V_{L(U)}$	lower (upper) bound of volume
V_U^d	an (imaginary) upper bound of volume for the deflation process

$\overline{V}$	non-dimensional volume, $(V - ((V_U + V_L)/2)/(\Delta V/2)$, (Eq.(1b))
$\widehat{V}_j$	volume of an element j
ΔV	$V_U - V_L = N\widehat{V}_0(\widehat{y}_{T0} + 1)$
$\widehat{V}_0$	'pop-open' volume $(= A_s\widehat{y}_0)$
$\widehat{y}_j$	piston displacement of an element j
$\widehat{y}_0$	$= \widehat{V}_0/A_s$
$\widehat{y}_T$	piston stroke limit
$\widehat{y}_{T0}$	$\widehat{y}_T/\widehat{y}_0$

Greek symbols:

α	constant of proportionality
Λ	$\alpha p_0 \Delta V$(non-dimensional parameter) (Eq.(1b))
σ	$(8/\pi)^{1/2}/\Lambda$, Standard deviation (Eq.(3b))
σ_D	$\sigma \cdot p_0$

Superscript:

$\widehat{\ }$	related to a single TRS element
d	deflation process

Acronym:

ARDS	acute respiratory distress syndrome
TRS	total respiratory system

Introduction

In Part I, the error function p-V model equation is shown to agree well with clinical p-V data. The equation and the corresponding non-dimensional form are,

$$V = V_U - \frac{\Delta V}{2} + \left(\frac{\Delta V}{2}\right) \cdot erf\left(C\left(\frac{p}{p_0} - 1\right)\right), \qquad \overline{V} = erf(C\overline{p}). \qquad (1a, b)$$

where $\Delta V = V_U - V_L$, V_U = upper volume asymptote, V_L = lower volume asymptote, p_0 = a pressure at the inflection point of the curve, $C = \sqrt{\pi}\Lambda/4$, $\overline{V} = [V - (V_U + V_L)/2]/(\Delta V/2)$, $\overline{p} = (p/p_0) - 1$.

The mechanistic model of a TRS element developed in Part I is a piston-spring-cylinder system with the alveolar recruitment and the elastic tissue distension represented respectively by the critical pop-open pressure, p_{cj}, and by the displacement of piston against the spring force, $\widehat{y}_j = A_s^2(p - p_{cj})/k$ (A_s = piston surface area, k = spring constant).

Based on the error function p-V equation and the mechanistic model, and allowing for a distribution of elements over p_{cj}, the following model-based p-V equations as well as the corresponding distribution function of TRS elements are derived,

$$V\,(0 \le p \le p_0 \cdot \widehat{y}_{T0}) = \frac{V_U + V_L}{2} + \frac{\Delta V}{\widehat{y}_{T0} + 1}\left(I_3(\overline{p}) + \frac{(1 - I_1)}{2}(\overline{p} + 1 - \widehat{y}_{T0}) - \frac{\widehat{y}_{T0} - 1}{2} I_4 + \frac{2(I_5 - I_2(\overline{p}))}{\pi\Lambda}\right), \quad (2a)$$

$$V\,(p_0 \cdot \widehat{y}_{T0} \le p) = \frac{V_U + V_L}{2} + \frac{\Delta V}{2} I_3(\overline{p}), \quad (2b)$$

$$\frac{dN_j}{N \cdot dp_{cj}} = f(p), \qquad f(p) = \frac{1}{\sqrt{2\pi}\,\sigma_D} \cdot exp\left(-\frac{1}{2}\left[\frac{p_{cj} - (p - p_0)}{\sigma_D}\right]^2\right), \quad (3a)$$

$$\frac{dN_j}{N \cdot d\widehat{p}_{cj}} = F(\overline{p}), \qquad F(\overline{p}) = \frac{1}{\sqrt{2\pi}\,\sigma} \cdot exp\left(-\frac{1}{2}\left[\frac{\widehat{p}_{cj} - \overline{p}}{\sigma}\right]^2\right) \quad (3b)$$

where

$$I_1 = erf(C), \quad I_2(\overline{p}) = exp(-C^2\,\overline{p}^2) - exp(-C^2), \quad I_3(\overline{p}) = erf(C\,\overline{p}),$$

$$I_4 = erf(C(1 - \widehat{y}_{T0})), \quad I_5 = exp(-C^2\,(\widehat{y}_{T0} - 1)^2) - exp(-C^2),$$

$$\sigma_D = (8/\pi)^{\frac{1}{2}}\, p_0/\Lambda, \qquad \sigma = (8/\pi)^{\frac{1}{2}}/\Lambda \qquad \widehat{p}_{cj} = p_{cj}/p_0.$$

Following the development of the mechanistic TRS model and the discussion on relations between the error function p-V equation and the the model-based p-V equation as well as between parameters of the two equations in Part I, our discussions here concentrate on various results that may be derived from applications of the model to the clinical p-V data sets.

Relationship between Inflation and Deflation Processes

Although this report is focused on the mechanistic model for the inflation process, there exist certain relations between the inflation and the deflation process that may be evaluated from the present inflation analyses. We consider a general case in which a quasi-static inflation process proceeds to a pressure, p_{ID} (= end-of-inflation pressure = initial pressure of the corresponding deflation process), followed by a quasi-static deflation process. In terms of the mechanistic model, TRS elements at $p = p_{ID}$ with its critical pop-open pressure less than zero ($p_{cj} < 0$) are still closed and have not contributed to the volume change during the inflation process from $p = 0$ to $p = p_{ID}$; hence, we may postulate that only those elements that are open at $p = p_{ID}$ participate in the deflation process to follow. Therefore, V_U^d (=an (imaginary) upper bound of volume for the deflation p-V curve) may be viewed as the volume which would be attained if the elements that are open at the end of the inflation process, $p = p_{ID}$, were all fully saturated; i.e.

$$V_U^d = V(p = p_{ID}) + \left[\int_0^\infty N\widehat{V}_0(1 + \widehat{y}_{T0}) \cdot F(\overline{p} = \overline{p}_{ID})\, d\widehat{p}_{cj} - V_p(\overline{p} = \overline{p}_{ID}) \right]$$

The first term on the right hand side is the inflation volume at $p = p_{ID}$. The second integral term is the volume summed over all open elements at $p = p_{ID}$ when they are saturated, and the last term is the actual volume increase in the inflation process from $p = 0$ to $p = p_{ID}$ with the two terms in the square bracket together representing a volume increase above $V(p = p_{ID})$ if all open elements at p_{ID} were saturated. Under the assumption that the magnitude of p_{ID} is greater than $B\,(\equiv p_0\,\widehat{y}_{T0})$ which is valid for all data sets analyzed, Eqs.(2,3) along with Eq.(9) of Part I for V_p are used to evaluate the right hand

side, yielding

$$V_U^d = V_L + \frac{2\Delta V}{\pi\Lambda(1+\widehat{y}_{T0})} \cdot I_5 + \frac{\Delta V}{2} \cdot [1 + I_3(\overline{p}_{ID})] + \frac{\Delta V}{2\,(1+\widehat{y}_{T0})} [1 - (2-\widehat{y}_{T0}) \cdot I_1 + (1-\widehat{y}_{T0}) \cdot I_4] \quad (4)$$

The clinical data sets made available to us contain both the inflation and the deflation p-V curves for each patient with ARDS; however, the p-V curves are obtained separately for the inflation and the deflation process. (See [1] for the procedure of data acquisition.) Fig.1 shows inflation (unfilled) and deflation (filled) data points, as well as the corresponding inflation (I) and deflation (D) curves for a typical data set we examined. The inflation curve in Fig.1 is Eq.(2) of the mechanistic model; while, the deflation curve is obtained by straight applications of the method of least squares between data points and the error function p-V equation, Eq.(1). As may be observed from Fig.1, the end-of-inflation point is quite different from the initial deflation point for most data sets. To accommodate the data into the analysis based on Eq.(4), the initial deflation data point is translated horizontally until it meets the inflation p-V curve, the pressure value of which is then defined as p_{ID} in Eq.(4), as indicated in Fig.1, implying that the deflation curve preceded by an inflation curve is assumed to be the same as the deflation curve of data sets horizontally translated until the beginning-of-deflation data point is on the inflation curve.

Fig.2 presents V_U^d of Eq.(4), predicted from the mechanistic model of the inflation process, plotted against V_U^d of the error-function p-V equation, Eq.(1). (For a complete list of numerical results relevant to the analysis, see Table 1.) A maximum and a minimum of a difference, $V_U^d\,(Eq.(4)) - V_U^d\,(Eq.(1))$, are 0.1113 [L] and -0.0352 [L] respectively with an average of the difference = 0.0460 [L]. Agreements are very good in view of the fact that Eq.(4) predicts the upper volume asymptote of the deflation process in terms of the conditions predicted by the mechanistic model of the corresponding inflation process; thus indirectly supporting a certain degree of validity of the mechanistic model. Also, the fact that the magnitude of p_{ID} is determined from the horizontal translation of the deflation

curve indicates that the deflation process may be relatively insensitive to the inflation history prior to $p = p_{ID}$. On the other hand, Eq.(4) for V_U^d contains p_{ID} as variable for specified inflation conditions, indicating that the magnitude of V_U^d (i.e. the shape of the deflation curve) changes as the end-of-inflation pressure is varied. A similar statement has been made previously by Jonson [2]. A closer examination of Fig.2 indicates that the mechanistic model slightly underpredicts V_U^d compared to that of the error-function equation for most of data sets. This could indicate either a quantitative limitation of the mechanistic model or the effects of the inflation process preceding the deflation. If $\widehat{y}_{T0}$ is set to zero, Eq.(4) is reduced to

$$V_U^d\,(\widehat{y}_{T0} = 0) \;=\; V_U \;-\; \Delta V\,(I_1 - I_3(\overline{p}_{ID}))/2. \qquad (4a)$$

Fig.3 plots V_U^d of Eq.(4a) vs V_U^d of the error function p-V equation for the deflation process. Agreements are fairly good between the two. Results presented in Fig.3 reflects that the p-V curve is relatively insensitive to the magnitude of $\widehat{y}_{T0}$; a reason why the antisymmetric error function p-V equation (for which $\widehat{y}_{T0}$ is zero) fits well with p-V curves.

The error function p-V equation fits well not only with the inflation but also with the corresponding deflation processes as shown in Part I. Therefore, regardless of the actual deflation process, we may define ΔV^d (ΔV of the deflation process) as the maximum possible volume change of a specified TRS during the deflation process; which, in our mechanistic model, yields the following equation for ΔV^d in terms of the inflation parameters:

$$\begin{aligned}\Delta V^d &= \widehat{V}_0\,(\widehat{y}_{T0} + 1)\int_0^{\infty} N \cdot F(p = \overline{p}_{ID})\,d\widehat{p}_{cj} \\ &= \frac{\Delta V}{2}\,(1 + I_3(\overline{p}_{ID})). \qquad (5)\end{aligned}$$

Fig.4 is ΔV of deflation, ΔV^d, predicted by Eq.(5) plotted against the corresponding ΔV^d of error-function p-V equation determined by the method of least squares. (See Table 1 for numerical values.) Agreements between the two are reasonably good for a majority of data sets, except for six data sets shown in filled circles accompanied by alphabetical

data numbers. Shown in Fig.5 for the six data sets are their deflation data points and two p-V curves; one (dotted) for the error function p-V equation with the method of least squares applied to determine (Λ^d, p_0^d, ΔV^d, V_U^d), and the other (solid) for the error function p-V equation with (ΔV^d, V_U^d) determined from Eqs.(4,5) and (Λ^d, p_0^d) determined by the method of least squares. Two curves are different in their approaches to different high and low asymptotes. Although agreements of the solid curves (with two adjusting parameters) with the data points are not as good as that of the dotted curves (with four adjusting parameters), the errors are small for the solid curves in view of the fact that the magnitude of ΔV^d is quite different between the two curves, indicating that a better understanding of relations between the p-V equation and the corresponding intra-respiratory changes helps interpret various characterisitcs of p-V curves accurately.

Interpretation of Inflation p-V Curves based on Mechanistic Model

Fig.6 shows ranges covered by all data sets analyzed in terms of p_0 (the inflection pressure of the high-pressure solution), ΔV (maximum volume available for inflation in the high-pressure solution) and $1/(1+\widehat{y}_{T0})$ (the fraction of total elemental volume available for the pop-open mechanism (alveolar recruitment), $N\widehat{V}_0/\Delta V$), all plotted against the non-dimensional parameter, Λ. The data sets with their alphabetical data numbers indicated in the figure are those to be analyzed in detail in comparative analyses to follow. (Various parameters of the six data sets are reproduced as Table 2. Parameters of all data sets are listed in Table 1 of Part I.) The range of Λ is between 1.5 and 3.6 except for Data T ($\Lambda = 5.47$). The six data sets (B, E, M, N, R, T) are different from each other in the following ways:

1. Data set B, E and N have roughly the same magnitude in both Λ ($=\sim 2.65 - 2.80$) and ΔV ($=\sim 1.55 - 1.68$) with significantly different values for p_0.

2. Data set E and T have substantially different values of Λ with p_0 and ΔV being approximately the same in magnitude.

3. N and R also show similar characteristics of being different in Λ and common in p_0 and ΔV; however, the pair covers lower range in both Λ and p_0 compared to E and T.

4. E and M are different in terms of the magnitude of ΔV with $p_{0\,E} \sim p_{0\,M}$, $\Lambda_E \sim \Lambda_M$.

5. T and R represent the data sets with very high and low values of Λ, respectively.

Figs.7 and 8 are p-V and the corresponding non-dimensional $\overline{p} - \overline{V}$ curves over their ranges of measurement for Data Set B, E and N in (a), Data Set E and T in (b), Data Set N and R in (c) and Data Set E and M in (d).

Referring to Fig.7 and noting that the dotted (broken) vertical lines are the location of $p = p_0\,(p_0 \cdot \widehat{y}_{T0})$, it may be observed that the range for the low pressure solution, $0 < p < p_0 \cdot \widehat{y}_{T0}$, in which all elements are active (unsaturated), is very narrow compared to the range for the high pressure solution with an exception of Data set M, for which the measurement does not reach the inflection pressure, p_0, with $p_0 \cdot \widehat{y}_{T0} > 15\,[cmH_2O]$.

The corresponding non-dimensional $(\overline{p} - \overline{V})$ curves, based on the definitions of $\overline{V}$ and $\overline{p}$ in Eq.(1), represent Eqs.(2a,b) in the following normalized form:

$$\begin{aligned}
&\overline{V}\,(-1 \le \overline{p} \le \widehat{y}_{T0} - 1\,) = \\
&\quad + \frac{2}{\widehat{y}_{T0} + 1}\left(I_3(\overline{p}) + \frac{(1 - I_1)}{2}(\overline{p} + 1 - \widehat{y}_{T0}) - \frac{\widehat{y}_{T0} - 1}{2} I_4 + \frac{2(I_5 - I_2(\overline{p}))}{\pi\Lambda} \right), \\
&\overline{V}\,(\widehat{y}_{T0} - 1 \le p) \qquad = I_3(\overline{p}),
\end{aligned} \tag{6}$$

The normalization of volume transforms the two volume asymptotes, V_U and V_L into $\overline{V} = +1$ and $\overline{V} = -1$ respectively; while, the pressure, $p = p_0$, at the inflection point is transformed into $\overline{p} = 0$. With both the location of p_0 and the volume asymptotes made common to all p-V curves, the resulting non-dimensional representations in Fig.8 are characterized by a single non-dimensional parameter, Λ. The parameter, Λ, is twice the maximum local compliance at $p = p_0$ $(d\overline{V}/d\overline{p}(\overline{p} = 0) = \Lambda/2)$. Since the compliance is maximum at the origin of $\overline{p} - \overline{V}$ diagram, the first quadrant $(\overline{V}, \overline{p} > 0)$ in Fig.8 is a region of decreasing local compliance with pressure; while, the third quadrant $(\overline{V}, \overline{p} < 0)$ is a region of increasing local compliance with pressure. The origin (p = 0, V = 0) of

dimensional p-V curves is transformed into ($\overline{p} = -1$, $\overline{V}(V = 0)$) on a $\overline{p}$-$\overline{V}$ curve; hence, the physiological lower limit of $\overline{p}$ is -1.

Fig.8 (a) compares the three data sets, B, E and N, among which the magnitude of p_0 is substantially different with Λ and ΔV being approximately the same in magnitude. Three curves are very close to each other because values of Λ are similar, and the difference between the three appears as the extent to which the p-V curves are measured in the region of decreasing compliance with pressure. In Fig.8 (b) and (c) differences between the two data sets occur in the magnitude of Λ ($\Lambda_T > \Lambda_E$, $\Lambda_N > \Lambda_R$), resulting in the T- and N- curves above the E- and R- curves respectively in the first quadrant. Since the magnitude of p_0 for the data set T and E are very high compared to those for N and R, the region of decreasing compliance covered by the T- and E- curves are narrower than N and R. Because both p_0 and ΔV are similar in magnitudes between the two data sets in Fig.8(b) and (c) the shape of $\overline{p} - \overline{V}$ curves is very similar to the corresponding p-V curves. In Fig.8 (d) two data sets with a high value of p_0 ($\sim 30\,[cmH_2O]$) are shown. For the data set M the high value of p_0 combined with a high value of ΔV limit the measured range of the p-V curve in the region of increasing compliance only, compared to the data set E with a smaller magnitude for ΔV.

Although the $\overline{p} - \overline{V}$ diagram helps distinguish differences among p-V curves and effectively bring out various characteristics of each p-V curve, it is the information from the elemental distribution that relates various parameters of p-V curves to TRS conditions quantitatively. On the normalized $\overline{p} - \overline{V}$ plane of Fig.8 the local compliance at $p = 0$ ($d\overline{V}/d\overline{p}\,(\overline{p} = 0)$) increases with Λ; while, as the standard deviation, σ, is proportional to $1/\Lambda$ in the normalized number distribution, Eq.(3b), the distribution becomes sharper and has a higher peak as Λ is increased. Fig.9 is a plot of the number distribution (not normalized) vs the critical pop-open pressure, p_{cj} in $[cmH_2O]$, for the six data sets analyzed in Figs.7 and 8. The number distribution, $dN_j/N \cdot dp_{cj}$, is a fraction in the number of elements, the critical pop-open pressure of which ranges between p_{cj} and $p_{cj} + dp_{cj}$ in $[1/cmH_2O]$. The

corresponding equation is Eq.(3a), which indicates that the maximum number of elements are present at $p_{cj} = p - p_0$ with its magnitude equal to $1/\sqrt{2\pi} \cdot \sigma_D$ $(= \Lambda/4 \cdot p_0)$. As σ_D decreases the distribution becomes sharper $(\propto 1/\sigma_D)$ and its peak value $(\propto \sigma_D)$ larger. (See Table 2 for the magnitude of σ_D for each data set.) Two distributions are shown in Fig.9 for each data set, one at $p = p_0$ (with its peak at $p = 0$) and the other at $p = p_f$ (end-of-inflation pressure) (with its peak at $p = p_f - p_0$). The vertical line, $p = p_0\,(p_f)$ for the distribution at $p = p_0\,(p_f)$ indicates the pressure above which the distribution is truncated. The dotted parts of the curves, as discussed in Part I, correspond to the elements that are open at p = 0. The normal distribution truncated at $p_{cj} = 0$ and $p_{cj} = p$ (i.e. the solid part of the curves in Fig.9) shifts to the right with an increase in p as more elements become open. When $p < p_0$, the peak of the distribution lies in the negative range of p_{cj}. It should be noted that in Data set M (Fig.9 (c)) the distribution at $p = p_f$ lies below that at $p = p_0$ because the measured range never reached $p = p_0$.

An integral of the distribution function over the critical pop-open pressure in Fig.9 should yield various fractions in number of elements (depending on the upper and lower limits of the integral) at each quasi-static state. Also an integral of a product of the distribution function and the elemental volume over the critical pop-open pressure should provide us with such quantities as the volume change due to alveolar recruitment, due to elastic wall distension and due to an increase in the saturated elements. The following equations may be obtained for changes in the number fractions:

Fraction of the number of open elements at p = p: $N_{open}(p = p)/N$

$$\frac{N_{open}(p=p)}{N}\left(\equiv \int_0^{p/p_0} F(\overline{p})\, d\widehat{p}_{cj}\right) = [I_1 + I_3(\overline{p})]/2, \quad for \quad p \geq 0, \tag{7a}$$

Fraction of the number of saturated elements at p = p: $N_{sat.}(p = p)/N$

$$\frac{N_{sat.}(p=p)}{N}\left(\equiv \int_0^{p/p_0 - \widehat{y}_{T0}} F(\overline{p})\, d\widehat{p}_{cj}\right) = \begin{cases} [I_4 + I_3(\overline{p})]/2, & \text{if } p_0 \cdot \widehat{y}_{T0} \leq p, \\ 0, & \text{if } 0 \leq p \leq p_0 \cdot \widehat{y}_{T0}. \end{cases} \tag{7b}$$

Fraction of the number of unsaturated elements at p = p: $N_{unsat.}(p=p)/N$

$$\frac{N_{unsat.}(p=p)}{N}\left(=\frac{N_{open}-N_{sat.}}{N}\right)=\begin{cases}[I_1-I_4]/2, & \text{if } p_0\cdot\widehat{y}_{T0}\le p,\\ [I_1+I_3(\overline{p})]/2, & \text{if } 0\le p\le p_0\cdot\widehat{y}_{T0}.\end{cases} \tag{7c}$$

Fraction of the number of open elements at p = 0: $N_{open}(p=0)/N$

$$\frac{N_{open}(p=0)}{N}\left(\equiv\int_0^{\infty}F(\overline{p}=-1)\,d\widehat{p}_{cj}\right)=[1-I_1]/2 \tag{7d}$$

It should be noted that (1.) the equation for $N_{open}(p)/N$ does not include the elements that are open at p = 0. (2.) the equation for $N_{sat.}(p)/N$ does not account for the elements that are open at p = 0 and saturated subsequently. (3.) $N_{open}(p=0)/N$ is a function of a single parameter, Λ. (4.) the number fraction of unsaturated elements, $N_{unsat.}(p)/N$, is independent of pressure for $p_0\cdot\widehat{y}_{T0}\le p$, indicating that as more elements are recruited in the region of the high pressure solution the same number of elements are saturated.

Similarly, the following equations are for volume changes as pressure is varied:

Total pop-open volume: $V_{pop-open}(p=p)$

$$V_{pop-open}(p=p)\left(\equiv N\widehat{V}_0\cdot\frac{N_{open}(\overline{p})}{N}\right)=\frac{\Delta V}{2}\frac{1}{1+\widehat{y}_{T0}}\cdot[I_1+I_3(\overline{p})]\quad for\quad p\ge 0. \tag{8a}$$

Total volume of saturated elements: $V_{sat.}(p=p)$

$$V_{sat.}(p=p)\left(\equiv N\widehat{V}_0(1+\widehat{y}_{T0})\cdot\frac{N_{sat.}(\overline{p})}{N}\right)$$
$$=\begin{cases}\Delta V\cdot[I_4+I_3(\overline{p})]/2, & \text{if } p_0\widehat{y}_{T0}\le p,\\ 0, & \text{if } 0\le p\le p_0\cdot\widehat{y}_{T0}.\end{cases} \tag{8b}$$

Total volume of elements open at p = 0 when they are all saturated: $V_{open-sat.}(p=0)$

$$V_{open-sat.}(p=0)\left(\equiv N\widehat{V}_0\widehat{y}_{T0}\cdot\frac{N_{open}(p=0)}{N}\right)$$
$$=\frac{\Delta V}{2}\frac{\widehat{y}_{T0}}{1+\widehat{y}_{T0}}(1-I_1)\quad for\quad p_0\widehat{y}_{T0}\le p. \tag{8c}$$

A number fraction of open elements, $N_{open\,total}(p=p)/N$, may be derived from Eqs.(7a) and (7d) as,

$$\frac{N_{open\,total}(p=p)}{N}\left(=\frac{N_{open}(p=0)}{N}+\frac{N_{open}(p=p)}{N}\right)=\frac{1+I_3(\overline{p})}{2}. \tag{9}$$

The function, $I_3(\overline{p})$ defined in Eq.(2), is an error function, the magnitude of which depends on Λ and p_0. Therefore, the number fraction of all open elements, $N_{open\,total}\,(p = p)/N$, has the point of antisymmetry at $p = p_0$ with two asymptotes of 0 and 1. Fig.10 shows $N_{open\,total}\,(p = p)/N$ vs p of the six representative data sets in solid lines. Due to the antisymmetry with respect to $p = p_0$, the fraction, $N_{open\,total}\,(p = p)/N$, is exactly equal to 0.5 when p is equal to p_0 as the peak of the distribution is located at p = 0. (See Fig.9.) Since the location of $p = p_0\widehat{y}_{T0}$ is the boundary between the low- and high-pressure solutions of the p-V equation, all open elements are still active and unsaturated for $p \leq p_0\widehat{y}_{T0}$. The fraction of open elements at $p = p_0\widehat{y}_{T0}$ is less than 0.2 for four data sets other than Data sets R and M for which the fraction is $\sim$ 0.25. As pressure increases beyond $p_0\widehat{y}_{T0}$, some of the open elements begin to be saturated, the fraction of which, $N_{sat.}(p = p)/N$ of Eq.(7b) is plotted in Fig.10 in broken lines. The number fraction saturated depends on $\widehat{y}_{T0}$ in addition to Λ and p_0. The difference between the two fractions plotted in Fig.10 varies with the magnitudes of the three parameters with $(N_{open\,total}/N - N_{sat.}/N)$ at a specified pressure ranging from $\sim$ 0.28 for Data R to less than 0.01 for Data T. It should also be noted that the two curves are parallel, indicating that the rate of increase in the number of saturated elements is equal to the corresponding rate of opening elements, once pressure exceeds $p_0\widehat{y}_{T0}$.

The number fraction of open elements at p = 0, $N_{open}(p = 0)/N$, of Eq.(7d) represents the percentage of elements that only experience elastic displacement, which may be interpreted as the elemental fraction representing a non-alveolar part of TRS such as airway tissues as well as a dysfunctional alveolar part which does not respond to the recruitment. Fig.11 depicts the fraction as a function of Λ, the only parameter affecting the fraction. As Eq.(7d) shows, the fraction, $N_{open}(p = 0)/N$, has two asymptotes of 0 (as $\Lambda \rightarrow \infty$) and 0.5 (as $\Lambda \rightarrow 0$). Fig.11 indicates that the number fraction of open elements at p=0 is very sensitive to the magnitude of Λ as its value drops from 0.5 to $\sim$ 0.1 when Λ is changed from 0 to 2. It should also be mentioned here that the total volume of elements

open at p = 0 when they are all saturated, $V_{open-sat.}(p=0)$ of Eq.(8c), depends on three parameters, Λ, ΔV and $\widehat{y}_{T0}$, of the mechanistic model. The last column of Table 2 lists $V_{open-sat.}(p=0)$ for the six data sets. Although their magnitudes are small (0.08 [L] or less), the value varies substantially among the data sets.

As mentioned in Part I, the optimization of the ventilator strategy is required for patients with acute lung injury in intensive care units in terms of pressure- and volume-ranges $[3-5]$, taking into account such considerations as a change in the recruited volume with pressure, a rate of recruitment and overdistension of the respiratory tissues. Results of the mechanistic model analyses relevant to the respiratory ventilation are presented in Figs.12 and 13. The volume, $V_{pop-open}$ of Eq.(8a), represents a volume change of TRS due to the pop-open mechanism (alveolar recruitment) only (that is, excluding the volume change due to the displacement of piston (elastic tissue distention)); on the other hand, the volume, $V_{sat.}$ of Eq.(8b), is the total volume of saturated elements of TRS. They both increase as pressure increases along an inflation path. Sketched in Fig.12 are $p-V$ curves (solid, Eq.(2)), $p-V_{pop-open}$ curves (dotted, Eq.(8a)) and $p-V_{sat}$ curves (broken, Eq.(8b)) for the six data sets. The vertical broken line in the figure is the location of $p=p_0$. The intersect between the $p-V_{sat}$ curve and the x axis in the figure is the pressure at the boundary $(=\ p_0\,\widehat{y}_{T0})$ between the low pressure p-V solution (in which all open elements are active (unsaturated)) and the high pressure solution (in which a part of open elements are saturated). Since both the $p-V_{pop-open}$ and the $p-V_{sat}$ relations as well as $p-V\,(p\ >\ p_0\,\widehat{y}_{T0})$ equation are represented by a common function, $I_3\,(\overline{p})$ $(=\ erf(C\,\overline{p})$, $C=\sqrt{\pi}\Lambda/4, \overline{p}=p/p_0-1)$, the pressure at the inflection point, p_0, is not only the pressure at which the local compliance, dV/dp, is maximum, but also the pressure location for a maximum rate of increase in $V_{pop-open}$ as well as in V_{sat} with their gradients given by the following equations;

$$\frac{dV_{sat}(p)}{dp}\left(=\frac{dV(p)}{dp}\right)=\frac{\Delta V\,\Lambda}{4p_0}\cdot exp(-(C\overline{p})^2)\quad for\quad p_0\widehat{y}_{T0}\le p\,,$$

$$\frac{dV_{pop-open}}{dp} = \frac{1}{1+\widehat{y}_{T0}} \cdot \frac{\Delta V\,\Lambda}{4p_0} \cdot exp(-(C\overline{p})^2) \quad for \quad p \geq 0\,. \tag{10}$$

The identity between dV_{sat}/dp and dV/dp implies that the shape of the p-V curves (in the range of the high pressure solution) closely represents the change in the saturated volume rather than the pop-open volume. Since the gradient of $V_{pop-open}$ is smaller than that of V_{sat} by a factor of $1/(1+\widehat{y}_{T0})\,(<1)$, the magnitude of V_{sat} eventually becomes greater than that of $V_{pop-open}$ as pressure increases. Also, $1/(1+\widehat{y}_{T0})$, a fraction of the pop-open volume (= pop-open volume/total volume of a single TRS element), may be interpreted as a gradient ratio of $V_{pop-open}$ to V_{sat}. A smaller value of $\widehat{y}_{T0}$ (i.e. smaller piston stroke limit) means that the element, once it pops open, reaches the saturated state earlier; hence, for Data T of Fig.12(f) ($\widehat{y}_{T0} = 0.289$, $p_0\,\widehat{y}_{T0} = 8.68\,[cmH_2O]$) V_{sat} becomes greater than $V_{pop-open}$ at a pressure close to $p_0\,\widehat{y}_{T0}$, while, for Data M of Fig.12(c) ($\widehat{y}_{T0} = 0.626$, $p_0\widehat{y}_{T0} = 18.98\,[cmH_2O]$) V_{sat} does not overtake $V_{pop-open}$ within the measured pressure range. The gradients, $dV_{pop-open}/dp$ between $p = 0$ and $p = p_f$ (=final pressure) (solid) and $dVsat/dp$ between $p = p_0\,\widehat{y}_{T0}$ and $p = p_f$ (broken) are plotted in Fig.13 for the six data sets. The gradients are symmetric with respect to p_0. The data sets with high gradients (Data set M, N, T) show high sensitivity of the gradients to pressure change near p_0. Other data sets with low gradients, particularly Data set E and R, indicate that the gradients (i.e. the local compliance) do not change too much over a substantial range in pressure around p_0.

Summary

The mechanistic model of TRS developed in Part I is applied to examine p-V curves (in a form of the error function p-V equation) of patients with ARDS with the following results:

1. Parameters of the deflation process, V_U^d in Eq.(4) and ΔV^d in Eq.(5), predicted by the mechanistic model of the corresponding inflation process agree well with those of the error function p-V equation for the deflation process (Figs.2, 4), indicating that the

mechanistic model has a certain validity to be used for improving our quantitative understanding of various intra-respiratory conditions, that the shape and characteristics of deflation curves depend not so much on the inflation history but on the end-of-inflation (the onset-of-deflation) pressure, and that relations between parameters in p-V equation and TRS conditions are needed to strengthen our applications of p-V curves in clinical settings (Fig.5).

2. The non-dimensional p-V curve, $\overline{p} - \overline{V}$ curve, is effective in distinguishing differences in magnitudes of model parameters among different p-V curves (Figs.7, 8).

3. In the mechanistic model, the distribution function, Eq.(3), and its change with pressure are the basis for evaluating alveolar recruitment and the elastic tissue distension. The shape of the distribution function (the peak value and the standard deviation) is determined by the magnitude of the non-dimensional parameter, Λ; while, the magnitude of the pressure at the maximum compliance, p_0, and its location relative to the range of the p-V curve are the important factors affecting changes of the distribution with pressure (Eqs.(7)(9), Figs.9,10,11).

4. In addition to Λ and p_0, other parameters of the model, ΔV, V_U and $\widehat{y}_{T0}$ influence the magnitude and changes of both $V_{pop-open}$ (volume increase due to alveolar recruitment) and V_{sat} (total volume of saturated (fully-distended) elements). The shape of the clinically-measured p-V curve represent the change in V_{sat}. The inflection pressure, p_0, is not only the pressure at which the local compliance, dV/dp, is maximum, but also the pressure location for a maximum rate of increase in $V_{pop-open}$ as well as in V_{sat} (Eqs.(8),(10), Figs.11,12).

The mechanistic model of a TRS element presented in this report consists of a simple piston-spring-cylinder system with the critical pop-open pressure of the element as distribution parameter. The pop-open volume (= volume that pops open at the critical pressure) as well as the spring constant are assumed constant and common to all elements. More comprehensive and detailed analyses of clinical data as well as advice from clinical experts are needed to advance the model further and also to make it a practical tool for

understanding various respiratory conditions. However, it is believed that the analyses presented here show the developments and use of a mechanistic model as a possible new approach to investigate respiratory systems.

Figure/Table Captions

Table 1. Summary of Deflation Data Analysis.

Table 2. Parameters of Inflation Data Sets Examined

Fig. 1. Data points for inflation (unfilled) and deflation (filled), and the corresponding p-V equation of mechanistic model for inflation (I). and the error function p-V equation for deflation (D),

p_{ID} = pressure at the intersect of the inflation curve and a line parallel to the x-axis passing through the initial deflation data point.

(See Table 1 of Part I (II) for numerical values of parameters for inflation (deflation).)

Fig. 2. V_U^d (predicted from the mechanistic model) vs V_U^d (of error-function p-V equation for deflation).

Fig. 3. V_U^d (predicted from the mechanistic model with $\widehat{y}_{T0} = 0$) vs V_U^d (of error-function p-V equation for deflation).

Fig. 4. ΔV^d (predicted from the mechanistic model) vs ΔV^d (of error-function p-V equation for deflation). Letters in the figure = Data No.

Fig. 5. Deflation curves.

triangle = data points, dotted = error function p-V equation with the method of least squares applied to determine (Λ^d, p_0^d, ΔV^d, V_U^d),

solid = error function p-V equation with (ΔV^d, V_U^d) determined from Eqs.(4,5) and (Λ^d, p_0^d) determined by the method of least squares.

Fig. 6. Ranges of parameters of inflation data sets.

(a) p_0 vs Λ, (b) ΔV vs Λ, (c) $1/(1+\widehat{y}_{T0})$ vs Λ. Letters in the figure = Data No.

Fig. 7. Model-based p-V equation.

(a) Data Set B, E and N. (b) Data Set E and T.

(c) Data Set N and R. (d)Data Set E and M.

Vertical lines: dotted = p_0, broken = $p_0 \widehat{y}_{T0}$.

Fig. 8. Non-dimensional $(\overline{p} - \overline{V})$ equation.

(a) Data Set B, E and N. (b) Data Set E and T.

(c) Data Set N and R. (d)Data Set E and M.

Fig. 9. Distribution of elements.

(a) through (f) for Data Sets B(=(a)), E, M, N, R and T(=(f)).

Fig.10. Number fraction of total open elements, $N_{open\,total}\,(p = p)/N$, vs pressure (solid) and number fraction of saturated elements, $N_{sat.}\,(p = p)/N$, vs pressure (broken).

(a) through (f) for Data Sets B(=(a)), E, M, N, R and T(=(f)).

Fig.11. Number fraction of open elements at p = 0, $N_{open}(p = 0)/N$ vs Λ

Fig.12. $p - V$ curve (solid, Eq.(2)), $p - V_{pop-open}$ curve (dotted, Eq.(8a)) and $p - V_{sat}$ curve (broken, Eq.(8b)) for six data sets.

(a) through (f) for Data Sets B(=(a)), E, M, N, R and T(=(f)).

Letters in the figure = Data No.

Fig.13. $dV_{pop-open}/dp$ $[L/cmH_2O]$ vs p $[cmH_2O]$ (solid) and $dVsat/dp$ $[L/cmH_2O]$ vs p $[cmH_2O]$ (broken) for six data sets.

(a) through (f) for Data Sets B(=(a)), E, M, N, R and T(=(f)).

Table 1. Summary of Deflation Data Analysis

Data No	Λ^d	p_0^d $[cmH_2O]$	ΔV^d [L]	V_L^d [L]	V_U^d [L]
A 1.	1.4712	11.410	1.9214	-0.1528	1.7685
2.			1.7567		1.7064
B 1.	1.5528	12.975	1.4115	-0.1227	1.2887
2.			1.3405		1.2808
C 1.	2.3293	14.808	1.1753	0.0800	1.2599
2.			1.2525		1.2259
D 1.	1.0772	6.846	2.7012	-0.6096	2.0915
2.			2.5850		2.0572
E 1.	2.2044	15.602	0.7009	0.0703	0.7712
2.			0.7784		0.7329
F 1.	1.7995	14.418	1.0476	-0.0527	0.9948
2.			1.0041		0.9252
G 1.	0.9839	8.140	1.2811	0.0454	1.3265
2.			1.6496		1.3455
H 1.	0.7147	6.472	2.0772	-1.0349	1.0423
2.			1.1910		1.0053
I 1.	2.1010	14.157	1.4798	0.5637	2.0435
2.			1.9943		1.9784
J 1.	1.6600	13.404	1.8960	-0.1250	1.7103
2.			1.7759		1.6858
K 1.	1.0577	9.778	1.5070	-0.3657	1.1412
2.			1.1620		1.0860
L 1.	0.3107	3.151	1.3930	-0.8076	0.5853
2.			0.8574		0.6206
M 1.	2.1702	14.989	1.4322	0.1442	1.5764
2.			1.4921		1.5163
N 1.	0.7220	6.45	2.4020	-1.1900	1.2140
2.			1.1654		1.1115
O 1.	1.0558	10.969	1.8684	-0.3195	1.5488
2.			1.6515		1.4375
P 1.	1.5406	12.231	0.7461	0.0684	0.8145
2.			0.8679		0.8154
Q 1.	1.1691	10.670	1.1801	-0.1515	1.0285
2.			1.0938		0.9857
R 1.	0.8643	8.1411	1.8260	-0.4893	1.3366
2.			1.7784		1.2923
S 1.	2.7458	17.050	2.0015	-0.5673	1.4341
2.			1.4461		1.3962
T 1.	4.5056	23.619	1.1748	0.1057	1.2805
2.			1.2115		1.2026
U 1.	2.9735	18.599	2.3404	0.0408	2.3812
2.			2.5197		2.3305

1. Obtained by method of least squares with error function p-V equation for deflation process.
2. Results from the mechanistic model of inflation process.

Table 2. Parameters of Inflation Data Sets Examined

Data	Λ	p_0	ΔV	$1/(1+\widehat{y}_{T0})$	$\widehat{y}_{T0}$	σ_D	$V_{open-sat.}(p=0)$
B	2.7304	21.999	1.5559	0.736	0.359	12.857	0.01789
E	2.6497	30.817	1.6847	0.676	0.480	18.559	0.02645
M	2.9972	30.327	4.2463	0.615	0.626	16.147	0.04932
N	2.8046	15.297	1.6219	0.736	0.358	8.704	0.01685
R	1.6209	16.352	1.7396	0.711	0.406	16.098	0.07779
T	5.4708	30.037	1.7694	0.766	0.289	8.761	0.00012

p_0 and σ_D in $[cmH_2O]$, ΔV and $V_{open-sat.}(p=0)$ in [L].

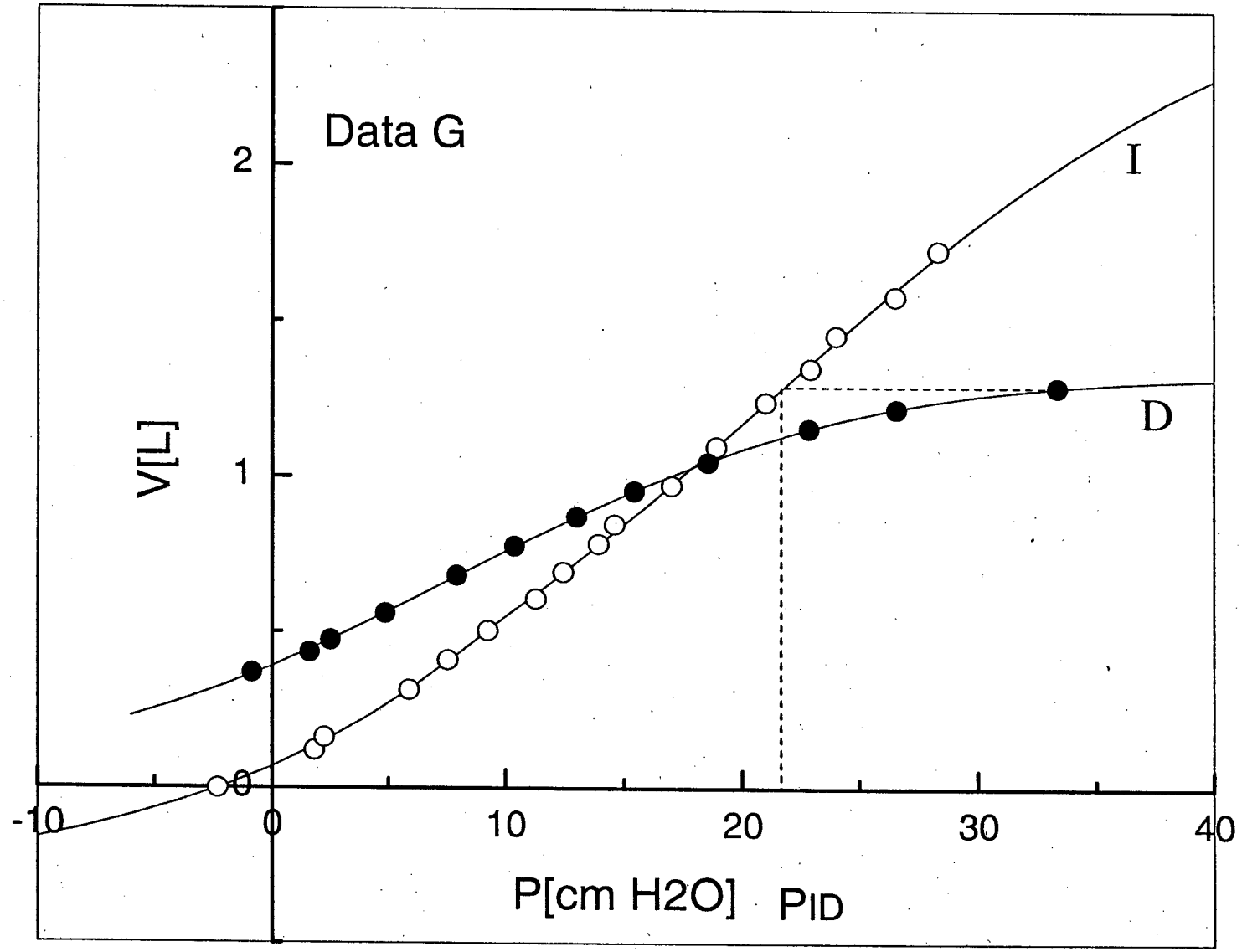

Fig. 1. Data points for inflation (unfilled) and deflation(filled), and the corresponding p-V equation of mechanistic model for Inflation (I) and the error function p-V equation for deflation (D). PID = pressure at the intersect of the inflation curve and a line parallel to the x-axis passing through the initial deflation data point.
(See Table 1 of Part I(II) for numerical values of parameters for inflation (deflation).)

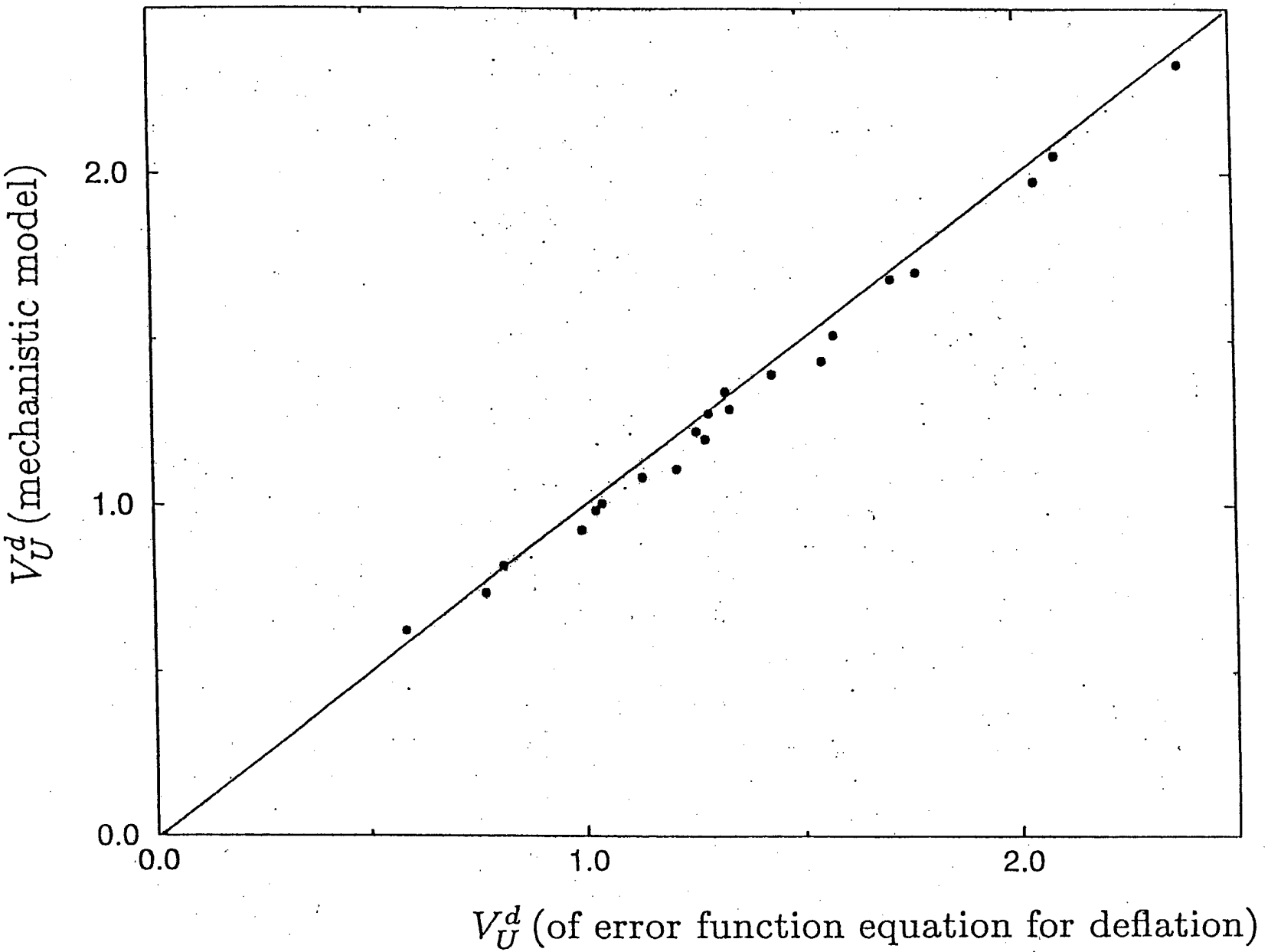
2.0
1.0
0.0
0.0
1.0
2.0
V_U^d (mechanistic model)
V_U^d (of error function equation for deflation)

Fig.2

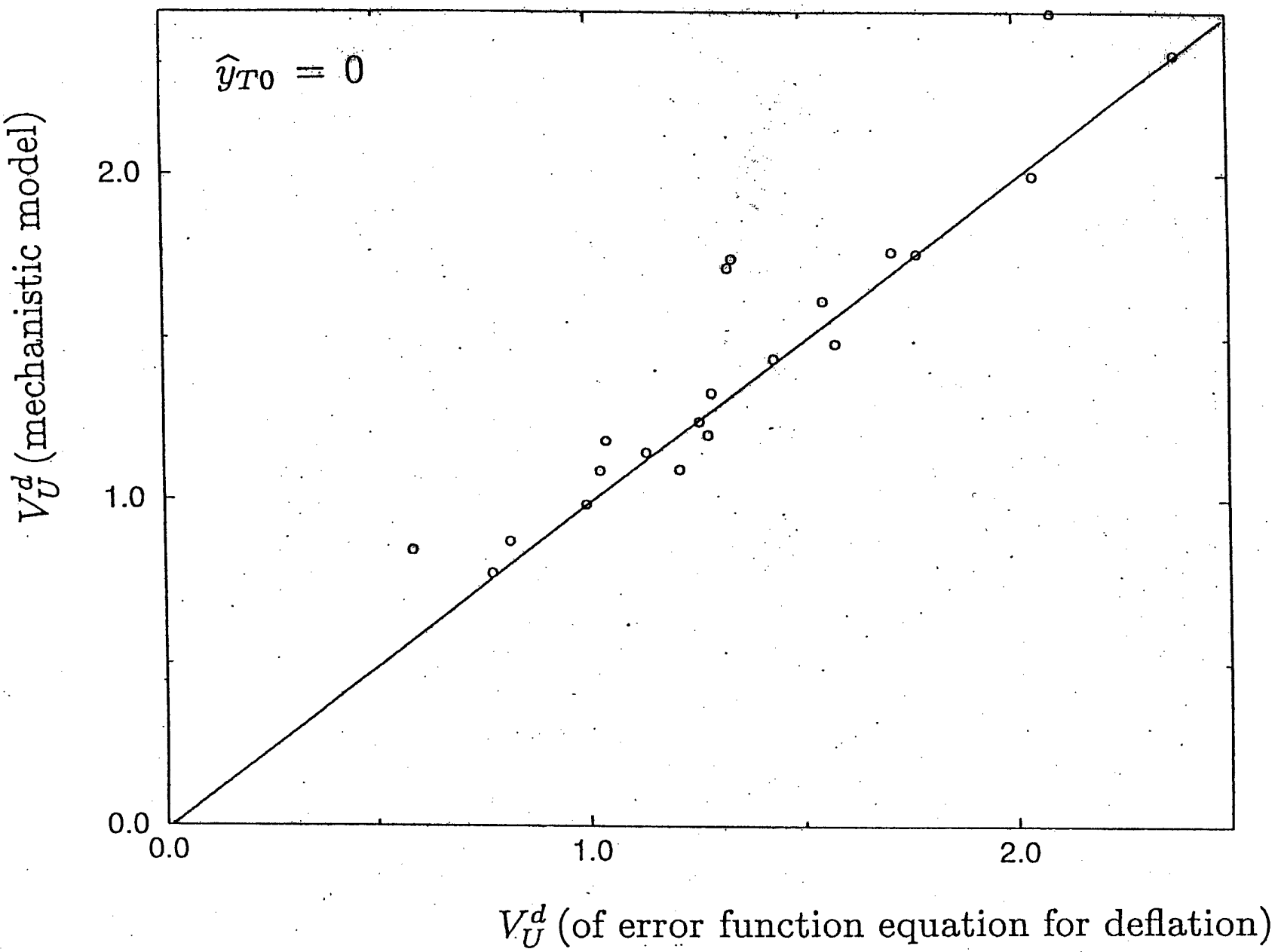
$\widehat{y}_{T0} = 0$
V_U^d (mechanistic model)
2.0
1.0
0.0
0.0
1.0
2.0
V_U^d (of error function equation for deflation)

Fig.3

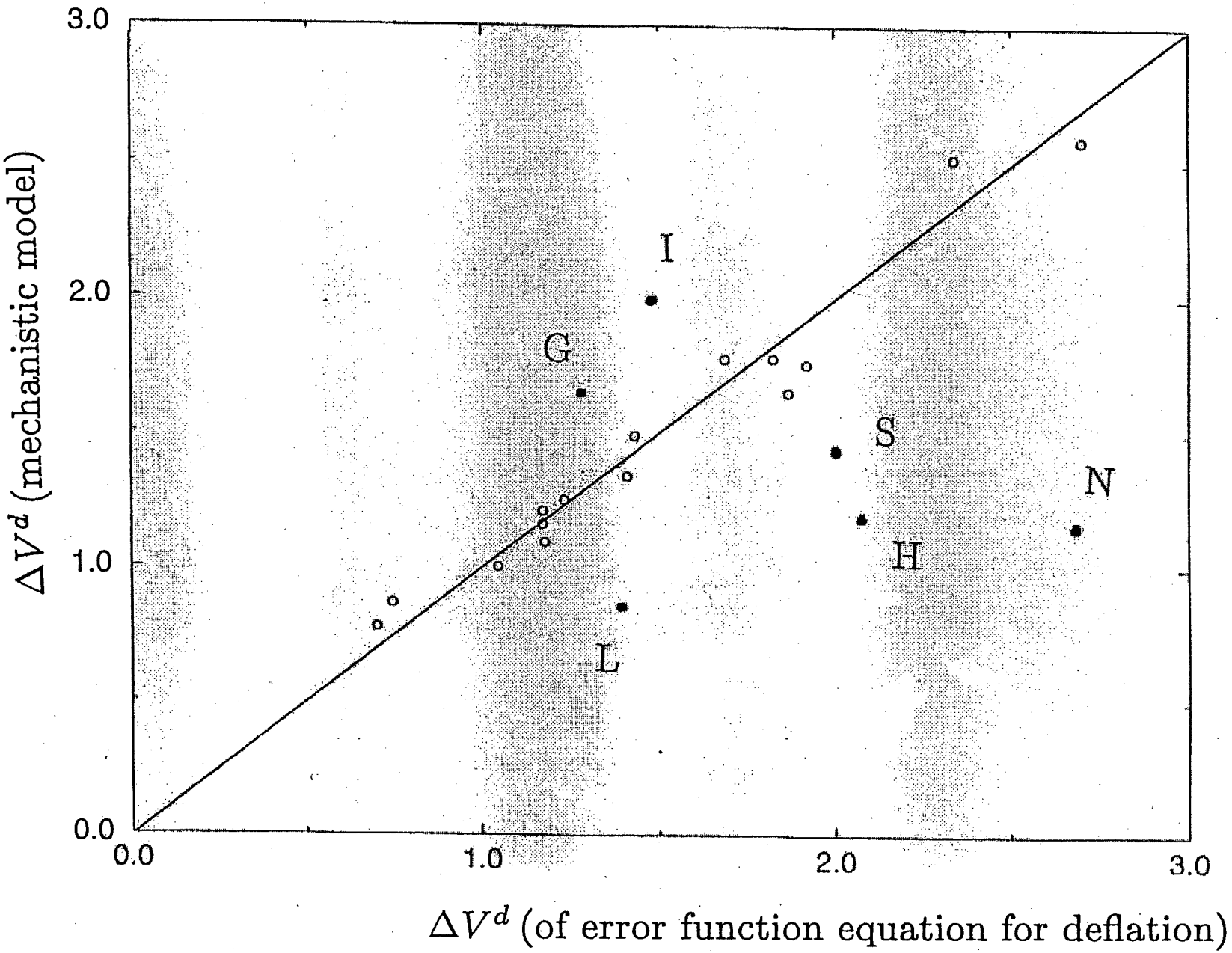
3.0
2.0
1.0
0.0
0.0
1.0
2.0
3.0
ΔV^d (mechanistic model)
ΔV^d (of error function equation for deflation)
I
G
S
N
H
L

Fig.4

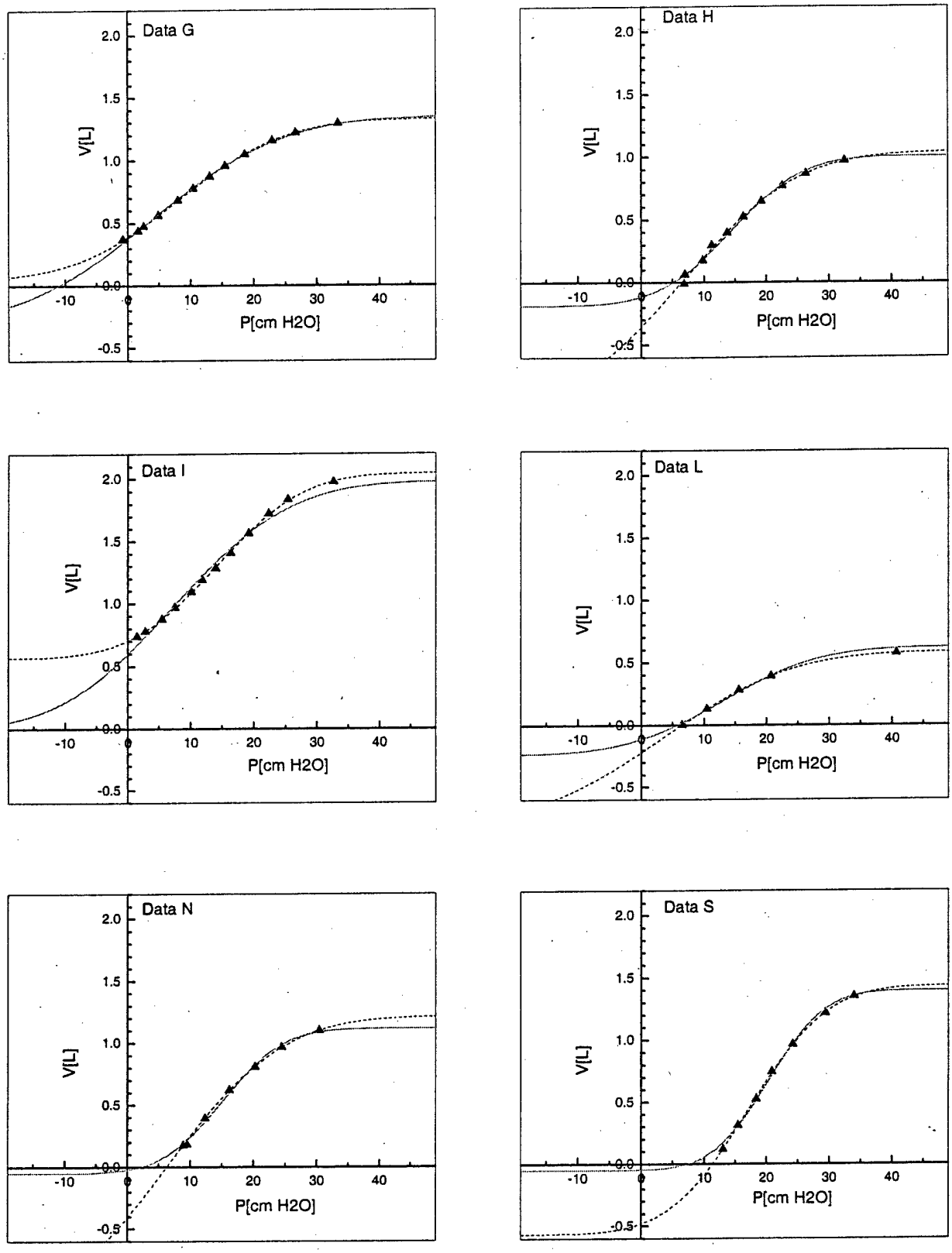

Fig 5. triangle = data points, dotted error function p-V equation with the method of least squares applied to determine ($\Lambda^d, p_0^d, \Delta V^d, V_U^d$) ,
Solid = error function p-V equation with ($\Delta V^d, V_U^d$) determined from Eqs. (4,5) and (Λ^d, p_0^d) determined by method of least squares.

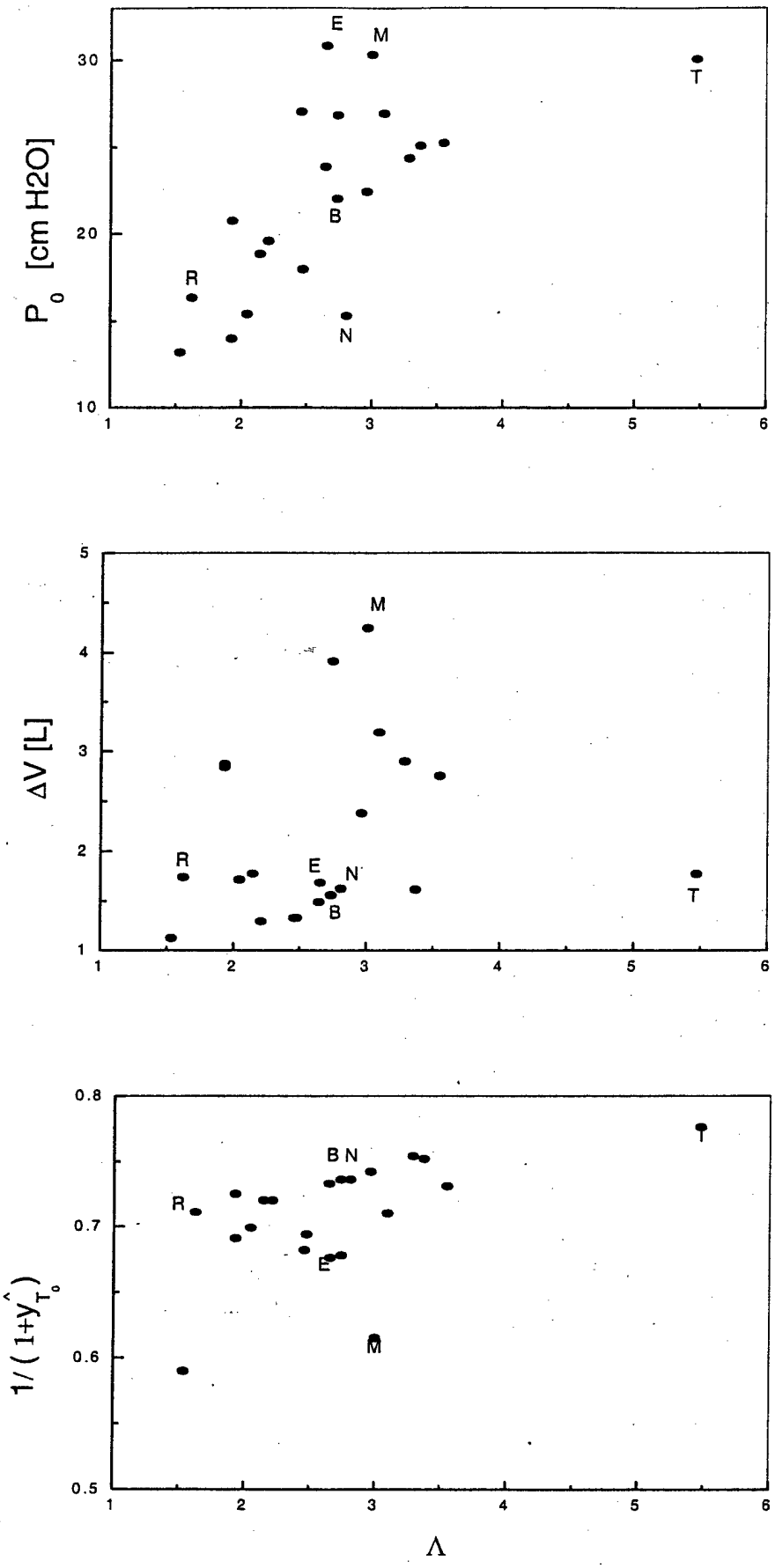

Fig 6. Ranges of Parameter of inflation data sets.(Letters in figure= Data No.)

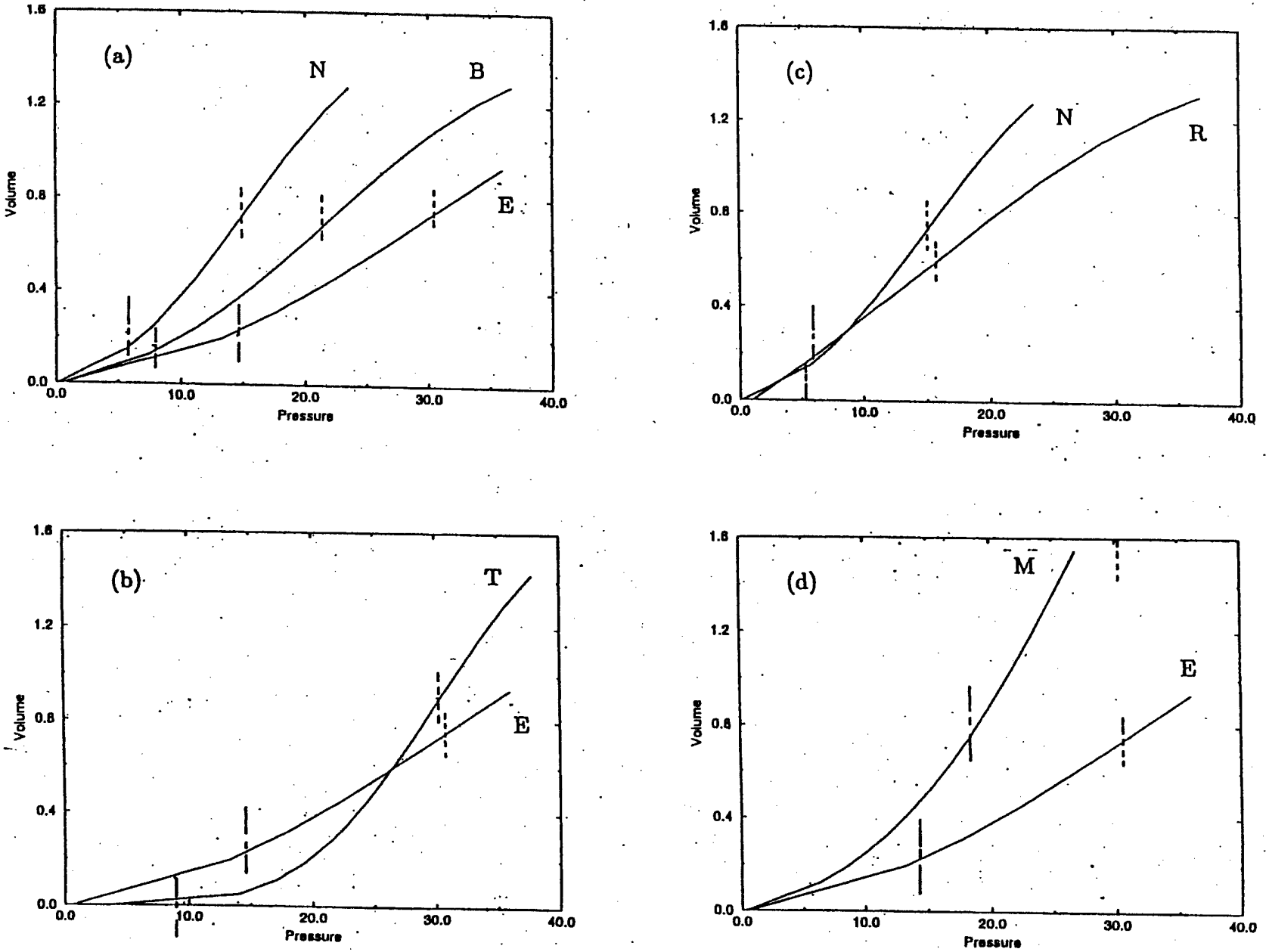

Fig. 7. Model-based p-V equation.

(a) Data Set B, E and N. (b) Data Set E and T.

(c) Data Set N and R. (d)Data Set E and M.

Vertical lines: dotted = p_0, broken = $p_0\,\widehat{y}_{T0}$.

Fig. 7

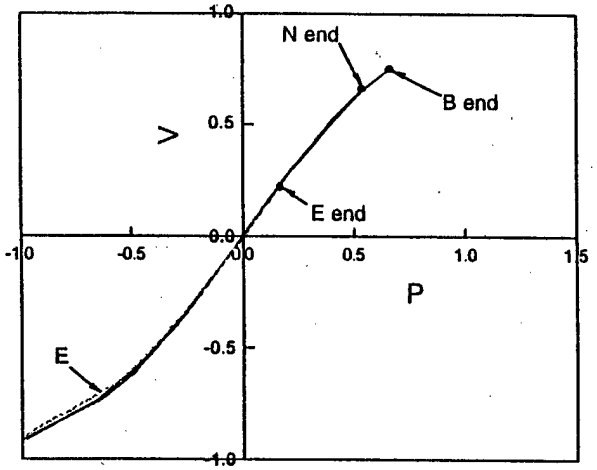

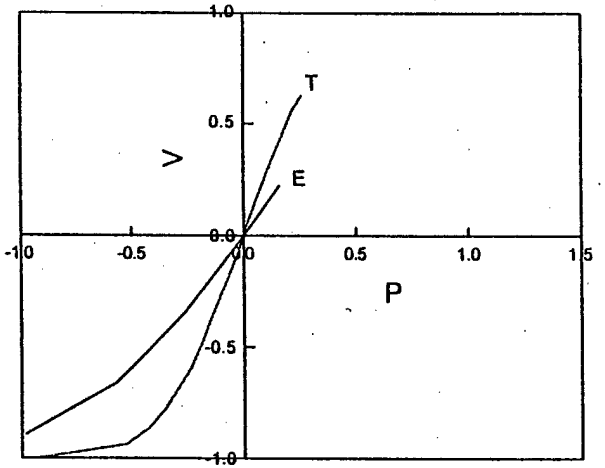

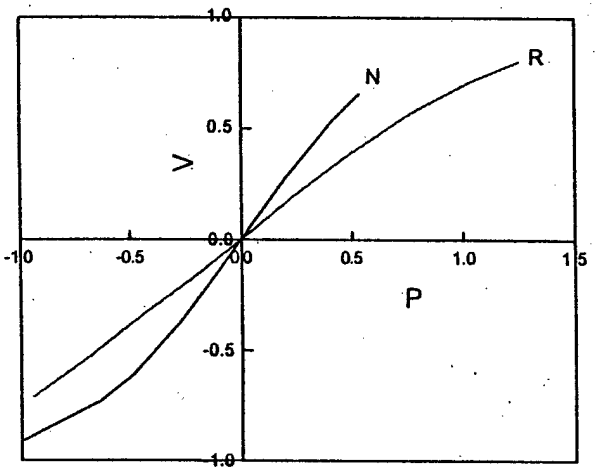

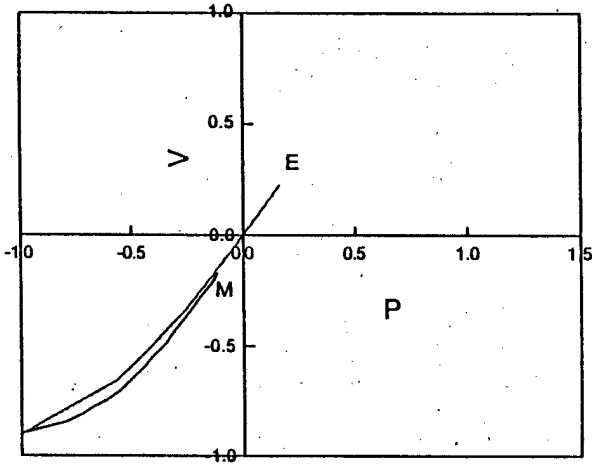

Fig. 8. Non-dimensional $(\overline{p} - \overline{V})$ equation.

(a) Data Set B, E and N. (b) Data Set E and T.

(c) Data Set N and R. (d)Data Set E and M.

Fig. 8

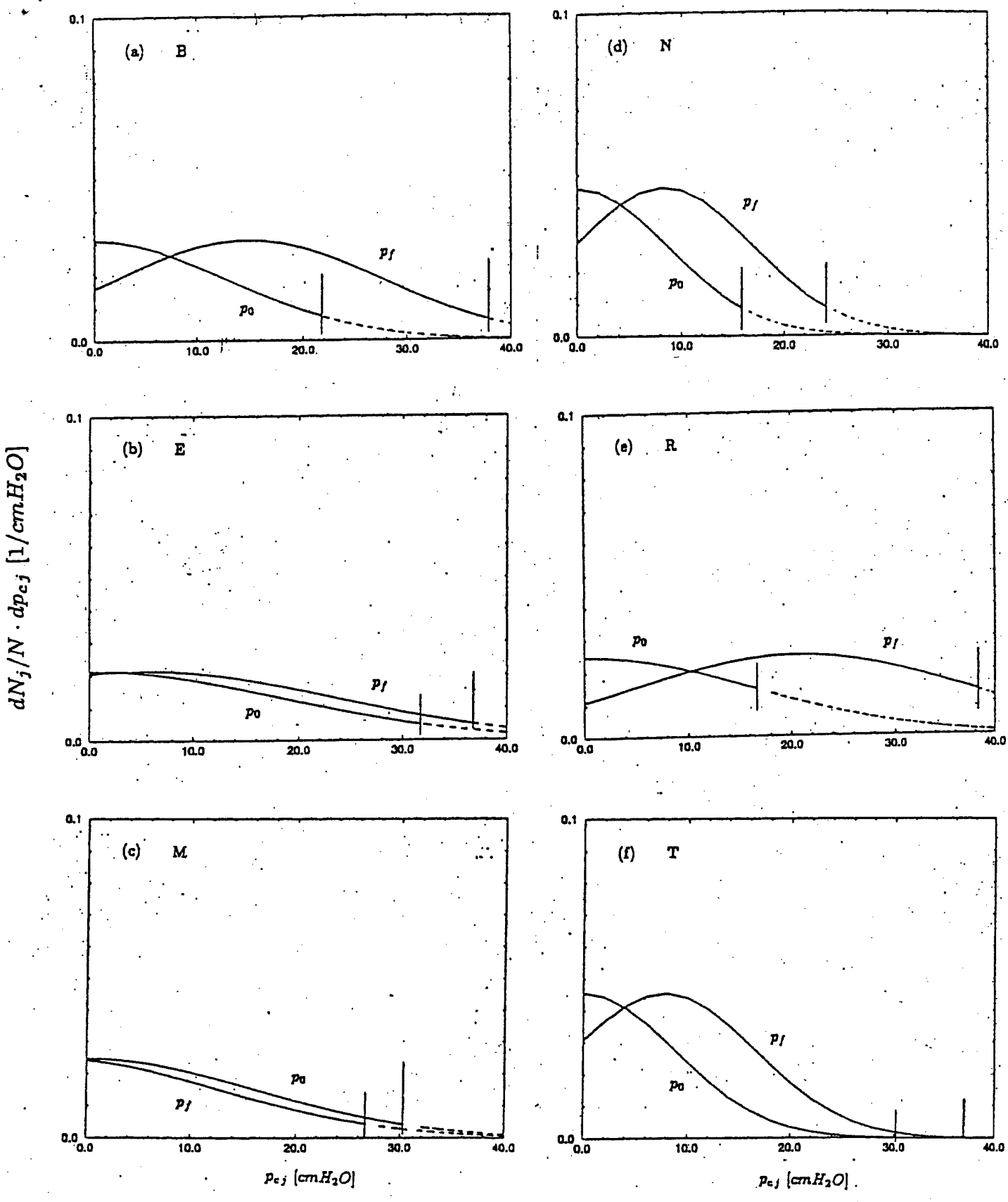

Fig. 9. Distribution of elements.

(a) through (f) for Data Sets B(=(a)), E, M, N, R and T(=(f)).

Fig.9

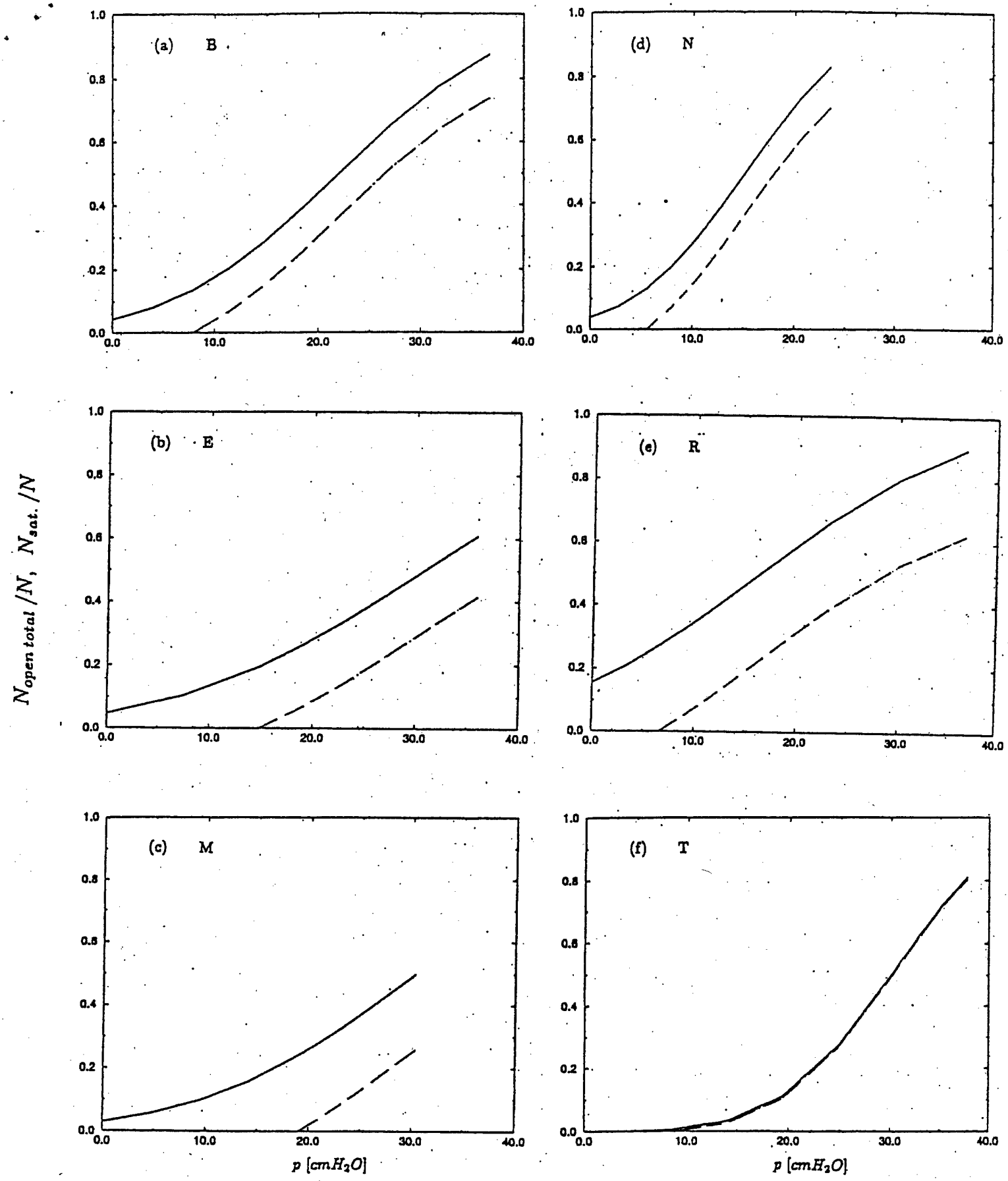

Fig.10. Number fraction of total open elements, $N_{open\ total}\ (p = p)/N$, vs pressure (solid) and number fraction of saturated elements, $N_{sat.}\ (p = p)/N$, vs pressure (broken). (a) through (f) for Data Sets B(=(a)), E, M, N, R and T(=(f)).

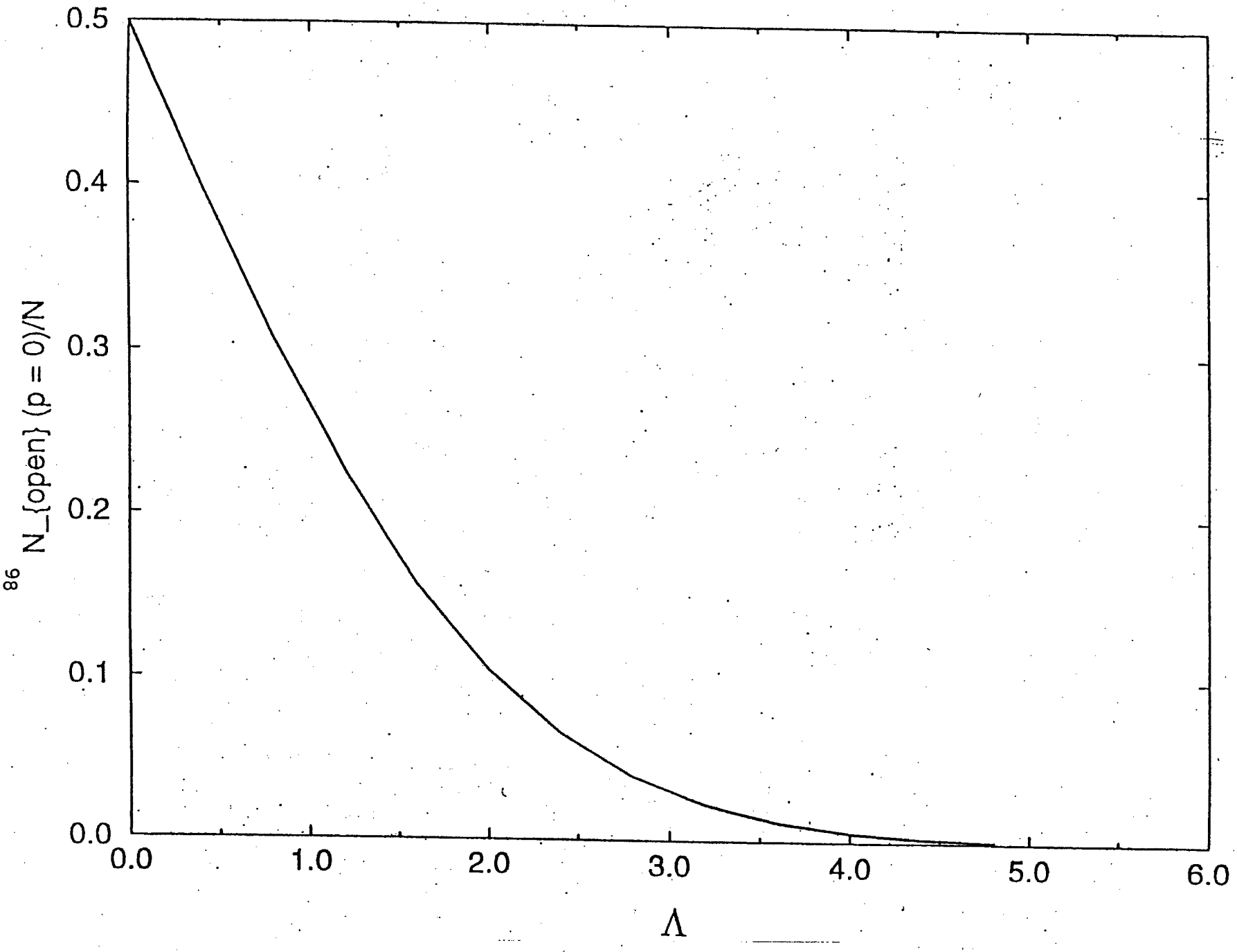

Fig.11. Number fraction of open elements at p = 0, $N_{open}(p = 0)/N$ vs Λ

Fig.11

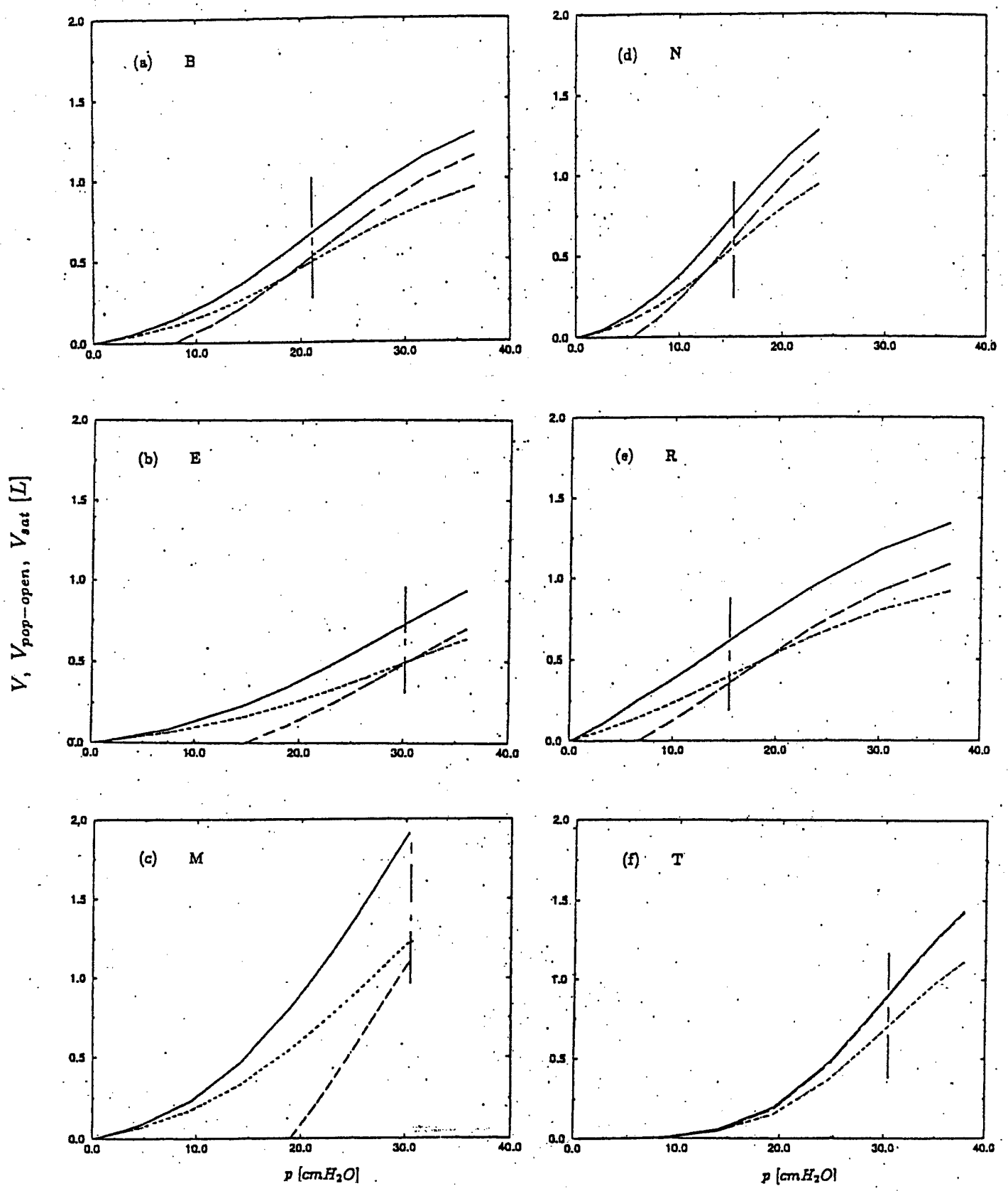

Fig.12. $p - V$ curve (solid, Eq.(2)), $p - V_{pop-open}$ curve (dotted, Eq.(8a)) and $p - V_{sat}$ curve (broken, Eq.(8b)) for six data sets.

(a) through (f) for Data Sets B(=(a)), E, M, N, R and T(=(f)).

Letters in the figure = Data No.

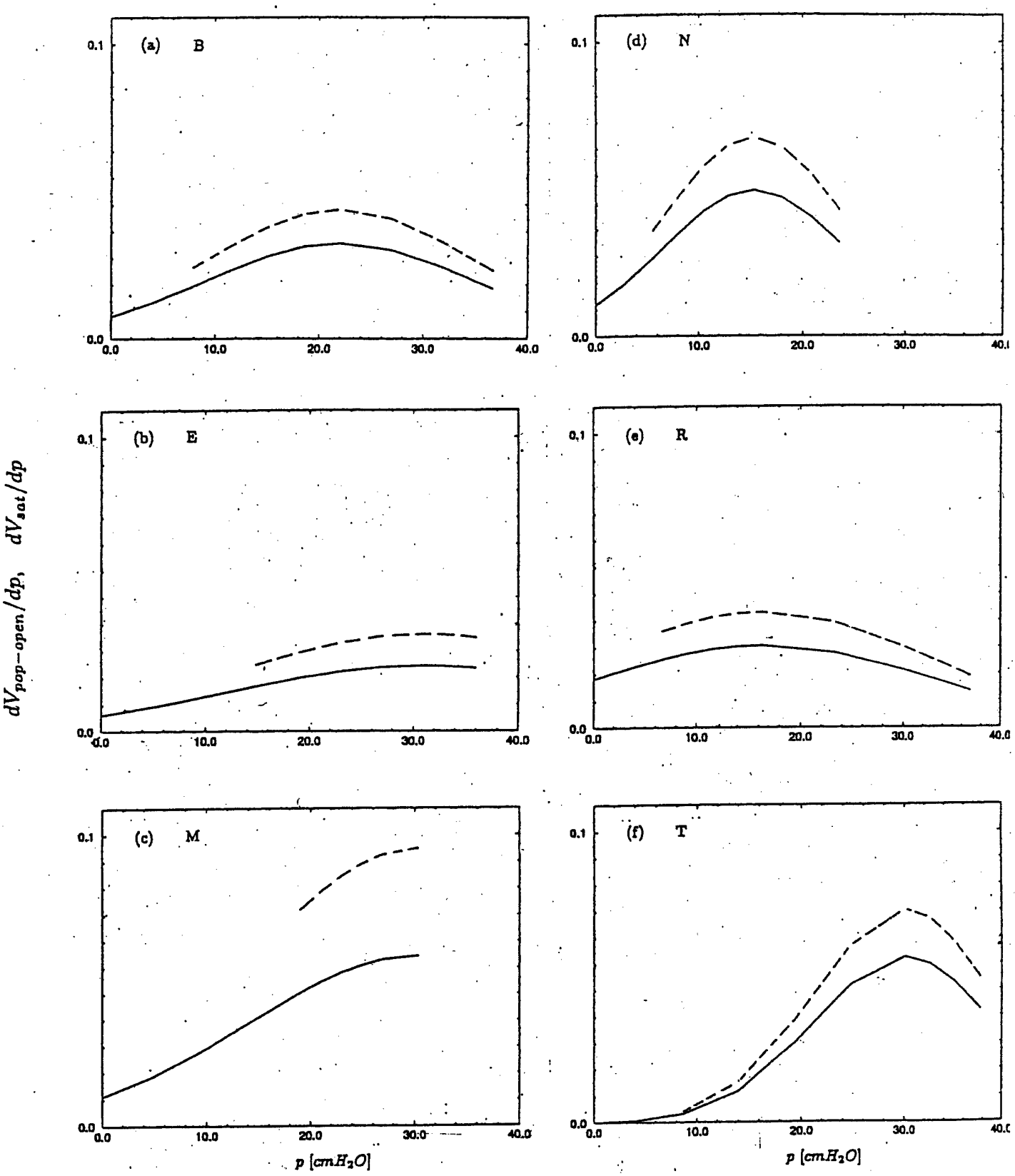

Fig.13. $dV_{pop-open}/dp$ $[L/cmH_2O]$ vs p $[cmH_2O]$ (solid)
and $dVsat/dp$ $[L/cmH_2O]$ vs p $[cmH_2O]$ (broken) for six data sets.
(a) through (f) for Data Sets B(=(a)), E, M, N, R and T(=(f)).

References

1. Harris, S.R., Hess, D.R., Venegas, J.G., An objective analysis of the pressure-volume curve in the acute respiratory distress syndrome. Am.J.Respir.Crit.Care Med., 161, 432-439, 2000.
2. Jonson, B., Svantesson, C., Elastic pressure-volume curves: What information do they convey ? Thorax, 54, 82-87, 1999.
3. Amato, M.B., Barbas, C.S., Medeiros, D.M., Schettino, G.D.P., Lorenzi, F.G., Kairalla R.A., Deheinzelin, D., Morais, C., Fernandes, E.D.O., and Takagaki, T.Y., Beneficial effects of the "open lung approach" with low distending pressures in acute respiratory distress syndrome. A prospective randomized study on mechanical ventilation. Am.J.Respir.Crit.Care Med., 152, 1835-1846, 1995.
4. Amato, M.B., Barbas, C.S., Medeiros, D.M., Magaldi, G.P., Schettino, G.D.P., Kairalla R.A., Deheinzelin, D., Munozs, C., Oliveira, R., Takagaki, T.Y., and Calvalho, C.R., Effect of a protective-ventilation strategy on mortality in the acute respiratory distress syndrome. New Engl. J. Med., 347-354, 1998.
5. ARDS Network, Ventilation with lower tidal volumes as compared with traditional tidal volumes for acute lung injury and the acute respiratory distress syndrome. N. Engl. J. Med. 342 (18), 1301-1308, 2000.

Key Research Accomplishments

1. A representation of p-V curves by a single (non-linear) model equation (either the error-function p-V model equation or the sigmoidal model equation) is confirmed to be an effective method for clinical data analyses.
2. A mechanistic model for the inflation process is constructed; which makes it possible to yield information on the internal conditions of the respiratory system from the p-V curve.
3. The ability of the mechanistic model of the inflation process to yield information on the deflation process correctly justifies its further development as a new tool for processing p-V curves in practical environments.

Reportable Outcomes

Degrees obtained that are supported by this award:

Reza Amini: Master of Science in Mechanical Engineering, August 2002

Funding applied for based on work supported by this award:

Title: P-V Curve Analyses based on a Respiratory System Model.

submitted to,

National Institute of Health (Assignment Number yet to be issued).

Principal Investigator: Narusawa, Uichiro

with two co-principal investigators.

Eighteen month project

Objective: To relate predictions of the mechanistic model developed under this award to clinical diagnoses of patients with acute lung injury, and to refine the model further if needed.

Research Experience for Undergraduate students

1 student for Honor's Thesis (March — June, 2002)

1 student for Undergraduate Special Project (March — June, 2002)

Note:

There is no journal publication resulting from this one-year research project yet. At this stage, we are in the process of applying for journal publications. Any articles based on work under this award will be reported to USAMRMC in future.

Conclusions

It is shown that both the sigmoidal (tangent hyperbolic) p-V model equation and the error function model equation represent quasi-static p-V curves well. Major parameters of both the sigmoidal and the error function model equations are the non-dimensional compliance, Λ, the maximum local compliance, p_0, the upper (or lower) volume asymptote, V_U (V_L), and the maximum volume available for inflation, ΔV. Although both continuous model equations are antisymmetric with respect to p_0, the non-dimensional parameter, Λ, as well as two volume asymptotes slightly differ between the two equations as those function-specific parameters are selected to follow a specified p-V curve as closely as possible. The p-V model equation in the form of the error-function (because of its relevance to the mechanistic model) is applied to data sources of patients with ARDS as well as of healthy adults to show that the the magnitudes of the model equation parameters distinguish various p-V curves clearly.

A mechanistic model of TRS elements, each consisting of a piston-spring system, is developed to analyze p-V curves for the inflation process. The model accommodates both the alveolar recruitment (in terms of the critical pop-open pressure) and the elastic distension of wall tissues (in terms of the piston displacement). Model-based relations are established between the parameters in the $p - V$ curve represented by the error function equation, and in the mechanistic model. The p-V equation derived from the mechanistic model consists of two equations; one for the low pressure region where all open elements are active (= unsaturated) as the piston of an element is yet to reach its stroke limit, and the other for the high pressure region where some open elements are saturated. The elemental distribution over the critical pop-open pressure is a normal distribution with its shape (the mean and the standard deviation) affected substantially by the magnitudes of two parameters of the model, Λ and p_0.

The mechanistic model is applied to p-V curves of patients with ARDS. Parameters of the deflation process, V_U^d and ΔV^d, predicted by the mechanistic model of the corre-

sponding inflation process agree well with those of the p-V model equation for the deflation process (Chapter 3, Figs.2, 4), thus providing justifications for its validity to be used for improving our quantitative understanding of various intra-respiratory conditions. In the mechanistic model, the distribution of TRS elements and its change with pressure are the basis for evaluating alveolar recruitment and the elastic tissue distension. The shape of the distribution function (the peak value and the standard deviation) is determined by the magnitude of the non-dimensional parameter, Λ; while, the magnitude of the pressure at the maximum compliance, p_0, and its location relative to the range of the p-V curve are shown to be important factors affecting changes of the distribution with pressure. The other parameters of the model, ΔV, V_U and $\widehat{y}_{T0}$ influence the magnitude and changes of both $V_{pop-open}$ (volume increase due to alveolar recruitment) and V_{sat} (total volume of saturated (fully-distended) elements).

We are currently in the process of developing a method of analyzing the deflation curve based on our mechanistic model. After a mechanistic model is derived for the deflation process, it is possible to analyze both the inflation and the deflation process together; which would yield a greater amount of quantitative information on the respiratory conditions than the analyses of the inflation process alone.

More comprehensive and detailed analyses of clinical data as well as advice from clinical experts are needed to refine the model further and also to relate predictions by the mechanistic model to clinical diagnoses. However, it is believed that the analyses presented here show the developments and use of a mechanistic model as a new, effective approach to investigate respiratory systems of patients with acute lung injury.

References

Chapter 1.

1. Salazar, E., Knowles., J.H., An analysis of pressure-volume characteristics of the lungs. J. Appl. Physiol., 1964, 19, 97-104.
2. Paiva, M., Yernault, J.C., VanErdeweghe, P., Englert, M., A sigmoidal model of the static volume-pressure curve of human lung. Respir. Physiol., 1975, 23, 317-323.
3. Murphy, B.G., Engel, L.A., Models of the pressure-volume relationship of the human lung. Respir. Physiol., 1978, 32, 183-194.
4. Gibson, G. J., Pride, J. B., Davis, J., Schroter, R. C., Exponential description of the static pressure-volume curve of normal and diseased lungs. Am. Rev. Respir. Dis., 1979, 120: 799-811.
5. Greaves, I. A., Colebatch, H. J., Elastic behavior and structure of normal and emphysematous lungs post mortem. Am. Rev. Respir. Dis., 1980, 121, 127-136.
6. Schroter, R. C., Quantitative comparisons of mammalian lung pressure-volume curves. Respir. Physiol., 1980, 42, 101-107.
7. Gugger, M., Wraith, P. K., Sudlow, M. F., A new method of analysing pulmonary quasi-static pressure-volume curves in normal subjects and in patients with chronic airflow obstruction. Clin. Sci. (Lond.), 1990, 78, 365-369.
8. Venegas, J.G., Harris, S.R., Simon, B.A., A comprehensive equation for the pulmonary pressure-volume curve. J. Appl. Physiol., 1998, 84, 1, 389-395.
9. Svantesson, C., Sigurdsson, S., Larsson, A., Jonson, B., Effects of recruitment of collapsed lung units on elastic pressure-volume relationship in anaesthetized healthy adults. Acta Anaesthesiol. Scand., 1998, 42, 721-728.
10. Jonson, B., Svantesson, C., Elastic pressure-volume curves: What information do they convey ? Thorax, 1999, 54, 82-87.
11. Harris, S.R., Hess, D.R., Venegas, J.G., An objective analysis of the pressure-volume curve in the acute respiratory distress syndrome. Am.J.Respir.Crit.Care Med., 2000, 161, 432-439.
12. Amato, M.B., Barbas, C.S., Medeiros, D.M., Schettino, G.D.P., Lorenzi, F.G., Kairalla R.A., Deheinzelin, D., Morais, C., Fernandes, E.D.O., Takagaki, T.Y., Beneficial effects of the "open lung approach" with low distending pressures in acute respiratory distress syndrome. A prospective randomized study on mechanical ventilation. Am.J.Respir.Crit.Care Med., 1995, 152, 1835-1846.
13. Amato, M.B., Barbas, C.S., Medeiros, D.M., Magaldi, G.P., Schettino, G.D.P., Kairalla R.A., Deheinzelin, D., Munozs, C., Oliveira, R., Takagaki, T.Y., Calvalho, C.R., Effect of a protective-ventilation strategy on mortality in the acute respiratory distress syndrome. New Engl. J. Med., 1998, 347-354.
14. ARDS Network, Ventilation with lower tidal volumes as compared with traditional tidal volumes for acute lung injury and the acute respiratory distress syndrome. N. Engl. J. Med., 2000, 342 (18), 1301-1308.
15. Narusawa, U., General characteristics of the sigmoidal model equation representing quasi-static pulmonary pressure-volume curves. J. Appl. Physiol., 2001, 91, 201-210.

Chapter 2.

1. Venegas, J.G., Harris, S.R., Simon, B.A., A comprehensive equation for the pulmonary pressure-volume curve. J. Appl. Physiol., 84, 1, 389-395, 1998.
2. Harris, S.R., Hess, D.R., Venegas, J.G., An objective analysis of the pressure-volume curve in the acute respiratory distress syndrome. Am.J.Respir.Crit.Care Med., 161, 432-439, 2000.
3. Jonson, B., Svantesson, C., Elastic pressure-volume curves: what information do they convey ? Thorax, 54, 82-87, 1999.
4. Amato, M.B., Barbas, C.S., Medeiros, D.M., Schettino, G.D.P., Lorenzi, F.G., Kairalla R.A., Deheinzelin, D., Morais, C., Fernandes, E.D.O., and Takagaki, T.Y., Beneficial effects of the "open lung approach" with low distending pressures in acute respiratory distress syndrome. A prospective randomized study on mechanical ventilation. Am.J.Respir.Crit.Care Med., 152, 1835-1846, 1995.
5. Amato, M.B., Barbas, C.S., Medeiros, D.M., Magaldi, G.P., Schettino, G.D.P., Kairalla R.A., Deheinzelin, D., Munozs, C., Oliveira, R., Takagaki, T.Y., and Calvalho, C.R., Effect of a protective-ventilation strategy on mortality in the acute respiratory distress syndrome. New Engl. J. Med., 347-354, 1998.
6. ARDS Network, Ventilation with lower tidal volumes as compared with traditional tidal volumes for acute lung injury and the acute respiratory distress syndrome. N. Engl. J. Med. 342 (18), 1301-1308, 2000.
7. Salazar, E., and J. H. Knowles. An analysis of pressure-volume characteristics of the lungs. J. Appl. Physiol., 19, 97-104, 1964.
8. Paiva, M., Yernault, J.C., VanErdeweghe, P. and Englert, M., A sigmoidal model of the static volume-pressure curve of human lung. Respir. Physiol., 23, 317-323, 1975.
9. Murphy, B.G., Engel, L.A., Models of the pressure-volume relationship of the human lung. Respir. Physiol. 32, 183-194, 1978.
10. Gibson, G. J., Pride, J. B., Davis, J. and Schroter, R. C.. Exponential description of the static pressure-volume curve of normal and diseased lungs. Am. Rev. Respir. Dis., 120: 799-811, 1979.
11. Bogaard, J. M., Overbeek,S. E., Verbraak, A. F., Vons, ,C., Folgering, H. T., Van, D. M. T. C., Roos, M. and Sterk, P. J.. Pressure-volume analysis of the lung with an exponential and linear-exponential model in asthma and COPD. Eur. Respir. J., 8, 1525-1531, 1995.
12. Svantesson, C., Sigurdsson, S., Larsson, A., Jonson, B., Effects of recruitment of collapsed lung units on elastic pressure-volume relationship in anaesthetized healthy adults. Acta Anaesthesiol. Scand., 42, 721-728, 1998.
13. Hickling, K.G., The pressure-volume curve is greatly modified by recruitment. A mathematical model of ARDS lungs. Am.J.Resp.Crit.CareMed., 158, 194-202, 1998.
14. Narusawa, U., General characteristics of the sigmoidal model equation representing quasi-static pulmonary pressure-volume curves. J. Appl. Physiol., 91, 201-210, 2001.
15. Sonntag, R.E. and Van Wylen, G.J., Fundamentals of Statistical Thermodynamics. John Wiley & Sons, 1966.
16. Fowler, R. and Guggenheim, Statistical Thermodynamics. Cambridge University Press. 1956.

Chapter 3.

1. Harris, S.R., Hess, D.R., Venegas, J.G., An objective analysis of the pressure-volume curve in the acute respiratory distress syndrome. Am.J.Respir.Crit.Care Med., 161, 432-439, 2000.
2. Jonson, B., Svantesson, C., Elastic pressure-volume curves: What information do they convey ? Thorax, 54, 82-87, 1999.
3. Amato, M.B., Barbas, C.S., Medeiros, D.M., Schettino, G.D.P., Lorenzi, F.G., Kairalla R.A., Deheinzelin, D., Morais, C., Fernandes, E.D.O., and Takagaki, T.Y., Beneficial effects of the "open lung approach" with low distending pressures in acute respiratory distress syndrome. A prospective randomized study on mechanical ventilation. Am.J.Respir.Crit.Care Med., 152, 1835-1846, 1995.
4. Amato, M.B., Barbas, C.S., Medeiros, D.M., Magaldi, G.P., Schettino, G.D.P., Kairalla R.A., Deheinzelin, D., Munozs, C., Oliveira, R., Takagaki, T.Y., and Calvalho, C.R., Effect of a protective-ventilation strategy on mortality in the acute respiratory distress syndrome. New Engl. J. Med., 347-354, 1998.
5. ARDS Network, Ventilation with lower tidal volumes as compared with traditional tidal volumes for acute lung injury and the acute respiratory distress syndrome. N. Engl. J. Med. 342 (18), 1301-1308, 2000.